COMPUTATIONAL BUCKLING ANALYSIS OF CYLINDRICAL THIN-WALLED ABOVEGROUND TANKS

by
Eduardo Manuel Sosa

A thesis submitted in partial fulfillment of the requirements for the degree of

DOCTOR OF PHILOSOPHY
in
CIVIL ENGINEERING

UNIVERSITY OF PUERTO RICO
MAYAGÜEZ CAMPUS
June, 2005

Approved by:

Luis E. Suárez, PhD Member, Graduate Committee	Date
Ricardo R. López, PhD Member, Graduate Committee	Date
Raúl E. Zapata, PhD Member, Graduate Committee	Date
Luis A. Godoy, PhD President, Graduate Committee	Date
Gustavo Gutiérrez, PhD Representative of Graduate Studies	Date
Ismael Pagán Trinidad, MS Chairperson of the Department	Date
José Mari Mutt, PhD Director of Graduate Studies	Date

ABSTRACT

This thesis evaluates the stability of cylindrical above-ground steel tanks under imposed support settlements and wind pressures. The tanks considered are representative of tanks constructed in Puerto Rico and in the Caribbean Islands. Typical tanks are constructed with a cylindrical shell with variable thickness and a conical roof supported by rafters. The behavior of these tanks is evaluated by means of computational experiments performed using finite element models developed with ABAQUS.

The influence of support settlements on the out-of-plane displacements in the cylindrical shell is investigated considering an elastic material behavior and using different types of analyses. Results are presented for geometric linear, geometric non-linear and bifurcation buckling analyses. Linear results provide a poor indication of the real displacements in the shell, so that geometric non-linearity is included in the analysis for working loads. Results show that the equilibrium path is highly non-linear and that the shell displays a stable symmetric bifurcation behavior.

The lower bound approach for the buckling load of imperfection-sensitive shells is implemented in this thesis. Initially, the formulation is presented in a way to highlight what computations can be done following a reduced energy model. Then, a proposed methodology is used in conjunction with a general purpose finite element program to compute the lower bound buckling load for tanks with different geometric and load configurations. Results show that the proposed reduced energy model can predict the lower bound load for cylindrical shells under uniform pressure distributions, but cannot estimate the lower bound for wind pressures.

The dynamic stability of an empty tank under wind pressures is investigated. An assumed space variation of pressures, and a simplified deterministic model of time fluctuating pressures due to wind, are applied. The response is calculated using explicit integration of the equations of motion and the dynamic buckling load is identified through a qualitative criterion. The response is analyzed in the time and in the frequency domain in order to recognize the nature of the problem. Results show that pressure fluctuations do not induce resonance of the structure, so that simpler pressure models may be used in practical analyses.

RESUMEN

Esta tesis estudia la estabilidad estructural de tanques cilíndricos de acero bajo la acción de desplazamientos impuestos en los apoyos y de presiones de viento. Los tanques analizados son representativos de los que se encuentran en Puerto Rico y en otras islas del Caribe. Éstos están compuestos típicamente de una cáscara cilíndrica de espesor variable y un techo cónico con su estructura de soporte. El comportamiento se evalúa por medio de modelos de elementos finitos desarrollados en ABAQUS.

El efecto del descenso de apoyos en los desplazamientos normales a la superficie de la cáscara cilíndrica se evalúa a través de análisis estáticos que consideran linealidad y no linealidad geométrica, y por medio de análisis clásicos de bifurcación. En todos los casos se considera que el material se comporta elásticamente. Los resultados muestran que los análisis lineales no predicen correctamente los desplazamientos reales en la cáscara cilíndrica y que es necesario incluir los efectos no lineales geométricos para amplitudes de descenso típicas. La cáscara cilíndrica muestra un comportamiento altamente no lineal caracterizado por una bifurcación simétrica estable.

En esta tesis se implementa el concepto de límite inferior de cargas de pandeo en cáscaras sensibles a imperfecciones a través de un modelo de energía reducida. Inicialmente se identifican las operaciones necesarias para determinar ese límite en el modelo de energía reducida y luego se ejecutan en un modelo de elementos finitos. La metodología propuesta se aplica a distintas configuraciones de tanques, en los cuales los resultados muestran que el modelo de energía reducida propuesto predice bien el límite inferior de carga de pandeo en los modelos sometidos a presión uniforme, pero no puede hacerlo correctamente en los modelos bajo presiones de viento.

Se evalúa la estabilidad dinámica de un tanque vacío sometido a presión de viento. Se asume una distribución espacial y se introduce un modelo determinístico simplificado para tener en cuenta las fluctuaciones temporales de las presiones de viento. La respuesta se calcula por medio de integración explícita de las ecuaciones de movimiento y la carga dinámica de pandeo se determina usando un criterio cualitativo. La respuesta se analiza en el dominio del tiempo y de las frecuencias para reconocer la naturaleza del problema. Los resultados muestran que las fluctuaciones temporales no

llevan la estructura a resonancia, con lo cual para efectos prácticos es posible usar modelos simplificados de presiones.

ACKNOWLEDGEMENTS

First of all, I want to express my sincere acknowledgements and appreciation to my advisor Dr. Luis A. Godoy, who encouraged me to join to the Ph.D. program at the University of Puerto Rico. Previously in Córdoba, Argentina and then in Puerto Rico, his help, support and guidance throughout my entire doctoral studies and research experiences made possible the completion of this thesis.

I would also like acknowledge the members of my graduate committee: Dr. Luis Suárez, Dr. Ricardo López and Dr. Raúl Zapata, for their patience, comments, and criticism to this work. I must also thank to Dr. Carlos Prato for his valuable observations and suggestions in some stages of the research.

My acknowledgements to the Department of Civil Engineering and Surveying and to its Director, Prof. Ismael Pagán for providing financial assistance during my doctoral studies.

Part of the research developed in this thesis was supported by US National Science Foundation grant CMS-9907440, and by US Federal Emergency Management Agency grant PR-0060-A. Their contribution is gratefully acknowledged.

Finally, I wish to thank my parents, Rodolfo and Elva, for their attention, patience, best wishes, and the love given at the distance, but that I perceived very close to me. Finally, my thanks to my brothers, Sergio and Liliana, for their continuous help in every situation I requested them.

TABLE OF CONTENTS

CHAPTER 1 .... **1**

INTRODUCTION **1**

1.1 MOTIVATION 1
1.2 IMPORTANCE 7
1.3 SCOPE 9
1.4 OBJECTIVES 9
1.5 METHODOLOGY 10
1.6 ORGANIZATION 11

CHAPTER 2 .... **13**

BASIC CONCEPTS ON BUCKLING OF TANKS **13**

2.1 INTRODUCTION 13
2.2 WHAT IS BUCKLING? 14
2.3 EQUILIBRIUM PATHS AND CRITICAL STATES 16
2.4 INFLUENCE OF IMPERFECTIONS 19
2.5 PLASTIC BUCKLING 22
2.6 THE MINIMUM POTENTIAL ENERGY CRITERION 22
2.7 DYNAMIC STRUCTURAL INSTABILITIES 27
2.8 APPROACHES TO EVALUATE BUCKLING 31

CHAPTER 3 .... **33**

LOCALIZED SUPPORT SETTLEMENTS OF THIN-WALLED STORAGE TANKS **33**

3.1 INTRODUCTION 33
3.2 LITERATURE REVIEW 34
3.3 CASE STUDIED 38
3.4 RESULTS FOR THE CASE STUDIED 41

3.4.1 LINEAR ANALYSIS ...41
3.4.2 GEOMETRIC NON-LINEAR ANALYSIS...44
3.4.3 BIFURCATION ANALYSIS ...47
3.5 EXPERIMENTAL RESULTS ON SMALL-SCALE MODEL ... 50
3.6 FINITE ELEMENT MODEL OF THE SMALL-SCALE TEST ... 53
3.7 CONCLUSIONS... 56

CHAPTER 4... 58

COMPUTATION OF LOWER-BOUND BUCKLING LOADS USING GENERAL-PURPOSE FINITE ELEMENT CODES ... 58

4.1 INTRODUCTION ... 58
4.2 LITERATURE REVIEW ... 60
4.3 BUCKLING ANALYSIS ... 64
4.3.1 CLASSICAL BIFURCATION ANALYSIS ...64
4.3.2 REDUCED STIFFNESS ANALYSIS ...65
4.3.3 REDUCED ENERGY ANALYSIS ...67
4.3.4 PROPOSED METHODOLOGY FOR LOWER BOUND ANALYSIS ...68
4.4 SHELL ELEMENTS AVAILABLE IN ABAQUS... 69
4.5 RESULTS FOR A CYLINDRICAL SHELL SIMPLY SUPPORTED AT THE ENDS UNDER UNIFORM PRESSURE ... 71
4.5.1 ANALYTICAL RESULTS ...71
4.5.2 COMPUTATIONAL RESULTS ...73
4.6 RESULTS FOR A CYLINDRICAL TANK CLAMPED AT THE BASE AND FREE AT THE TOP UNDER UNIFORM PRESSURE... 76
4.7 RESULTS FOR CONICAL ROOF TANKS UNDER UNIFORM PRESSURE ... 79
4.8 CONCLUSIONS... 86

CHAPTER 5... 87

COMPUTATION OF LOWER-BOUND BUCKLING LOADS FOR TANKS UNDER WIND PRESSURES... 87

5.1 INTRODUCTION ... 87

5.2 CONICAL ROOF TANKS UNDER WIND PRESSURE 88
5.2.1 GEOMETRY AND LOAD DESCRIPTION 88
5.2.2 COMPUTATIONAL MODEL FOR CLASSICAL BUCKLING ANALYSIS 91
5.2.3 COMPUTATIONAL MODEL FOR REDUCED ENERGY ANALYSIS 98
5.2.4 LOWER BOUND VIA NON-LINEAR ANALYSIS 99
5.2.5 DISCUSSION 103
5.3 OPEN TANKS UNDER WIND PRESSURE 104
5.3.1 GEOMETRY AND LOAD DESCRIPTION 104
5.3.2 COMPUTATIONAL MODEL FOR CLASSICAL BUCKLING ANALYSIS 105
5.3.3 LOWER BOUND USING REDUCED ENERGY METHOD 106
5.3.4 LOWER BOUND VIA NON-LINEAR ANALYSIS 108
5.4 ALTERNATIVES FOR IMPROVING THE LOWER BOUND COMPUTATIONS 109
5.4.1 CHANGE IN THE BUCKLING MODE 109
5.4.2 CHANGE IN THE MODE NORMALIZATION TO COMPUTE THE ENERGY 113
5.5 CONCLUSIONS 122

CHAPTER 6 124

NON-LINEAR DYNAMICS OF ABOVE-GROUND THIN-WALLED TANKS UNDER FLUCTUATING PRESSURES 124

6.1 INTRODUCTION 124
6.2 LITERATURE REVIEW 125
6.3 WIND ACTION 129
6.4 THEME STRUCTURE AND COMPUTATIONAL MODEL 133
6.5 NON-LINEAR DYNAMIC RESPONSE 135
6.5.1 RESULTS FOR PERFECT GEOMETRY WITHOUT DAMPING 135
6.5.2 RESULTS INCLUDING DAMPING 140
6.5.3 RESULTS INCLUDING IMPERFECTIONS 141
6.6 FREQUENCY DOMAIN ANALYSIS 145
6.7 CONCLUSIONS 151

CHAPTER 7 153

CONCLUSIONS 153

7.1 SUMMARY OF CONTENTS 153
7.2 MAIN CONCLUSIONS 155
7.3 ORIGINAL CONTRIBUTIONS OF THIS THESIS 157
7.4 RECOMMENDATIONS FOR FUTURE WORK 157
7.4.1 ON THE REDUCED ENERGY METHOD 157
7.4.2 ON FLUCTUATING LOADS IN TANKS 158
7.4.3 OTHER TOPICS 160

APPENDIX A 161

CONSTITUTIVE RELATION FOR THE REDUCED ENERGY METHOD.... 161

APPENDIX B 167

INPUT FILES FOR THE PROPOSED REDUCED ENERGY METHOD 167

REFERENCES 170

LIST OF FIGURES

Figure 1.1. Aerial view of a tank farm located in Puerto Rico (Caribbean Petroleum)...... 2
Figure 1.2. Tank farm located in Saint Lucia, during construction. 2
Figure 1.3. Tank farm located in Puerto Rico (Caribbean Petroleum). 3
Figure 1.4. Cone roof tanks connected to pipelines (Caribbean Petroleum). 3
Figure 1.5. Cylindrical tanks in Yabucoa, Puerto Rico. 3
Figure 1.6. Collapsed tanks in St. Croix after hurricane Hugo (1989). 5
Figure 1.7. Local buckling and collapsed dome roof tank after Georges (1998), Puerto Rico. 5
Figure 2.1. A tank that buckled in Peñuelas, Puerto Rico. 15
Figure 2.2. Load deflection diagrams showing equilibrium paths (a) limit point, and (b) bifurcation point.. 15
Figure 2.3. Three basic types of bifurcation for isolated modes...................................... 18
Figure 2.4. (a) Almost-coincident and (b) coincident critical states: Two or more critical modes are associated to the same critical load. 18
Figure 2.5. Influence of imperfections on bifurcation behavior of structural systems. 20
Figure 2.6. Imperfection sensitivity plot showing how the maximum load decreases with the amplitude of an imperfection. 21
Figure 2.7. Time invariant instability phenomena. 28
Figure 2.8. (a) Motion as time history; (b) Motion plotted in the phase space................. 29
Figure 2.9. Limiting situations of blast loading (a) Impulse like, short duration; (b) Steady like, long duration. 30
Figure 3.1. A typical tank considered for the analysis... 39
Figure 3.2. Geometry of the tank considered in the computations. 39
Figure 3.3. (a) Scheme of central angle with support settlements. (b) Finite element mesh used for the discretization of half of the structure and configuration of imposed displacements. 40
Figure 3.4. Linear results: Maximum out-of-plane displacements for different values of central angle of settlement. 42

Figure 3.5. Deflected shapes and contours of out-of-plane displacements for geometrical linear results: (a) θ = 15°; (b) θ = 30° and (c) θ = 45°. 43

Figure 3.6. Geometrically non-linear results for central angle θ = 15º. (a) Initial part of the equilibrium path; (b) Equilibrium path up to u_{max}=20mm. 45

Figure 3.7. Deflection pattern of the shell for central angle θ = 15°. 45

Figure 3.8. Geometrically non-linear results for central angle θ = 30º: (a) Initial part of the equilibrium path; (b) Deflection pattern of the shell for central angle 30º. 46

Figure 3.9. Geometrically non-linear results for central angle θ = 45º: (a) Initial part of the equilibrium path; (b) Deflection pattern of the shell for central angle 45º. 47

Figure 3.10. Normalized critical and non-linear settlements for different values of central angle of settlement. 48

Figure 3.11. Bifurcation modes for central angle θ (a) 15º, (b) 30º, (c) 45º. 49

Figure 3.12. Experimental set-up to induce vertical displacements at the base of the shell. 51

Figure 3.13. Deflected shape of the experimental model with a settlement of u_{max}=1 mm. 52

Figure 3.14. (a) Radial displacement for θ = 0°; (b) Radial displacement for θ = 30°; (c) Maximum radial displacement in FEM and experimental model (for θ = 18° and u_{max} = 1 mm). 52

Figure 3.15. Finite element mesh for the small-scale model. 54

Figure 3.16. Equilibrium paths at: a) θ = 0º and b) θ = 18°. 54

Figure 3.17. Sequence of deflected shapes. 55

Figure 3.18. Complete deflected shape for the computational model with a settlement of u_{max} = 1 mm. 55

Figure 4.1. Critical load for different load paths. 66

Figure 4.2. Analytical results for a cylindrical shell under uniform pressure................... 72

Figure 4.3. Energy spectrum $U_{[Total]} = U^{2m} + U^{2b}$ for different values of α 72

Figure 4.4. Variation of η for different shell elements. 75

Figure 4.5. Comparison of η for analytical and numerical model. 75
Figure 4.6. Geometric properties of the open tank. 76
Figure 4.7. (a) Deflected shape from classical eigenvalue analysis; (b) Expanded modes at the top of the open tank model... 77
Figure 4.8. Open tank model: knock-down factors η for different values of α. 78
Figure 4.9. (a) Non-linear paths for different level of imperfections; (b) Imperfection sensitivity curve. 79
Figure 4.10. Relative proportions of the models with conical roof. 81
Figure 4.11. First classical eigenmodes for all the models considered............................ 81
Figure 4.12. Knock-down factor calculated using the first eigenmode in the reduced energy method. 82
Figure 4.13. Non-linear equilibrium paths and imperfection sensitivity curves for all models.. 84
Figure 4.14. Imperfection sensitivity curves for all models. 85
Figure 4.15. Eigenmodes of Model 1 for: (a) classical buckling analysis; (b) imperfection sensitivity analysis for $\xi / t_{min} = 0.5$ at maximum load................................ 85
Figure 5.1. (a) Pressure distribution used in the conical roof. (b) Wind pressure distribution assumed around the circumference. 89
Figure 5.2. Relative proportions of the models with conical roof. 90
Figure 5.3. Eigenvalues for the geometric configurations of Figure 5.2. 92
Figure 5.4. First classical buckling mode, models MC1, MC2, MC3. 94
Figure 5.5. Second classical buckling mode, models MC1, MC2, MC3.......................... 95
Figure 5.6. First classical buckling mode, models MC4, MC5, MC6. 96
Figure 5.7. Second classical buckling mode, models MC4, MC5, MC6.......................... 97
Figure 5.8. Knock-down factors calculated using the reduced energy method for: (a) first eigenmode, and (b) second eigenmode.. 99
Figure 5.9. Non-linear equilibrium paths and imperfection sensitivity curves for selected models.. 101

Figure 5.10. Knock-down factor calculated with non-linear imperfection sensitivity analysis using as imperfection shape: (a) First eigenmode, and (b) Second eigenmode. 102
Figure 5.11. Comparison between the model geometries investigated. 105
Figure 5.12. First classical buckling modes for all models. The amplification factor is one for all four cases. 107
Figure 5.13. Lower bound estimate for open tank models. 108
Figure 5.14. Results of non-linear imperfection sensitivity analysis. 109
Figure 5.15. Lower bound calculated using non-linear mode. 111
Figure 5.16. Mode comparison for model M1. 112
Figure 5.17. Variation of η as a function of ψ, ρ and the membrane reduction coefficient α, for model M1. 117
Figure 5.18. Variation of η as a function of ψ, ρ and the membrane reduction coefficient α, for model M4. 118
Figure 5.19. (a) Variation of $\overline{\rho}^*$ as a function of H/D and Z. (b) Variation of η as a function of $\overline{\rho}^*$, for all open tank models. 120
Figure 5.20. (a) Variation of $\overline{\rho}^*$ as a function of H/D. (b) Variation of η as a function of $\overline{\rho}^*$, for selected cone roof tank models. 121
Figure 6.1. Model of pressure variation with time. Rectangular impulse with fluctuations. T_f: period of the fluctuation; T_3: 3 sec interval; P_f: fluctuation amplitude of the; P_3: average amplitude pressure. 130
Figure 6.2. (a) Pressure coefficient distributions on the cylindrical shell (b) Contours of pressure coefficient distribution on the conical roof reported by Macdonald et al. (1988) (c) Contours of pressure coefficient distribution on the conical roof reported by Portela and Godoy (2005); (d) Contours of wind pressures coefficient used in computations. 132
Figure 6.3. Details of the tank considered in the analyses: (a) Dimensions; (b) Overview of conical shell and configuration of the rafters. 134
Figure 6.4. Tank under constant impulsive load: (a) Time response for different load levels (b) Deflected shapes at four instant times. 137

Figure 6.5. (a) Time response of tank with impulsive load and fluctuation with $T_f = T_N$ and $\varphi = 0.1$; (b) Deflected shapes at four instant times. 139
Figure 6.6. Critical dynamic load λ_D for different normalized load periods $\tau = T_f / T_3$ using $\varphi = 0.1$. 140
Figure 6.7. Summary of analysis of sensitivity to imperfections of λ_D for $\varphi = 0.1$ and $T_f =$ 0.3562 seg. 142
Figure 6.8. Time response for two levels of imperfections for a tank with impulsive load plus a fluctuation with $T_f = T_N$ and $\varphi = 0.1$. 144
Figure 6.9. Dynamic buckling load for different levels of imperfections. 145
Figure 6.10. Maximum response of Node A recorded during 10 sec for constant load: — $\lambda_D = 2.515$ and fluctuating load: – – – $\lambda_D = 2.34$ ($\varphi = 0.1$, $T_f = 0.3562$ sec). 146
Figure 6.11. FFT of (a) Response to a constant amplitude pressure in time; (b) Constant amplitude load function. 148
Figure 6.12. FFT of (a) Response to a fluctuating load; (b) Fluctuating load function.. 149
Figure 6.13. FFT of the response in the buckled state considered separately: (a) Constant load, high amplitude oscillations; (b) Fluctuating load, high amplitude oscillations. 150

LIST OF TABLES

Table 3.1. Lowest eigenvalues leading to bifurcation buckling under support settlements 48
Table 4.1. Dimensions adopted of the cylindrical part of the model. 80
Table 4.2. Thickness adopted for each model.. 80
Table 5.1. Dimensions adopted of the cylindrical part of the model. 90
Table 5.2. Thickness adopted for each model.. 90
Table 5.3. Critical pressures for wind loaded tanks... 92
Table 5.4. Geometric properties... 104
Table 5.5. Classical critical loads (eigenvalue analysis).. 106
Table 5.6. Normalized factor for open tank models. 120
Table 5.7. Normalized factor for cone roof tank models... 121
Table 6.1. Natural frequencies and periods of the tank model. 138

CHAPTER 1

INTRODUCTION

1.1 MOTIVATION

Above ground storage tanks are vital facilities in Puerto Rico and in the Caribbean Islands. Large thin-walled tanks are employed by various industries to mainly store oil, water, and petrochemical products. Tanks are complex structures, frequently built with a cylindrical body clamped at the base, a roof, and an additional structure to support the roof. Usually, they have a fixed conical or dome roof. It is also common to find floating roofs or tanks open at the top. Tanks are frequently constructed as part of "tank farms" or large industrial plants with dozens or even hundreds of tanks. Figures 1.1 and 1.2 show typical tank farm configurations in Puerto Rico and Saint Lucia.

Typical designs of tanks make use of very thin shells, with ratios between the radius of the cylinder and the wall thickness of the order of 1,500-2,000, and height to diameter ratios on the order of 0.15 to 1.0. For short tanks such ratio is less than 0.5. The cylindrical part of a tank is constructed by welding steel plates in courses of eight feet (2.4 m) and is designed to perform under internal or wind pressures, temperature differentials and earthquake actions. Tanks may be anchored or unanchored at the base depending on the soil conditions, which may vary at a particular site. Figures 1.3 to 1.5 show typical cone roof cylindrical tanks located in Puerto Rico.

Figure 1.1. Aerial view of a tank farm located in Puerto Rico (Caribbean Petroleum).

Figure 1.2. Tank farm located in Saint Lucia, during construction.

Figure 1.3. Tank farm located in Puerto Rico (Caribbean Petroleum).

Figure 1.4. Cone roof tanks connected to pipelines (Caribbean Petroleum).

Figure 1.5. Cylindrical tanks in Yabucoa, Puerto Rico.

Damage in steel tanks has been identified each time a hurricane affects the Caribbean. During hurricane Hugo (1989), severe damage and collapse of oil tanks were detected in St. Croix (Figure 1.6) with consequences for the production, the local economy, and the environment. Damage of tanks in Antigua occurred during hurricane Luis in 1995, followed a week later by hurricane Marilyn leading to damage of a number of tanks in St. Thomas. Hurricane Georges (1998) produced local buckling of tanks in Yabucoa and Guayanilla, in southern Puerto Rico. Although damage was not severe, repairing was needed to reestablish the storage capacity and optimal operation conditions. Figure 1.7 illustrates some examples of local buckling of the cylindrical shell and collapse of a dome roof in Puerto Rico.

During hurricanes, the occurrence of moderate damage to total failure was mainly associated to buckling of the cylindrical shell of the tank. In some cases, the top enclosure of a water storage tank failed and left the short cylindrical shell to resist wind loading, so that a second failure occurred in the form of buckling of the top part of the shell. Buckling was detected in St. Croix during hurricane Hugo, with large distortions in the shape of the shell (Figure 1.6).

Most studies on the effect of wind pressures on cylindrical shell have been carried out in short open top tank models or in silos that are taller than the tanks previously described. It has been usual to assume that the wind pressure is constant in time. In previous studies models were analyzed using static approaches and did not pay attention to the possibility of dynamic effects induced by wind. Observing the damaged tanks, one may wonder if wind gusts with very high speeds associated to hurricanes are capable of inducing transient vibrations in the shell during short times, which may eventually lead to dynamic buckling. This is one of the questions that this thesis attempts to answer.

Other identified source of failure in tanks is the loss of the soil foundation strength. Such failure is sometimes due to severe windstorms with heavy rains or to excessive compressibility of the soil deposit due to other reasons. This leads into differential settlements in some part at the base circumference affecting, not only the tank bottom, but also the cylindrical shell.

Figure 1.6. Collapsed tanks in St. Croix after hurricane Hugo (1989).

Figure 1.7. Local buckling and collapsed dome roof tank after Georges (1998), Puerto Rico.

Such differential settlements in tanks may have several consequences and there are many reasons to be concerned about stresses and distortions generated by the local settlements. Reported studies on shell structures under support settlement are restricted to linear analysis despite of large out-of-plane displacements identified in the field and in laboratory experiments. Most of the studies are focused in reinforced concrete cooling towers and equivalent studies in steel tanks are restricted to open tanks models. This is another research topic that motivated this thesis. The goal is to find displacement patterns induced by vertical settlements in cylindrical tanks and to investigate if they occur in the geometrically linear range, as suggested in previous studies.

The evaluation of accurate buckling loads in shell structures has been of great concern in the past, motivated by the continuous use of shell structures not only in civil engineering, but also in aeronautical, space and naval engineering. In all these engineering fields, shell structures have to be stable under different load conditions and the designer is required to determine a critical load for a specific load condition. Much of the research effort has been oriented to find such critical load given that in most cases, experimental tests predicted lower critical loads than those computed with analytical models.

For shell structures like cylindrical tanks, it is known that imperfections play an important role in reducing the load carrying capacity. Different techniques have been used to make the analytical results closer to the experimental ones. They include complex non-linear models implemented in numerical test or most recently, energy based models as the lower bound theory, which may be an adequate tool to estimate safe critical loads. However, those techniques have only been applied to problems using complex analytical solutions or else special purpose programs developed for a particular case. A more extensive application of the lower bound theory by engineers will only be possible if general purpose finite element codes may be used without any need to develop special computer subroutines. This is another motivation of this thesis and it is generated by the need to generalize ways to implement the lower bound theory for cylindrical tanks.

1.2 IMPORTANCE

During field inspections around Puerto Rico and other islands, it was common to find tank farms where tanks were not isolated from other parts in an industrial plant, and have pipes and connections to other facilities that may be damaged due to the vertical displacements. Even if the pipelines are not affected by such vertical displacements, the cylindrical shell may significantly change its original geometric configuration. There are several reasons to be concerned about such changes in the geometry. First, direct structural failure may occur. Second, imperfection-sensitivity is increased by a damaged geometry and may trigger an early failure under further loads. Indeed, it is well known that Caribbean islands are prone to hurricanes several months a year and tanks may be exposed to extreme wind conditions recurrently for which the presence of geometric distortions would affect the buckling capacity. Third, operational problems may arise due to distortions of the cylindrical shell, particularly in floating roof tanks; excessive displacements of the cylindrical shell may affect the normal roof operation. There is a huge economic loss for each day that a tank does not operate due to structural problems, in which case the owner of the tank, the oil or water supplier companies, the consumers, the insurance companies, and the environmental protection agencies may start an investigation.

Design codes for wind loads requires considering wind gusts of at least 3 seconds at 10 m above ground surface. According to the region, maximum wind gust velocities for design in Puerto Rico during a hurricane are about 145 miles per hour. Probably such speed was exceeded by far in coastal zones where many damaged tanks were located. Typical wind records store wind speeds at 3 second intervals as minimum time between two consecutive records. Then, there is limited or no information about the fluctuation of the wind velocity for intervals smaller than 3 seconds. Preliminary studies in silos using wind pressures in the form of a rectangular impulse with 3 seconds duration appear to indicate that the dynamic effects are not significant in terms of the buckling capacity of the shell. However, the question remains if pressure fluctuations due to wind speed fluctuations within a 3 sec impulse may have a more damaging effect on the stability of the shell, and thus, if this justifies the need to obtain more detailed information in the records with less than 3 seconds intervals.

For buckling analysis, particularly in wind buckling analysis of tanks, it is not possible to find analytical (closed-form) solutions, so that computational mechanics is often the only choice to model the behavior under critical load conditions. However, there are different levels of complexity in the available tools that requires advanced skills and additional resources, not always necessary or available at the preliminary stages of the design. Considering that most tanks are designed by engineering firms that have standard finite element computer packages (including linear/non-linear static analysis, bifurcation-buckling analysis, and non-linear dynamic analysis), the implementation of a reliable methodology to find lower bound critical loads, would contribute not only to the understanding of the mechanics of the problem, but also to its solution using common practice engineering tools.

1.3 SCOPE

This thesis considers cylindrical above-ground steel tanks with cone roof or open at the top. Height to diameter ratios considered are in the range of 0.17 to 1.0 and the general structural configuration adopted is similar of what was observed in field inspections in Puerto Rico. The analyses are restricted to isolated tanks and the interaction with surrounding structures and topographic effects are not considered. The theme structures are analyzed under three loads configurations: localized support settlements, uniform lateral pressure and wind fluctuating pressures.

1.4 OBJECTIVES

The main objective of this thesis is:

● To evaluate the stability of cylindrical above-ground tanks under imposed support settlements and wind pressures.

The specific objectives of this thesis are:

• To evaluate the behavior of cylindrical cone roof steel tanks under different configurations of support settlements.

• To determine the effect of fluctuations in pressures and the importance of inertial effects on the behavior of cylindrical tanks.

• To find the deflected patterns due to dynamic pressures associated to hurricane wind speeds.

• To evaluate the effect of imperfections in the critical wind pressures.

• To develop a reduced energy approach in cylindrical tanks under uniform lateral pressures and wind pressures.

1.5 METHODOLOGY

The work reported in this thesis is carried out within the frame of computational mechanics. In order to reach the proposed objectives, computational experiments are performed using general purpose finite element codes. The effects of support settlements are analyzed using classical linear bifurcation, geometrically linear and non-linear static analysis. Additionally, in the evaluation of the behavior of the cylindrical tank under support settlements, experiments in small-scale-model are performed to confirm the computational results.

Deterministic fluctuations of wind pressures applied to cylindrical tanks are studied using geometric non-linear dynamic analysis. Wind pressures distributions available from previous research are adopted in the modeling.

The reduced energy method is implemented using classical linear bifurcation analysis and static linear analysis, in conjunction with geometric non-linear analysis to validate the results.

1.6 ORGANIZATION

This thesis is divided in seven chapters and two Appendixes. Chapter 1 introduces the theme structures investigated in this work, i.e. cylindrical above-ground steel tanks. The motivation, scope, the main objectives and the methodology employed in this thesis are also presented in this chapter.

Chapter 2 gives an introduction to the buckling of tanks in the context of the theory of elastic stability. This chapter provides a conceptual framework for the following chapters and facilitates the explanation of the results of the computational experiments.

Chapters 3 to 6 constitute the central chapters of this thesis. Chapter 3 analyzes the effect of support settlements on a tank with a conical roof. Results using linear, geometric non-linear and bifurcation analysis are presented for a typical tank and for a small-scale model.

Chapter 4 introduces a methodology proposed in this thesis to compute lower bound buckling loads for different cylindrical tank configurations under uniform external pressure. The reduced energy method to find the knock-down factor that reduces the classical critical load is described and implemented in this chapter. Results are compared with analytical and numerical results available to validate the applicability of the new proposed procedure.

Chapter 5 is a continuation of the topics discussed in Chapter 4, in which the proposed reduced energy method is implemented for tanks similar to those considered in Chapter 4, but under a different load configuration. That chapter presents the results for wind pressures acting in different tank geometries, in order to find the variation of the knock-down factor as the geometry changes. Appendixes A and B are directly related to Chapters 4 and 5, and contains detailed derivations of the constitutive model implemented in the reduced energy approach.

Chapter 6 describes the results of computational experiments to evaluate the importance of dynamic effects on the theme structure under wind loads. A simplified time variation of wind gusts applied in conjunction with an adopted spatial variation, are used to compute the non-linear dynamic response. The effect of imperfections and damping are evaluated and results in the frequency domain are presented as an alternative way to explain the effect of inertial forces.

Finally, general conclusions and topics for future work are presented in Chapter 7.

CHAPTER 2

BASIC CONCEPTS ON BUCKLING OF TANKS

2.1 INTRODUCTION

This chapter presents an introduction to the buckling of tanks in the context of the theory of elastic stability. The main purpose of the following sections is to provide a conceptual framework to facilitate the explanation of the results obtained in the next chapters. Fundamental concepts are presented in a simple way without using complex formulation and information is presented emphasizing the aspects related to the buckling of tanks. Additional and expanded treatment of each topic presented in this chapter may be found in Godoy (2000), Brush and Almorth (1975), Croll and Walker (1972), Yamaki (1984) and others texts.

The outline of the chapter is as follows: the concept of buckling is introduced in Section 2.2. A notion of equilibrium paths and critical states are presented in Section 2.3. The effect of the presence of imperfections is introduced in Section 2.4. Section 2.5 introduces plastic buckling. Section 2.6 introduces the minimum potential energy criterion. Section 2.7 gives some notions on dynamic structural instabilities. Section 2.8 summarizes ways to evaluate buckling loads using finite element packages.

2.2 WHAT IS BUCKLING?

A structural system is formed by a structure and the loads acting on it. There are two main properties that make a structure withstand loads:

- The constitutive material, and
- The geometric shape.

Every structure is designed with a specific shape and it is expected that it should retain this shape during the service life. For example, a tank that is designed with a circular shape and a conical roof is expected to retain this shape under the loads considered in the design.

Buckling is a process by which a structure cannot withstand loads with its original geometry, so that it changes this shape in order to find a new equilibrium configuration. This is an undesired process (from the point of view of the engineer), and occurs for a well-defined value of the load. The consequences of buckling are basically geometric: There are large displacements in the structure, to such an extent that the shape changes. There may also be consequences for the material, in the sense that deflections in the tank may induce plasticity in the walls of the structure. Figure 2.1 shows a buckled tank.

Buckling is associated not just to a structure, but to the complete structural system. To visualize a buckling process it is necessary to consider the load-deflection (P-Δ) diagrams, as shown in Figure 2.2. Here we plot the equilibrium states of the structure in terms of the load applied (P) and the deflection (Δ) obtained. Depending on the structure behavior, diagram shown in Figure 2.2(a) or 2.2(b) will be discussed in the next section. Of course, there are deflections in almost every point of the structure. Therefore, it is necessary to choose a convenient point and follow the process by looking at the displacements of this specific point.

Figure 2.1. A tank that buckled in Peñuelas, Puerto Rico.

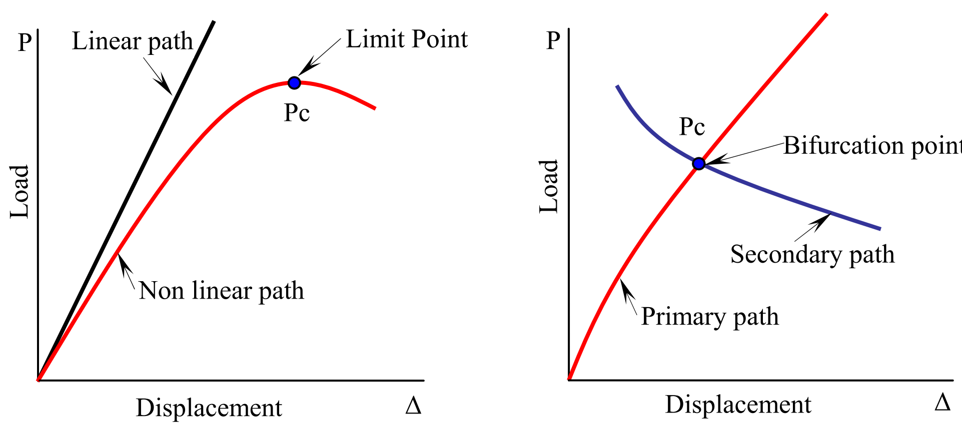

(a) (b)

Figure 2.2. Load deflection diagrams showing equilibrium paths (a) limit point, and (b) bifurcation point.

2.3 EQUILIBRIUM PATHS AND CRITICAL STATES

The sequence of equilibrium points in the P-Δ diagrams shown in Figure 2.2 is known as an equilibrium path. The equilibrium path emerging from the unloaded configuration is called the fundamental or primary path, also the pre-buckling path. This path may be linear (or almost linear) or may be non-linear depending on the structural system.

The load level in which there is a change of the shape is called buckling load P_C, and the emerging geometry is called the buckling mode. There are several ways in which this process may occur:

● In "snap buckling", the fundamental path is non-linear and reaches a maximum load, when the tangent to the path is horizontal. This state is called limit point (Figure 2.2(a)). The change in the shape occurs in a violent way.

● In "bifurcation buckling", the fundamental path may be linear and it crosses another equilibrium path, which was not present at the beginning of the loading process (Figure 2.2(b)). The state at which both paths have intersection is called a bifurcation point. Both limit and bifurcation points are called critical points or critical states.

Buckling is associated to a property of the equilibrium states known as stability. A stable equilibrium state is one in which if there is a small disturbance to the system at the same load level, then the system oscillates but returns to the original state after a while. If the system does not return to the original state and moves to a new state, perhaps far from the original one, then the original was an unstable equilibrium state. At a critical point, the stability changes from stable to unstable.

The process that occurs following buckling is called post-buckling:

● There are structures with a load capacity in their post-buckling behavior, which can adjust to changes in shape and resist additional loads after buckling. Thus, there is a post-buckling equilibrium path, which may be stable.

● Other structures do not have stable post-buckling equilibrium states, so that the critical load is the maximum load of the structure.

Koiter (1945) showed that the critical states of bifurcation might be of the following types (see Figure 2.3):

● Stable symmetric bifurcation. The post-buckling path (also called secondary path) has a horizontal tangent at the critical point, and the path is stable, so that the structure can carry further load increments (Figure 2.3(a)). This behavior is found in columns and plates.

● Unstable symmetric bifurcation. The post-buckling path has a horizontal tangent at the critical point, but the energy path is unstable, so that the structure cannot carry further load increments (Figure 2.3(b)). This behavior is typically found in shells.

● Asymmetric bifurcation. The post-buckling path has a non-horizontal tangent at the critical point, and the path is stable on one side and unstable on the other, depending of the displacements (Figure 2.3(c)). Then, the structure can carry further load increments only on the stable branch. This behavior is found in frames.

The type of behavior of Figure 2.3 occurs whenever there is an isolated critical state, also called distinct critical point. This means that the critical state is associated to just one buckling mode.

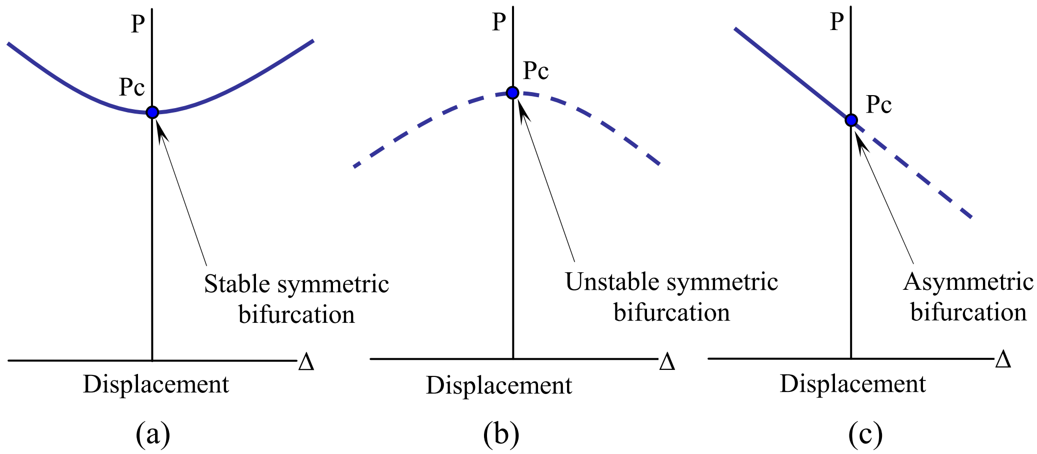

Figure 2.3. Three basic types of bifurcation for isolated modes.

There are also cases in which there are two modes associated to the same critical load, and this is known as a "coincident critical state", or a "compound critical point" ($P^1_c = P^2_c$) This situation is shown in Figure 2.4. The case of almost coincident critical loads is presented in Figure 2.4(a), while coincident critical loads are shown in Figure 2.4(b).

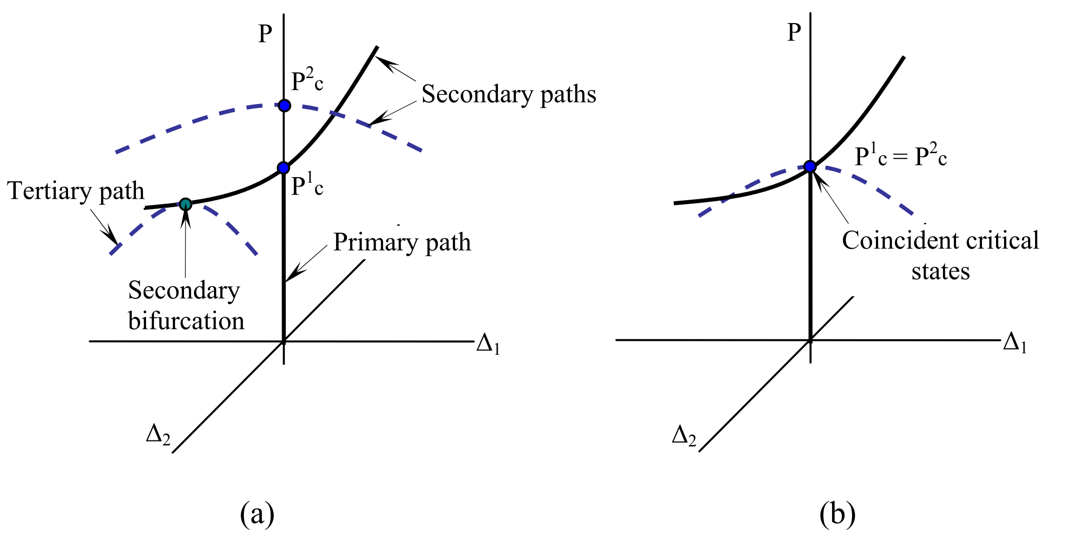

Figure 2.4. (a) Almost-coincident and (b) coincident critical states: Two or more critical modes are associated to the same critical load.

There are two reasons to explain how two or more modes can be coincident (or almost coincident):

● Due to the selection of some design parameters, two modes that may otherwise take different values of critical load, could result coincident. In this case, coincidence is the exception, not the rule.

● Due to a problem of the structure and the loading considered. For example, cylindrical shells under axial load or spherical shells under uniform external pressure (two common geometries in the design of tanks) develop many coincident modes for the lowest critical state. In this case, it does not matter how we design the shell, it will have coincident critical states, and coincidence is the rule, not the exception.

Two or more coincident (or almost coincident) critical states may have mode-coupling to form a new equilibrium path, different from the isolated equilibrium paths. For example, in Figure 2.4(a), the coupling of two modes produces a new secondary bifurcation state and a new tertiary equilibrium path. Not all coincident states couple, and there are several ways in which they may couple.

In many cases at the critical state the structure has a critical mode, and as the structure follows the post-critical equilibrium path the mode of deflections change. This is called “mode-jumping”.

2.4 INFLUENCE OF IMPERFECTIONS

Many structural systems (including tanks under lateral loads) are sensitive to the influence of small imperfections. Examples of imperfections are geometric deviations of the perfect shape, eccentricities in the loads, local changes in the properties, and others. An imperfection is usually characterized by its variation in space and its amplitude ξ.

An imperfection destroys a bifurcation point, and a new equilibrium path is obtained for each imperfection amplitude ξ. As the amplitude of the imperfection increases, the paths deviate more from the path of the perfect system. This is shown in Figure 2.5.

● Structural systems that display stable symmetric bifurcations have a non-linear path due to imperfections, and the bifurcation point is not reached (Figure 2.5(a)).

● Systems with unstable symmetric bifurcation in the perfect configuration, when an imperfection is included, have a non-linear path with a maximum in the load, after which the path descends (Figure 2.5(b)). Thus, the maximum load that the system can reach depends on the amplitude of the imperfection, and this maximum is lower than what would be computed using the perfect geometry.

● Finally, systems with asymmetric bifurcation have a maximum load on the unstable branch, leading to a maximum load (Figure 2.5(c)).

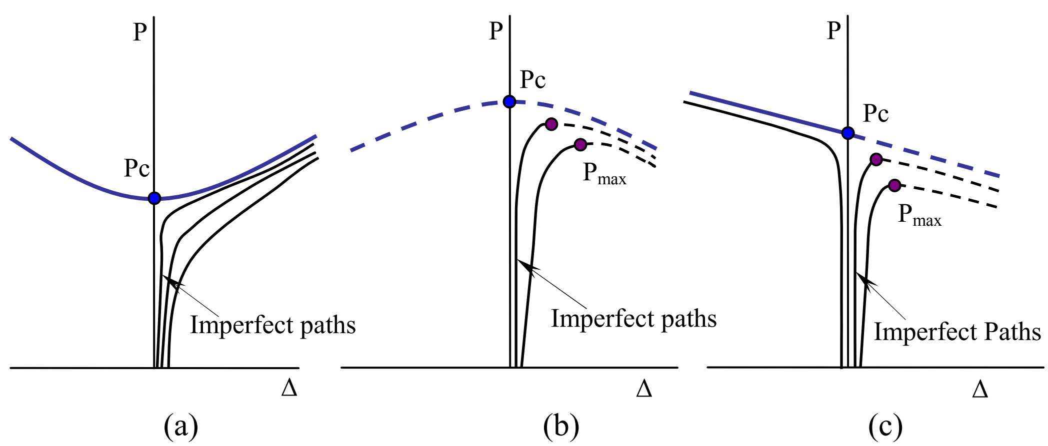

Figure 2.5. Influence of imperfections on bifurcation behavior of structural systems.

A typical plot is made showing the maximum load versus the amplitude of the imperfection; that is known as an imperfection-sensitivity plot. An example is shown in Figure 2.6. Some structures have a loss of buckling-carrying capacity of 50 % or more, including cylinders under axial load and spheres under pressure; they have high imperfection sensitivity. Other structures have moderate sensitivity, like cylinders under lateral pressure, which have a loss of about 20-30 %. Finally, there are structures with small sensitivity, like arches under transverse loads.

Problems with coincident (or almost coincident) critical states that have mode coupling may display high imperfection-sensitivity. This occurs in the cylinder and the sphere. In other cases (for example, an I-column under compression), there is mode-coupling but the imperfection-sensitivity is moderate.

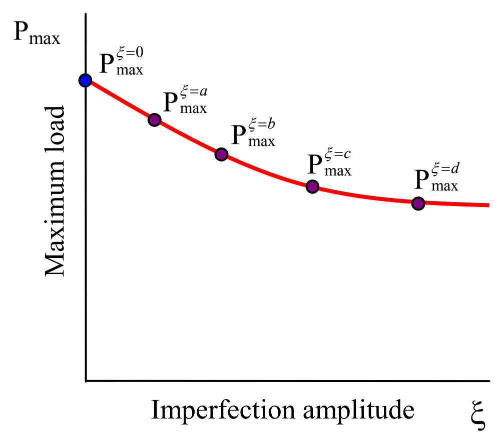

Figure 2.6. Imperfection sensitivity plot showing how the maximum load decreases with the amplitude of an imperfection.

2.5 PLASTIC BUCKLING

Figure 2.1 illustrates a frozen image of the buckled tank. Perhaps the steel was elastic at the onset of buckling, but as post-critical deflections grew the material had plastic deformations. The material properties during the buckling process are very important:

● Elastic buckling: is a process that initiates at the critical states with elastic material properties. Thus, instability occurs before plasticity: when the structure reaches plastic deformations it already experienced buckling. This occurs in most thin-walled shells, such as tanks.

● Plastic buckling: is a process that initiates with plastic deformations. Thus, plasticity occurs before instability: when the structure reaches a buckling load it already had plastic deformations. This occurs in thick shells.

● Elastic-plastic buckling: This occurs when plasticity and instability occur almost at the same load level. This occurs in moderately thin shells.

2.6 THE MINIMUM POTENTIAL ENERGY CRITERION

In the field of elastic stability, it is common to adopt the point of view expressed by Hutchinson and Koiter (1970): “The energy criterion of stability for elastic systems subject to conservative loadings is almost universally accepted by workers in the field of structural stability. A positive definite second variation in the potential energy about a static equilibrium state is accepted as a sufficient condition for stability of that state. Numerous attempts to undermine these two pillars of structural stability theory have been made, but confidence in them remains undiminished. Whit a proper shoring-up of certain aspects of these criteria, they will undoubtedly continue to serve as the foundation of elastic stability theory".

The potential energy criterion has been the basis of almost all the structural stability investigations that are known. This criterion has found widespread application because, in general, it leads to results that have been verified by experience. The lack of correlation of theory and practice has been in the analysis of what are now termed 'imperfection-sensitive structures'. Such structures are not stable at the critical or buckling load (the equilibrium points), and their proper analysis requires the inclusion of non-linear effects.

The total potential energy Π of a stressed body under load is defined as:

$$\Pi = U + \Omega \tag{2.1}$$

where U is the internal strain energy and Ω is the load potential. The internal strain energy in a thin walled element is composed by membrane and bending contributions given by:

$$U = U_m + U_b \tag{2.2}$$

where U_m is the membrane contribution and U_b is the bending contribution.

Slender and thin-walled structures (like tanks) which are prone to buckling are not modeled using three-dimensional elasticity. For those structures it is usual to employ technical theories, particularly thin-shell structures are often studied by means of the Love-Kirchhoff hypothesis. For a cylindrical shell of radius R and length l, membrane and bending contributions to the total strain energy are expressed in terms of stress resultants and deformations as:

$$U_m = \frac{R}{2} \int_0^{2\pi} \int_0^{l} N_{ij} \varepsilon_{ij} \; dx d\theta \tag{2.3}$$

$$U_b = \frac{R}{2} \int_0^{2\pi} \int_0^{l} M_{ij} \kappa_{ij} \; dx d\theta \tag{2.4}$$

Here, N_{ij} are the in-plane stress resultant; ε_{ij} are the membrane strains in the mid-surface; M_{ij} are the components of moments; κ_{ij} are the changes in curvatures of the mid-surface. For thin walled structures shear components are assumed that produce negligible strain energy.

The load potential depends on the type of load acting on the shell structure. For a cylindrical shell under uniform lateral pressures, the load potential is:

$$\Omega = -R \int_0^{2\pi} \int_0^{l} pw \; dx d\theta \tag{2.5}$$

where p is the unit pressure and w is the out-of-plane displacement. Throughout this thesis it is assumed that the forces are increased in the same rate. So that there is only one parameter λ that controls the increments of all loads components. With this assumption, the load potential given in equation 2.5 takes the form:

$$\Omega = -\lambda \, R \int_0^{2\pi} \int_0^{l} pw \; dx d\theta \tag{2.6}$$

Substituting equations 2.3, 2.4 and 2.6 in equation 2.1 we get the total potential energy for cylindrical shell under uniform pressures, that is:

$$\Pi = \frac{R}{2} \left[\int_0^{2\pi} \int_0^{l} (M_{ij} \kappa_{ij} + N_{ij} \varepsilon_{ij}) \, dx d\theta \right] - \lambda \, R \int_0^{2\pi} \int_0^{l} pw \; dx d\theta \tag{2.7}$$

In equation 2.7 it is necessary to introduce kinematic relations that include linear and non-linear contributions to each strain ε_{ij} and curvature κ_{ij} components. In the evaluation of stability it is usual write the kinematic relations for an incremental state with respect to the critical state (an incremental state has incremental displacements or buckling modes). In such state, the increments in the displacements are not associated to increments in the external load. The strains in the incremental state are expressed in terms no linear kinematic relations which relate variations in the displacements with variations in the coordinates. Kinematic relations proposed by Donnell (1976) allow separating the contributions to the total strain in: strains due to the displacements in the fundamental state, linear strains in the incremental state, and quadratic strains in the incremental state. As an example, for x coordinate in equation 2.7, the total strain can be expressed as:

$$E_x = E_x^F + \varepsilon_x^{'} + \varepsilon_x^{"} \tag{2.8}$$

where E_x^F is the deformation due to displacements in the fundamental state, $\varepsilon_x^{'}$ is the linear strain due to displacements in the incremental state, and $\varepsilon_x^{"}$ is the quadratic strain due to displacements in the incremental state. Total resultant forces can be expressed in a similar way as:

$$N_x = N_x^F + n_x^{'} + n_x^{"} \tag{2.9}$$

where N_x^F is the resultant force in the fundamental state, $n_x^{'}$ is the linear resultant force in the incremental state, and $n_x^{"}$ is the quadratic resultant force in the incremental state. Appling the same decomposition for the other coordinates and replacing in equation 2.7, we have:

$$\Pi = \frac{R}{2}\int_0^{2\pi}\int_0^{l}(N_x E_x + N_\phi E_\phi + 2N_{x\phi}E_{x\phi})\,dxd\theta$$
$$+\frac{R}{2}\int_0^{2\pi}\int_0^{l}(M_x \mathrm{X}_x + M_\phi \mathrm{X}_\phi + 2M_{x\phi}\mathrm{X}_{x\phi})\,dxd\theta + \Omega \tag{2.10}$$

Introducing in equation 2.10 the decomposition given in equations 2.8 and 2.9 for all coordinate components, we have the total potential energy for the incremental state. As example of this substitution, for *x* coordinate we have:

$$\Pi = \frac{R}{2}\int_0^{2\pi}\int_0^{l}(N_x^F + n_x^{'} + n_x^{''})(E_x^F + \varepsilon_x^{'} + \varepsilon_x^{''})\,dxd\theta$$
$$+\frac{R}{2}\int_0^{2\pi}\int_0^{l}(M_x^F + m_x^{'})(\mathrm{K}_x^F + \kappa_x^{'})\,dxd\theta + \ldots.. \tag{2.11}$$

Substituting for the other coordinates and expanding equation 2.11, the total potential energy takes the form:

$$\Pi = \Pi_0 + \Pi_1 + \Pi_2 + \Pi_3 + \ldots\ldots \tag{2.12}$$

where Π_0 only includes terms in the fundamental state, Π_1 includes linear terms in the incremental state, Π_2 includes quadratic terms in the incremental state and so on. Here the term Π_0 represents the potential energy in the primary or fundamental path. The term $\Pi_1 \equiv \delta\Pi$ represents the first variation of the fundamental state. This term satisfy equilibrium, so it must be zero, then $\Pi_1 \equiv \delta\Pi = 0$. The term $\Pi_2 \equiv \delta^2\Pi$ represents the second variation of the potential energy of the fundamental state and normally is not zero. Reminding the stability criterion presented at the beginning of this section, we have that:

$\delta^2\Pi > 0$ If the second variation is positive, then the state is stable.

$\delta^2\Pi < 0$ If the second variation is negative, then the state is unstable.

$\delta^2\Pi = 0$ If the second variation is zero, then it is a critical state of stability.

Incremental displacements and loads that satisfy the last condition, determine a critical state which can be evaluated equating the second variation to zero and neglecting the non-linear contributions in the secondary o post-critical path. This generates a new eigenproblem in which the eigenvalues are used to compute the resultant forces in the fundamental path. Expanded computations for this state can be found in Godoy (2000).

For simple geometric and load configurations it is possible evaluate the stability of the system computing the strain energy and the second variation analytically. For complex structures, like tanks analyzed in this thesis, such computations are performed numerically in finite element models.

Some remarks regarding the total potential energy criterion are (Godoy, 2000):

● The energy criterion of stability is based on a global measure, the energy of the complete body, and not in local measures like stresses.

● The applicability of this criterion is restricted to elastic behavior. The stability evaluation in plastic states cannot be determined using this criterion.

2.7 DYNAMIC STRUCTURAL INSTABILITIES

The occurrence of dynamic instability phenomena in engineering structures may be caused by time-dependent or time-invariant loads. For dynamic stability analysis, uniform computer-oriented stability criteria become more required as the various analytical methods that can only be employed to ‘simple’ structures.

Time-invariant responses are depicted in Figure 2.7. There, the sequence of points of equilibrium is called time-invariant structural response. From the response we distinguish primary, secondary and high order response paths separated by:

● Bifurcation points, in particular simple, multiple and tangent bifurcation points.

● Limit points, in particular snap-through and snap-back points.

● Isolated or multiple critical equilibrium points.

Response shows non-linearities which can be physical (associated to the material) or geometrical (associated to the kinematic of the problem).

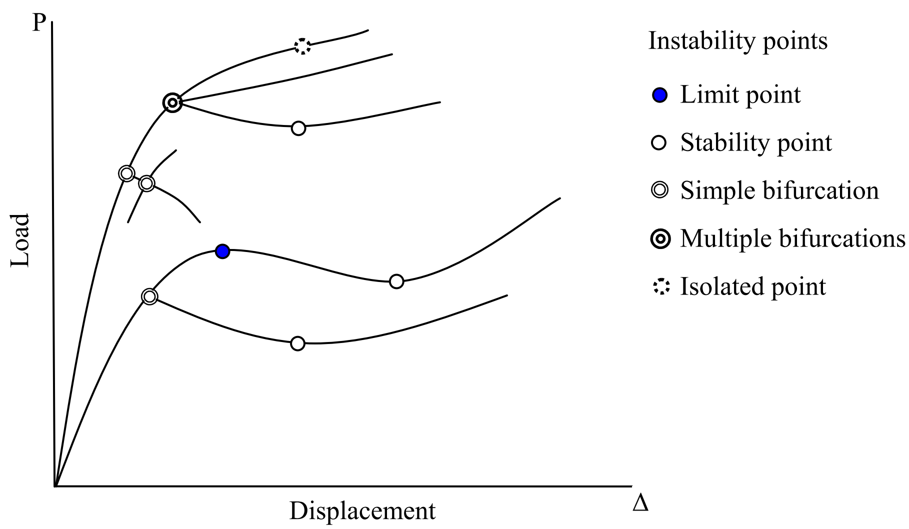

Figure 2.7. Time invariant instability phenomena.

Time-dependent responses as structural motions can be described as:

● Time-histories, where displacements for certain point is plotted versus time, as Figure 2.8(a) depicts.

● State-space diagrams, where the displacement is plotted versus the velocity, in this case the time is a parameter along the path, as Figure 2.8(b) shows.

However, with both diagrams depicted in Figure 2.8 in general it is not possible to decide whether a response is linear or non-linear, stable or unstable. Compared with the static case, the classification of kinetic instabilities is neither fundamental nor straight forward. Most phenomena are grouped together with those which are governed by similar mathematical equations or methods (Krätzig and Niemann, 1996). In a relatively superficial manner we distinguish kinetic instabilities caused by:

● Parametric resonance.

● Impulsive loading.

● Circulatory loads.

● Aeroelastic problems.

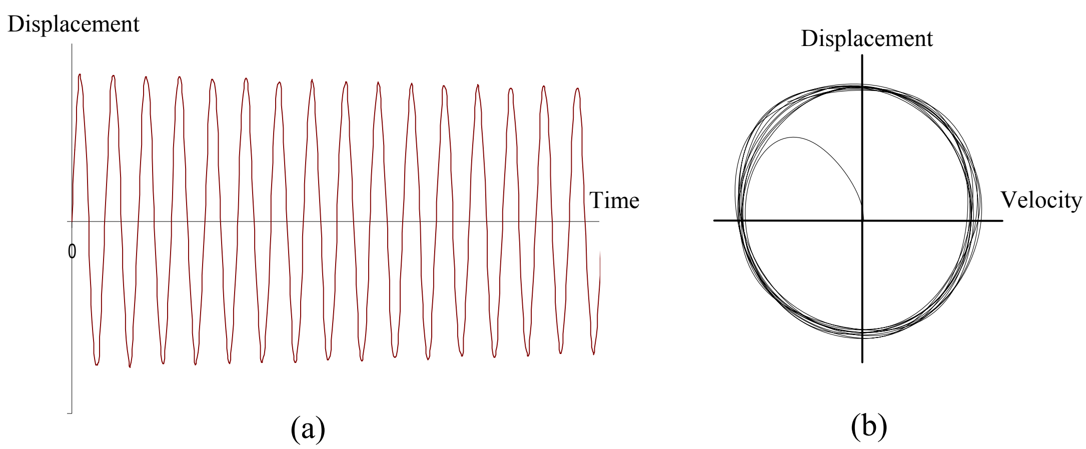

Figure 2.8. (a) Motion as time history; (b) Motion plotted in the phase space.

Particularly, impulsive loading is a case of interest in this work. In the evaluation of the stability of structures under transient loading, there are two situations of interest:

● Impulse or short term loading, as depicted in Figure 2.9(a), and

● Long term loading such as a suddenly applied load, which remains constant as Figure 2.9(b) shows.

The first could be associated to an impact loading and the second is the rapid application of a nominally quasi-static load. The second case has particular importance for this thesis because previous studies on dynamic wind effects have considered such type of loading. For this loading type, Doyle (2001) recognizes three situations in which the stability is evaluated:

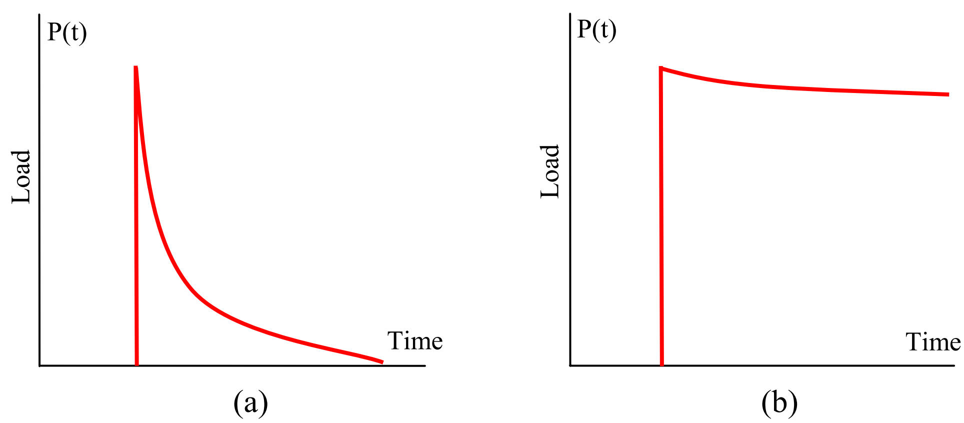

Figure 2.9. Limiting situations of blast loading (a) Impulse like, short duration; (b) Steady like, long duration.

I – Stiff systems, identified as those that exhibit increasing stiffness with increasing deformation. These are globally stable when the loads are applied quasi-statically.

II – Bifurcational systems, identified as those systems which have a primary loading path that does not change in the bifurcated degrees of freedom. Examples of these cases are Euler buckling columns and flat plates.

III – Limit point systems, in contrast to the bifurcational systems, the limit-point systems show change of deformation in the degrees of freedom along the primary loading paths. Snap-through buckling of a shallow arch is an example, but also is the buckling way of shells. Particularly for this situation, Budiansky and Roth (1962) proposed a "…qualitative, but fairly well defined, criterion…" for determining dynamic buckling load. This criterion is based in computing the time-dependent response for gradually raising load amplitudes. When response, measured in a control point, shows a very steep rise in the maximum amplitude for a very small change in the load amplitude, it is said that the dynamic buckling load is identified. Such critical pressure corresponds, qualitatively, to a transition from moderate to severe deformations.

Given the complexity of the structures analyzed in this work, it is not possible to obtain an analytic exact solution. Instead, finite element models in conjunction with non-linear geometric effects and explicit integration of the equations of motions are employed to determine the dynamic buckling load, so that a criterion as described above is helpful in the evaluation of the dynamic stability of tanks under time-variant loads.

2.8 APPROACHES TO EVALUATE BUCKLING

At present, most structures are analyzed using a finite element model, and more specifically, a commercial computer package is employed like ABAQUS, ALGOR, ADINA, ANSYS, and others. There are basically three ways in which buckling may be evaluated using a finite element program:

● Bifurcation analysis. The program performs first a static analysis of a linear fundamental equilibrium path, and then computes the eigenvalues and eigenvectors of the system using the stiffness and the load-geometry matrices. The results are the buckling load and the buckling mode. No information is provided regarding the post-buckling path or sensitivity analysis.

● Non-linear analysis. A step-by-step analysis is performed considering an initial imperfection and geometrical and material non-linearity. Only limit points can be detected, and bifurcations are not taken into account. Sometimes the program may fail to detect a bifurcation state. The results are a list of load and displacement configurations.

● Initial post-critical analysis. Koiter (1945) developed a theory in which the stability of the critical state provides information about the post-critical states close to the critical point. A perturbation analysis is performed to compute the initial post-critical secondary path. Commercial computer programs do not have this capability, and it has been incorporated into many special purpose finite element programs for shells.

CHAPTER 3

LOCALIZED SUPPORT SETTLEMENTS OF THIN-WALLED STORAGE TANKS

3.1 INTRODUCTION

Thin-walled metal tanks may be supported in various forms, including compact soil foundation, ring walls, slabs or pile-supported foundations. The support may be lost in some part of the base circumference affecting the cylindrical shell and the tank bottom. The causes of such differential settlements may include “non homogeneous geometry or compressibility of the soil deposit, non uniform distribution of the load applied to the foundation, and uniform stress acting over a limited area of the soil stratum” (Marr, *et al*, 1982). Heavy rains, such as those that happen during tropical storms and hurricanes, may aggravate the situation. The differential settlements in tanks may have several consequences:

(a) Out-of-plane displacements are induced into the shell in the form of buckling under a displacement-controlled mechanism;

(b) High stresses develop at the base of the shell and in the region of the settlement;

(c) High stresses develop in the tank bottom.

There are many reasons to be concerned about such stresses and distortions. First, tanks are not isolated from other parts in an industrial plant and have pipes or connections to other facilities that may be damaged due to the vertical displacements. Second, excessive displacements of the cylindrical shell affect the normal operation of a floating roof. Third, a geometric distortion greatly affects the buckling resistance of the shell under wind pressure. Fourth, plasticity may occur in parts of the shell wall.

In this chapter, the geometrically linear and non-linear behavior of thin-walled tanks under localized settlements is considered. Experiments on a small-scale acetate model of a tank with a flat roof, and the computer analysis carried out to validate the geometrically non-linear behavior of this model are discussed.

The outline of the chapter is as follows: A revision of previous research on the topic is presented in Section 3.2. The case studied is described in Section 3.3. Results for this case are presented in Section 3.4. Experimental and computational results for a small scale model are presented in Section 3.5 and 3.6, respectively. Finally, some conclusions are presented in Section 3.7.

3.2 LITERATURE REVIEW

The settlement of the foundation in large, thin walled shells has been of great concern in the past. Studies on large reinforced concrete cooling towers shells constructed in the form of hyperboloids of revolution indicate ratios of maximum amplitude of the out-of-plane displacement versus the vertical settlement of the support between 3.5 and 6. See for example Gould (1972), Koluza and Mateja (1976), Croll and Billington (1979) and Lu, *et al*. (1986). Equivalent studies for thin-walled tanks are also found in Bell and Iwakiri (1980), Brown and Peterson (1964), Green and Hight (1964) and Clark (1969). However, all the computer simulations carried out by those authors employed a geometrically linear formulation in spite of the fact that significant displacements were identified. Myers (1997) indicates a possible mechanism of settlement at the base of tanks, but does not provide information regarding actual displacements in the shell. An interesting observation in the change from reinforced concrete cooling towers to steel tanks is that there is a shift of interest from the evaluation of stresses to the assessment of radial deflections.

According to D'Orazio and Duncan (1987), "…examination of the settlement measured for the tanks… shows one fact clearly: steel tank bottoms can undergo a wide variety of types of distortion as they settle". However, most analytical studies concentrate on just one type of distortion: a vertical displacement pattern at the base of the shell that follows a harmonic shape. D'Orazio *et al*. (1989) report: "Because their walls have significant stiffness and ability to span local soft spots, the settlement profiles of tank walls tend to be smooth and free of sharp variations. Through examination of measured settlement profiles and approximate theoretical analysis, the writers have concluded that for the tanks studied, which are typical floating-roof oil-storage tanks, significant distortion will not occur over circumferential distances shorter than about 20 to 30 m" (D'Orazio, *et al*. 1989, pp. 875). For a tank with R = 25.6 m, as the authors considered, the central angle associated to 20 m is 45º or 1/8 of the circumference.

Failures of tanks have been reported in the literature; see for example Marr *et al*. (1982), Bell and Iwakiri (1980), Clark (1969) and D'Orazio *et al*. (1989). Remarkable is the report of the failure of a 26.15 m radius shell storing hot oil in Japan in 1974. The consequences of this failure were multiple: "The contents flooded much of the refinery property and flowed into the adjacent inland sea causing severe damage to the fishing industry. As a result, the 270,000 bbl/day refinery was shut down for about nine months, largely because of public reaction. By the time the refinery was permitted to resume operation, the accident had cost the refinery more than $ 150,000,000" (Bell and Iwakiri, 1980).

Because of dramatic cases as described before, there is a need to establish some criteria to limit support settlements to admissible values. Such criteria do not consider buckling of the shell: "We assume that buckling resulting from differential settlement would occur in the top course, would not rupture the shell and would not result in loss of oil. However, failure by buckling requires more studies" (Marr *et al*., 1982, pp. 1028 and Jonaidi and Ansourian, 1998).

To evaluate the distortions in the cylindrical part of the tank, various models have been proposed. One of them is the use of a harmonic shape to account for the vertical displacement at the base and written in the form:

$$u = u_n \cos(n\varphi) \tag{3.1}$$

where φ is the angle around the circumference and n is the wave number. Malik, *et al*. (1977) used an inextensional theory of shells and derived the relation

$$w_n = (\mathrm{H/R})\, n^2 \; u_n \tag{3.2}$$

where w_n is the maximum amplitude of the out-of-plane displacement induced by the settlement, H is the height and R the radius of the cylinder. This equation has many drawbacks: it is independent of the thickness of the shell, it does not account for localized settlements, and it is based on a simplified and linear shell theory. Kamyab and Palmer (1989) derived another expression based on linear membrane shell theory, i.e

$$w_n = (H/R)\, n^2\; u_n\; [\frac{1}{(1+\alpha\; I_{ratio})}] \tag{3.3}$$

where α is function of the wave number n, the thickness t and of the Poisson's relation ν. I_{ratio} is the ratio between the circumferential bending stiffness of a ring stiffener on the top and the bending stiffness of the cylindrical shell. Jonaidi and Ansourian (1998) argued that errors in the range of 10-18% are obtained from the use of this membrane model.

More refined analysis have used finite element models for the shell and assumed harmonic settlement including more realistic features such as tapering wall thickness and the influence of the top ring stiffener (wind girder) as reported by Jonaidi and Ansourian (1998). These authors used ABAQUS (2002) to evaluate out-of-plane displacements, bending and membrane stress resultants as a function of the wave number n. Their numerical results showed that there is a critical value of n (close to 8) and central angle of 45°, for which the displacements w_n reach a maximum value.

Experiments on small scale models have been done by D'Orazio *et al*. (1989) for an open cylinder supported on eight points around the perimeter, and the settlement in the laboratory model are related to wall movements in real tanks by:

$$w_{real} = (H/R)_{real}\; K_s\; (w\, R/H)_{model} \tag{3.4}$$

where w is the change in radius and K_s is a factor of scale. Again, these expressions are independent of the slenderness of the shell and represent a linear relation.

Tests were also reported by Jonaidi and Ansourian (1998) on steel open cylinders with variable thickness and a simulation of the top ring. The mean wall slenderness is R/t = 375 and R/H = 1.88. The tests were performed at low amplitude settlements, consistent with the linear shell theory, and also for large deflection, the main purpose being the evaluation of stress mechanisms. Most of these studies refer to open tanks. "Little data and few analyses exist to set a criterion for the validity of coned-roof tanks" (Marr *et al.*, 1982, pp. 1024).

3.3 CASE STUDIED

For the current study, a specific tank with a conical roof shown in Figure 3.1, which was found at several locations in Puerto Rico, was investigated to study the radial deflections due to settlements over part of the shell foundation. The geometric parameters for this structure are shown in Figure 3.2, and are H = 12.191 m, D = 30.48 m (H/D = 0.40), with a tapered thickness as in the real structure in which the first course of the tank is built with t_1 = 11.4 mm, the second course has t_2 = 9.5 mm and the remaining three top courses have t_3 = 7.9 mm, such that, the average R/t is about 1,700. The tank is made of steel with a modulus of elasticity E = 206 GPa and a Poisson's ratio ν = 0.3. The thickness of the conical roof is 12.5 mm and for this chapter the details of the stiffeners on the roof were not included in the model. An empty tank is assumed fixed at the base, except for an arc where a settlement is imposed.

Figure 3.1. A typical tank considered for the analysis.

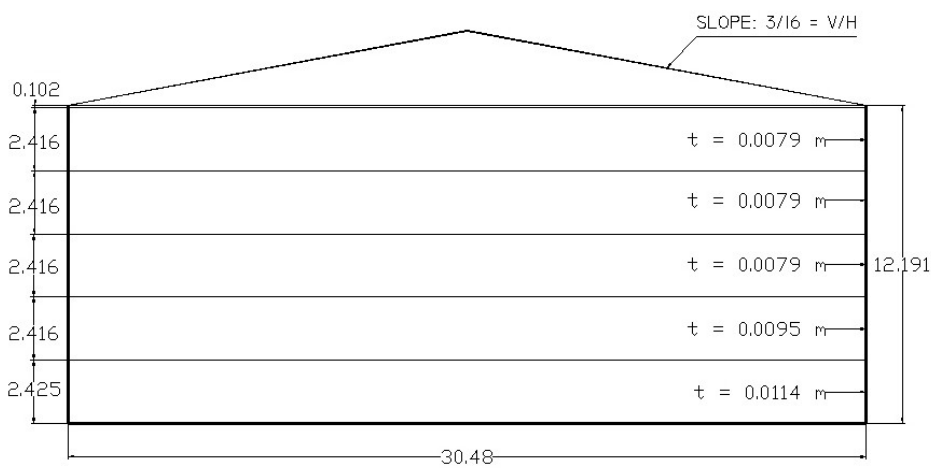

Figure 3.2. Geometry of the tank considered in the computations.

It is assumed that the settlement occurs on a small central angle of the circumference at the bottom of the tank, with a symmetric pattern and a linear variation between the point of maximum settlement and the edge of the region. Typical configurations covered a range of central angle between 6° and 150°.

The finite element computer package ABAQUS (2002) was used in this research to obtain displacements of the shell under vertical settlement. Quadrilateral shell elements with eight nodes (S8R5) were used to model the cylinder and most of the shell roof, while triangular elements (STRI65) were required for the center of the roof. Figure 3.3(b) shows the finite element mesh used for the discretization of half of the shell, with 1,500 elements for the cylindrical part and 1,200 for the roof (of which 1,140 are S8R5 elements and 60 are STRI65 elements).

Static analyses were performed under imposed displacements in the vertical direction at certain nodes in the circumference. Several settlement configurations were studied in each case, including a linear variation of the vertical displacements up to a maximum value at the center of the zone of settlement. The main parameters controlling the response are the central angle θ of the zone of settlement and the maximum amplitude of the vertical displacement. Figure 3.3(a) illustrates a scheme of the arc of applied vertical settlements and Figure 3.3(b) shows the linear variation in the amplitude.

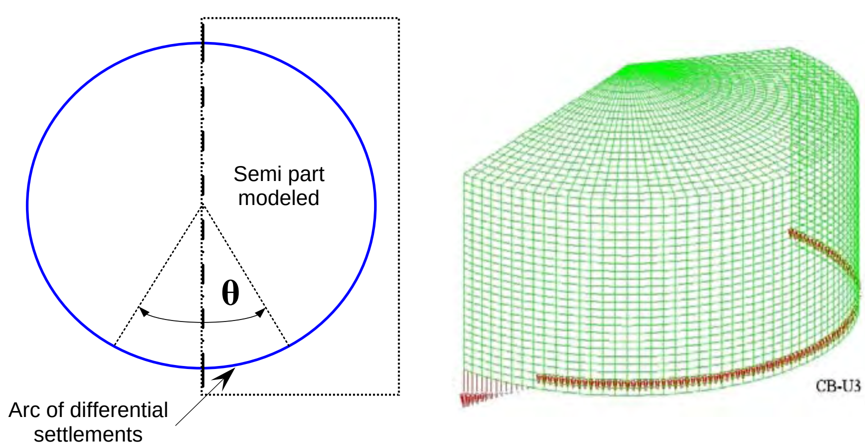

(a) (b)

Figure 3.3. (a) Scheme of central angle with support settlements. (b) Finite element mesh used for the discretization of half of the structure and configuration of imposed displacements.

3.4 RESULTS FOR THE CASE STUDIED

3.4.1 GEOMETRIC LINEAR ANALYSIS

Three types of analysis are reported in this chapter: a linear analysis, a geometrically non-linear analysis and a bifurcation buckling analysis. All models considered linear constitutive relations.

First, the structure was studied with a geometrically linear analysis. A plot of the maximum out-of-plane displacement w_{max} (normalized with respect to u_{max}) is shown in Figure 3.4 for several values of central angle of the region of settlement. This type of sensitivity analysis was performed previously by other authors (see for example Joinadi and Ansourian, 1998) for harmonic settlement, and they showed that there is a value of the arc (associated to the wave number n) from which the radial displacements reach a maximum.

The results obtained in the current study, indicate that for small central angles the shell does not notice the effect, while for large angles the influence tends to vanish, but there is a range of angles up to about 45º in which a significant distortion is computed in the shell response. The maximum in this case was computed for an angle of 15º and reached values of w_{max} / u_{max} of 12. The linear results predicted values of displacements much higher than what was observed in the experiments, and with a different pattern of deflections. Because of the large displacements computed using the linear analysis, it is expected that geometrically non-linearity plays a significant role in this problem. Notice that the trend in tanks and other shells has been to employ linear analysis for the settlement, as reviewed in Section 3.2.

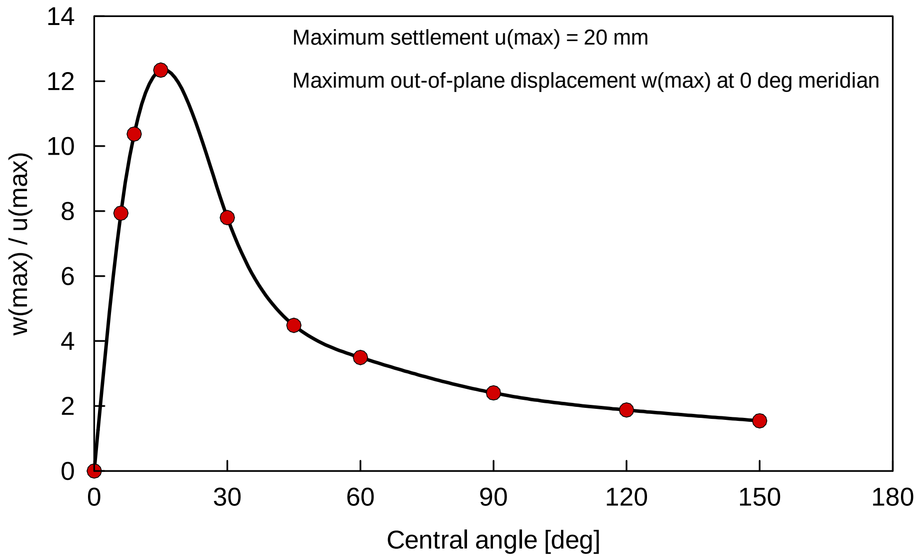

Figure 3.4. Linear results: Maximum out-of-plane displacements for different values of central angle of settlement.

For a maximum settlement u_{max}, the shell deflects with out-of-plane displacements w_{max} that are several times larger than the imposed displacements. Drawings of the pattern of linear displacements are shown in Figure 3.5 for three central angles: θ = 15°, θ = 30° and θ = 45°.

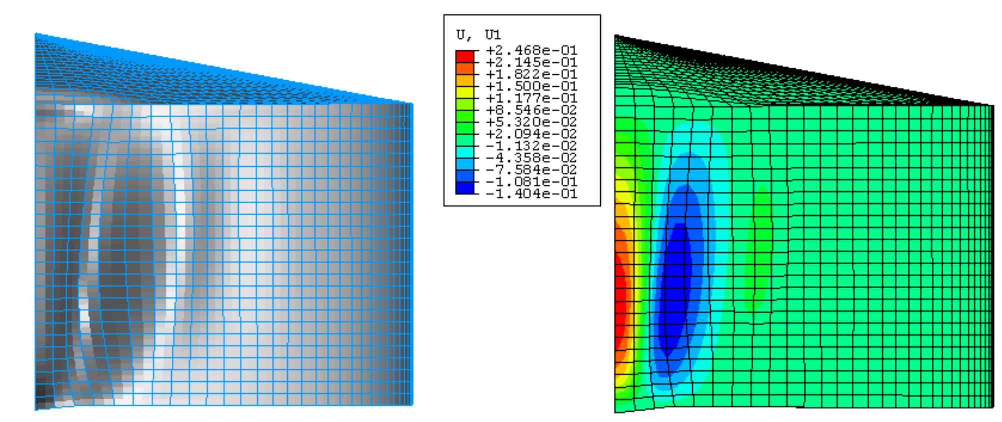

(a)

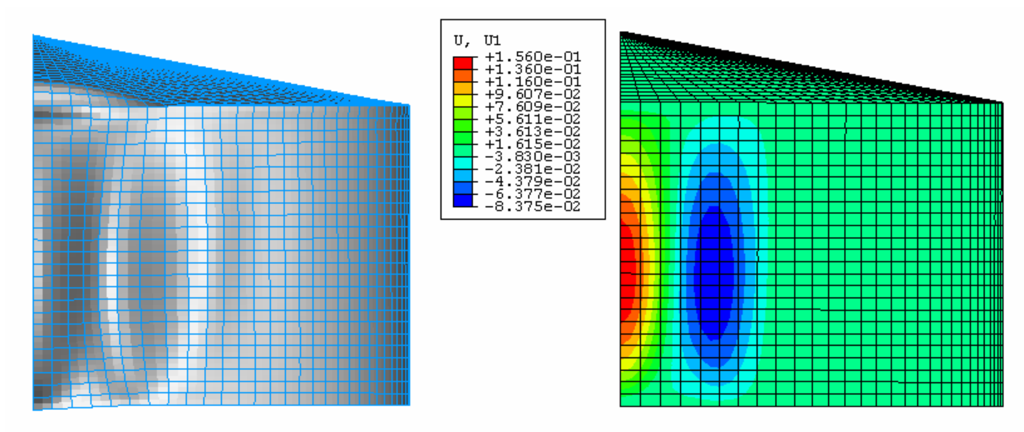

(b)

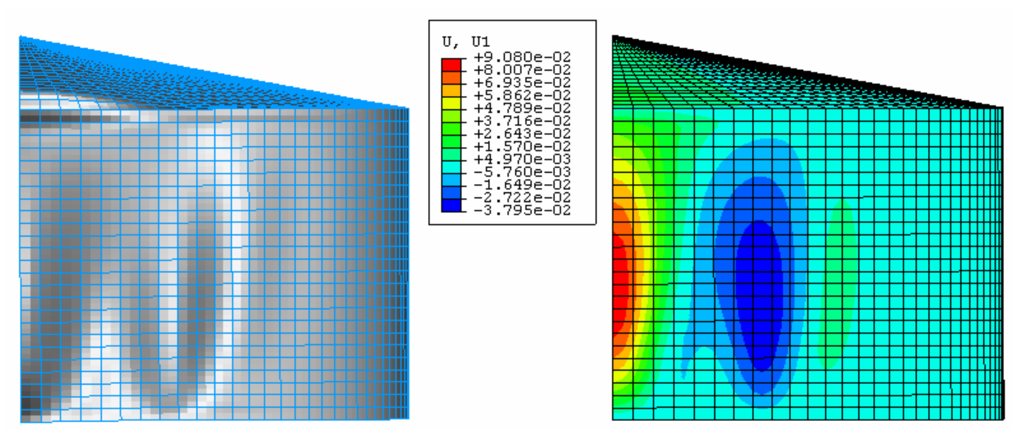

(c)

Figure 3.5. Deflected shapes and contours of out-of-plane displacements for geometrical linear results: (a) θ = 15°; (b) θ = 30° and (c) θ = 45°.

3.4.2 GEOMETRIC NON-LINEAR ANALYSIS

A geometrically non-linear analysis was carried out. Three settlement configurations were considered, with central angles of 15º, 30º and 45º. Results for a central angle of 15º, which was identified as the most critical case in the linear model, is reported first in Figure 3.6(a). For small values of u_{max}, the linear and non-linear plots are relatively close, but as the settlement reaches half the thickness of the shell (if one takes the smallest thickness as a reference value, t_3 = 7.9 mm), the out-of-plane deflections tend to increase in a plateau. This seems to be a clear sign of instability of the shell. To better understand the behavior, the settlement u_{max} is increased up to about 2.0 times the thickness (i. e. u_{max} / t_3 = 2.0), and the results of Figure 3.6(b) show a stable, stiffening path with very large deflections. For example, for u_{max} / t_3 = 2.25, the maximum out-of-plane normalized displacement is w_{max} / t_3 =35. The results show that there is a small range in which it may be reasonable to employ linear analysis, and this is for values of u_{max} / t_3 < 0.5.

The patterns of deflections of the shell are presented in Figure 3.7; this is significantly different from what may be obtained in the linear analysis and shows a V-shape with outward displacements on the meridian of symmetry and inward displacements for the meridian at the edge of the zone of settlement.

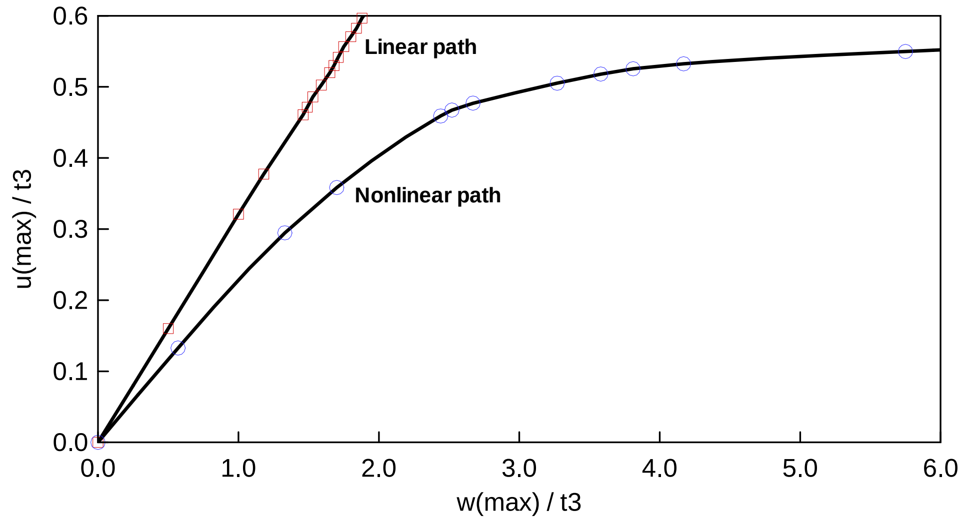

(a)

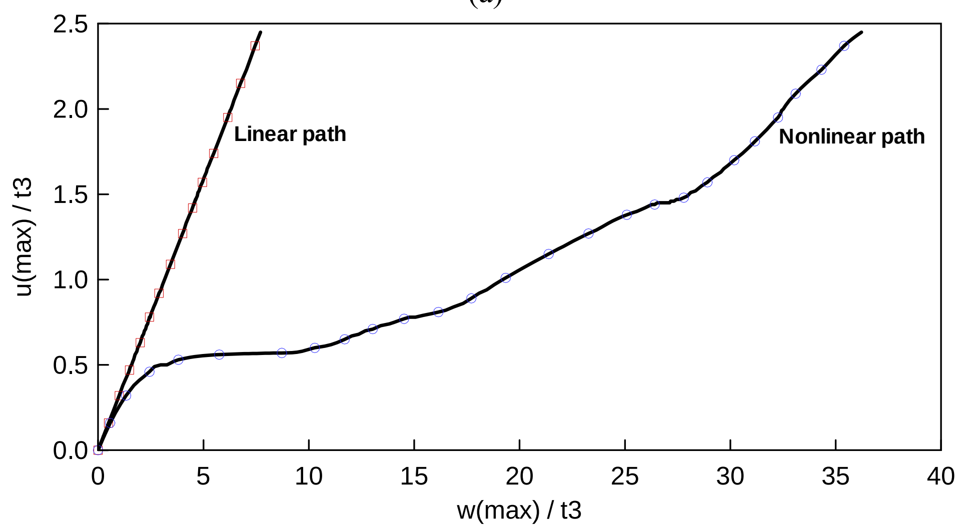

(b)

Figure 3.6. Geometrically non-linear results for central angle θ = 15º. (a) Initial part of the equilibrium path; (b) Equilibrium path up to u_{max}=20mm.

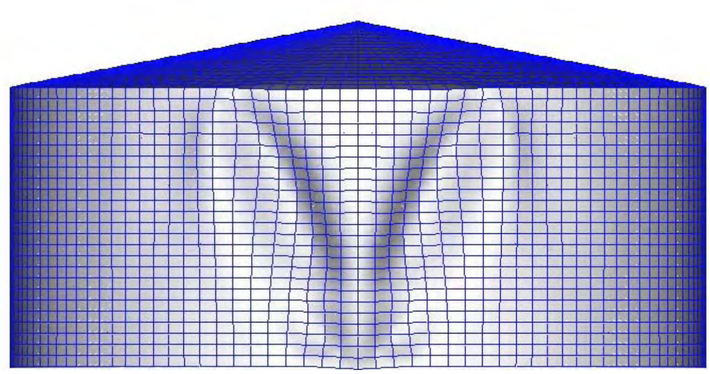

Figure 3.7. Deflection pattern of the shell for central angle θ = 15°.

Figure 3.8 shows that the behavior for a central angle of 30º is similar to the previous case, with a maximum less than 4 mm (u_{max} / $t_3 \approx 0.5$). For 45º the results are plotted in Figure 3.9. The slope in the linear response is different in each case, with a maximum for 30º and lower slopes are obtained for larger angles. However, the actual value at which the plateau is detected remains almost constant and close to the value of 4 mm (or u_{max} / $t_3 \approx 0.5$), as shown in Figure 3.9. This indicates that the high sensitivity in the response with respect to the central angle, detected in the lineal model of Figure 3.4, is not detected for the levels of settlement leading to instability.

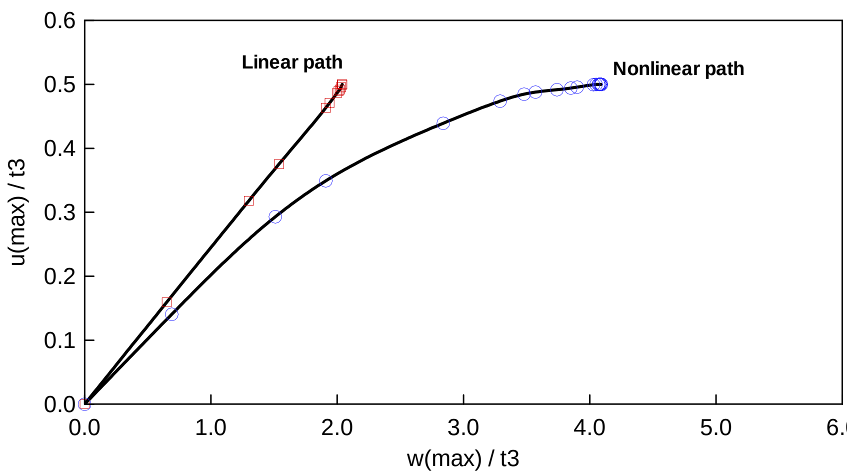

(a)

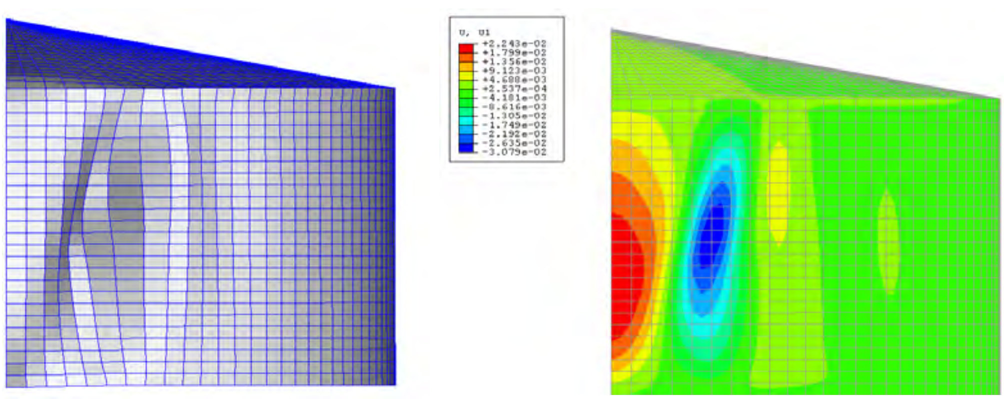

(b)

Figure 3.8. Geometrically non-linear results for central angle θ = 30º: (a) Initial part of the equilibrium path; (b) Deflection pattern of the shell for central angle 30º.

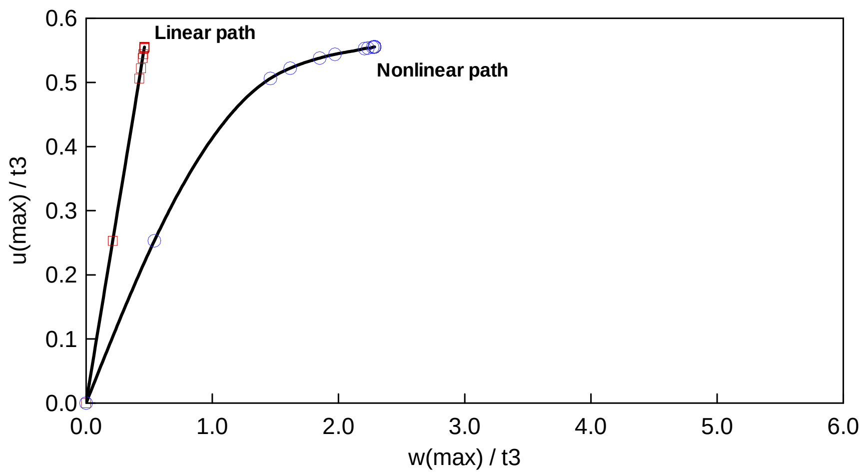

(a)

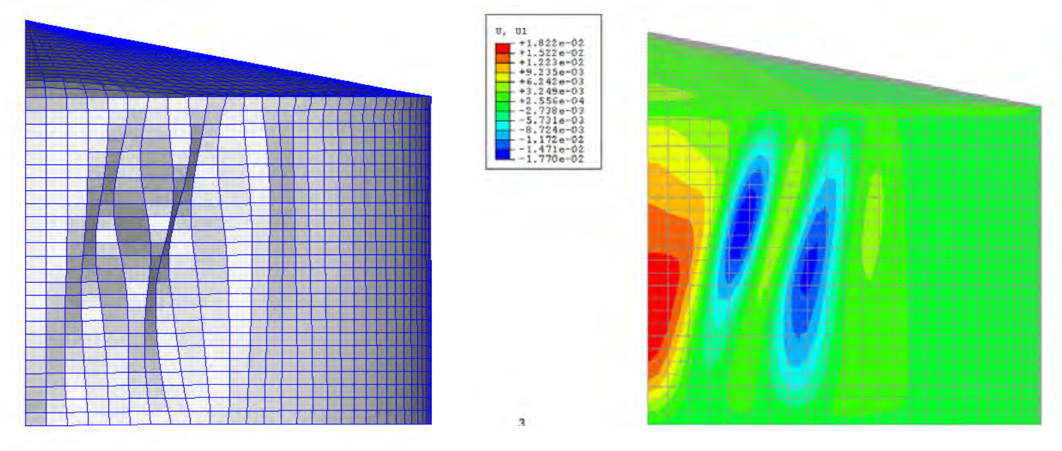

(b)

Figure 3.9. Geometrically non-linear results for central angle θ = 45º: (a) Initial part of the equilibrium path; (b) Deflection pattern of the shell for central angle 45º.

3.4.3 BIFURCATION ANALYSIS

The identification of an unstable behavior in the non-linear model indicates that a bifurcation analysis may be a good representation of the shell behavior under settlement. This bifurcation model has not been considered by other authors in the context of support settlement of shells. For the linearized fundamental equilibrium path, the control parameter is the settlement with a value of 2 mm. The bifurcation buckling was investigated by means of an eigenvalue analysis, in which the eigenvalue was the multiplier scaling the initial value of 2 mm. For the same central angles considered previously, the lowest eigenvalues are shown in Table 3.1, and the critical settlement obtained is compared in each case with the onset of instability in the non-linear analysis in Figure 3.10. The critical settlement depends on the central angle, with lower values for larger angles. The buckling modes are shown in Figure 3.11. Comparing each mode bifurcation analysis (Figure 3.11) with those obtained using non-linear analysis (Figures 3.7 to 3.9), it is seen that they have comparable deflection patterns.

Table 3.1. Lowest eigenvalues leading to bifurcation buckling under support settlements

CENTRAL ANGLE	EIGENVALUE	IMPOSED SETTLEMENT [m]	CRITICAL SETTLEMENT [m]	NON-LINEAR PLATEAU [m]
15°	4.0236	0.002	0.008047	0.004504
30°	2.5673	0.002	0.005135	0.003924
45°	2.3051	0.002	0.004610	0.004388

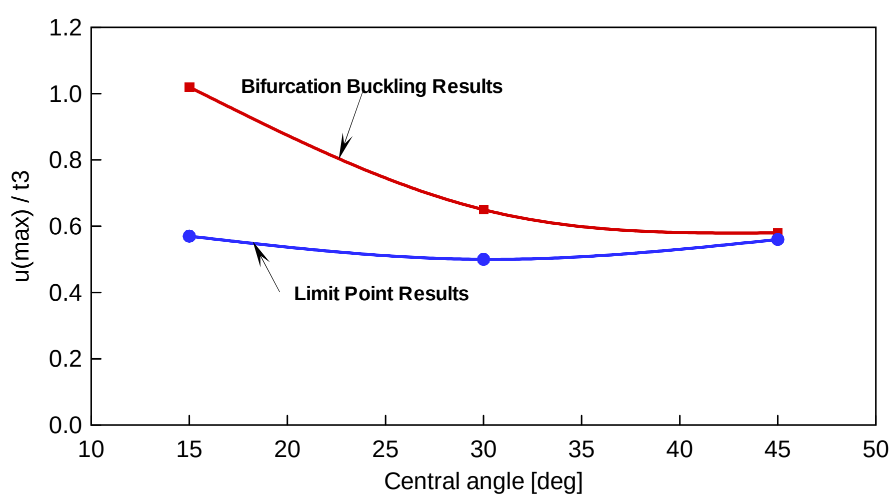

Figure 3.10. Normalized critical and non-linear settlements for different values of central angle of settlement.

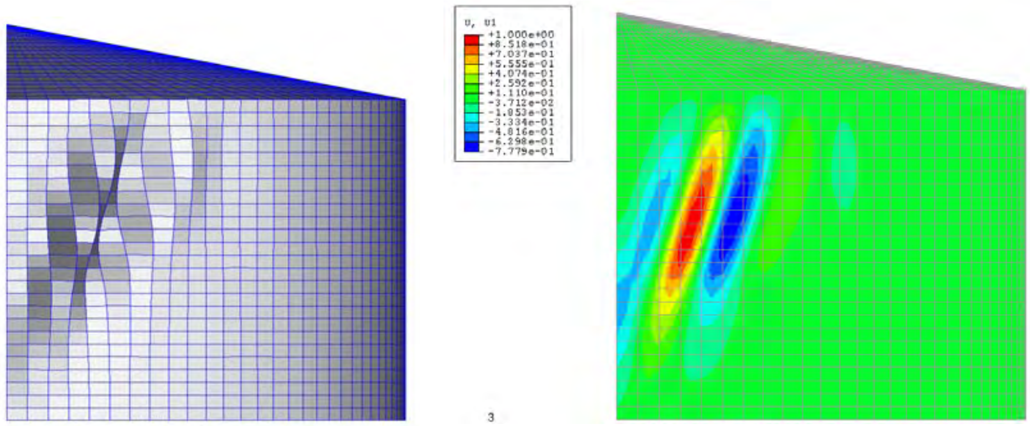

(a)

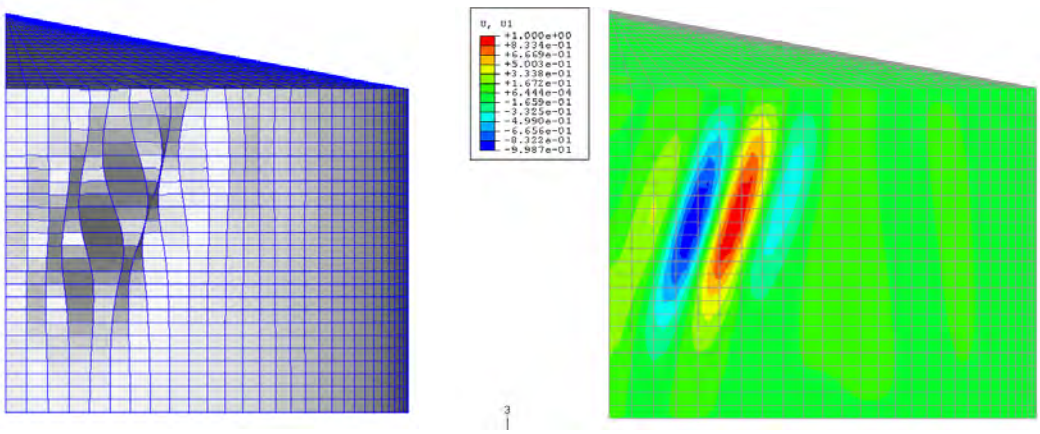

(b)

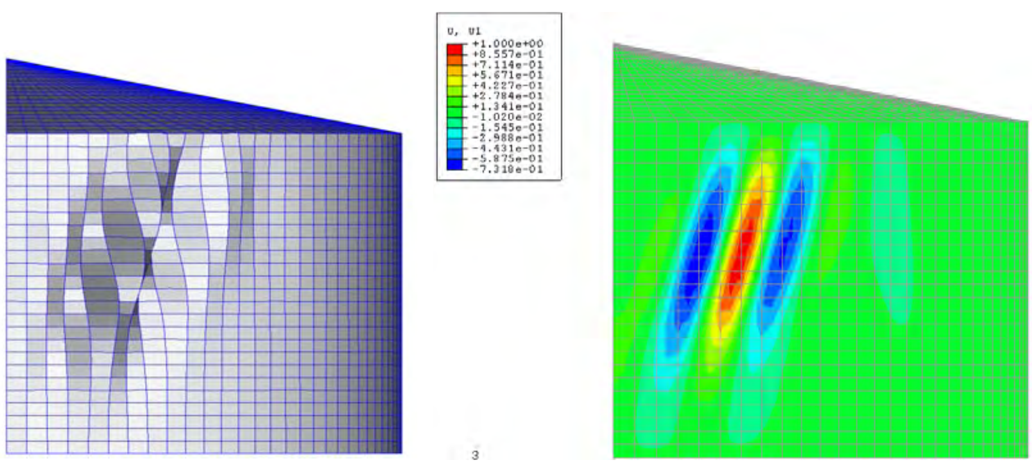

(c)

Figure 3.11. Bifurcation modes for central angle θ (a) 15º, (b) 30º, (c) 45º.

3.5 EXPERIMENTAL RESULTS ON SMALL-SCALE MODEL

A small-scale elastic model was tested to observe the main features of the behavior of the shell as the supports settle. The small-scaled tank was constructed using an acetate sheet, which was curved to form a cylinder, and a circular plate of acetate was cut to make the roof. The experiments did not use similitude theory so that only the phenomenological behavior was identified from the test. The dimensions were H = 90 mm, D = 226 mm and t = 0.2 mm, leading to ratios H/D = 0.39 and D/t = 1130. This model is about 135 times smaller than several tanks that have been constructed in Puerto Rico. Because of the difficulties in constructing a conical roof, only cases of flat roof were tested. The object of the test was to induce a vertical displacement at the base (over an arc covering 30º of the circumference) in order to measure the out-of-plane displacements of the shell and to obtain the general pattern of displacements.

The mechanical properties of the material were approximately E = 0.464 GPa and ν = 0.3. The cylinder was fixed to a rigid wooden base (with dimensions 600 × 400 × 12 mm) by means of a ring with an "L" cross section in order to maintain the circular shape of the tank at the base, but this ring was discontinued over a central angle of 30º to allow for the vertical displacements. Small holes were drilled on the cylinder at the base in the region chosen for the settlement, so as to fix a set of fine threads that were pulled down to produce the settlement. An arc of 30º was cut in the base to allow for vertical displacement of the shell. The displacements were induced by hand using the set-up shown in Figure 3.12, so that it was possible to measure the vertical displacement at each point.

Figure 3.12. Experimental set-up to induce vertical displacements at the base of the shell.

The buckled pattern of the shell is shown in Figure 3.13, for a maximum vertical displacement of u_{max} = 1 mm, or u_{max} / t = 5. A grid formed by squares with sides of 2.5 mm, was attached to the shell in order to identify the location of the points during the test. Dial gauges were used to obtain the radial displacement at different location in the shell, and photographs of the displacement pattern were obtained for different values of vertical displacements. The error in the measured radial displacement is estimated to be in the order of half of the shell thickness, i.e. ± 0.1 mm.

Results were obtained for various configurations and amplitudes of settlement patterns *u*. The pattern change as the settlement is increased, displaying a geometric non-linear behavior. The displacements shown in Figure 3.14 were obtained for u_{max} = 1 mm and are shown for two meridians, one located in coincidence with the meridian of maximum settlement, θ = 0º, and a second one for a meridian at θ = 30º. For θ = 0º, the radial displacements are positive (outward direction) with a maximum at about H/3 and with *w/u* = 1.2. Larger displacements (inward direction) are obtained for θ = 30º, with values in the order of *w/u* = 6 at an elevation of about H/2. Such large displacements are clearly outside a linear theory of shell. The pattern of displacements follow a “V” shape, with a large inward displacement along a diagonal at 45º with respect to a horizontal plane, and almost zero displacement at the top of the shell, where the roof restrains the radial deflections.

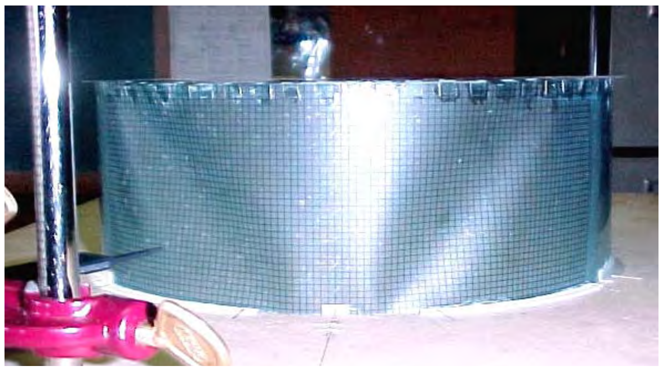

Figure 3.13. Deflected shape of the experimental model with a settlement of u_{max}=1 mm.

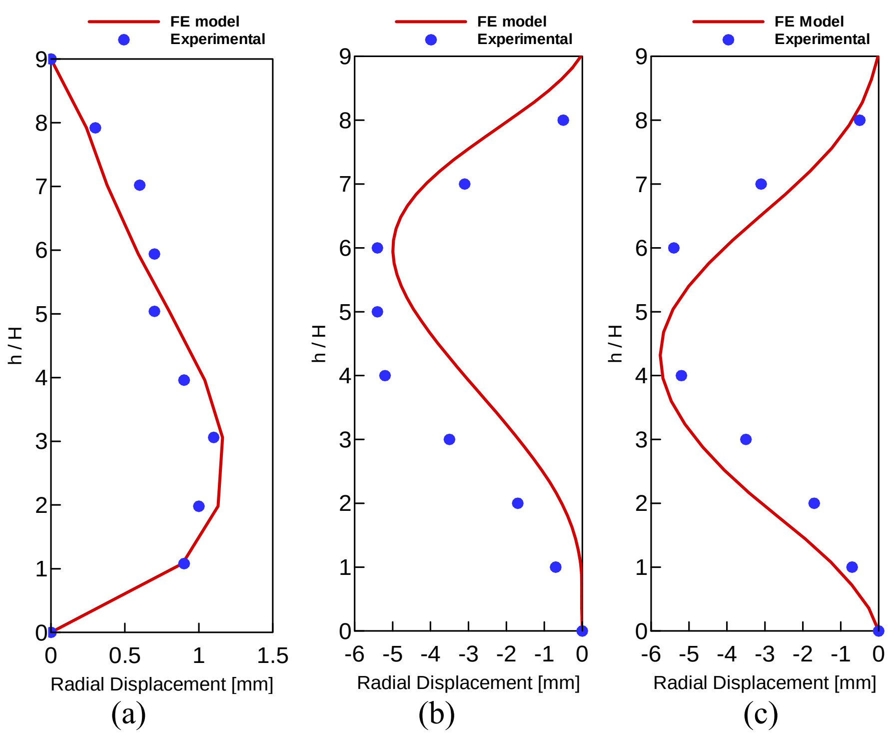

Figure 3.14. (a) Radial displacement for θ = 0°; (b) Radial displacement for θ = 30°; (c) Maximum radial displacement in FEM and experimental model (for θ = 18° and u_{max} = 1 mm).

3.6 FINITE ELEMENT MODEL OF THE SMALL-SCALE TEST

The finite element computer package ABAQUS (2002) was used to obtain the displacements of the shell under vertical settlement. To build the mesh, quadrilateral shell elements with eight nodes (S8R5) were used to model the cylinder and most of the shell roof (about 2,640 elements), while triangular elements (STRI65) were required for the center of the roof (about 60 elements). The finite element mesh used in the model is shown in Figure 3.15. Static analyses were performed under displacements in the vertical direction at certain nodes. Several settlement configurations were studied in each case, including a linear variation of the vertical displacements up to a maximum value at the center of the zone of settlement.

First, the structure was studied with geometric linear analysis, and the results predicted values of displacements much higher than what was observed in the experiments, with a different pattern of deflections. Second, a geometric non-linear analysis was carried out. For this non-linear models, plots of maximum vertical settlement (the control parameter) and the out-of-plane displacements (response parameter) are shown in Figure 3.16(a) and Figure 3.16(b) for two meridians at $\theta = 0°$ and $\theta = 18°$, respectively.

The radial displacements seems to follow the linear response up to a value of the order of the thickness of the shell, both at $\theta = 0°$ and $\theta = 18°$. But for further increases in the control parameter, the results show that the out-of-plane displacements departed significantly from the linear solution. The equilibrium path shown in Figure 3.16(b) display a non-linear behavior similar to a stable symmetric bifurcation; however, there is only one branch of equilibrium. The tangent to the path becomes almost zero for approximately $u/t = 1$, then it increases for higher values of u. The results suggest that the shell buckles for a small value of the control parameter, and then deflects into a post-buckling mode.

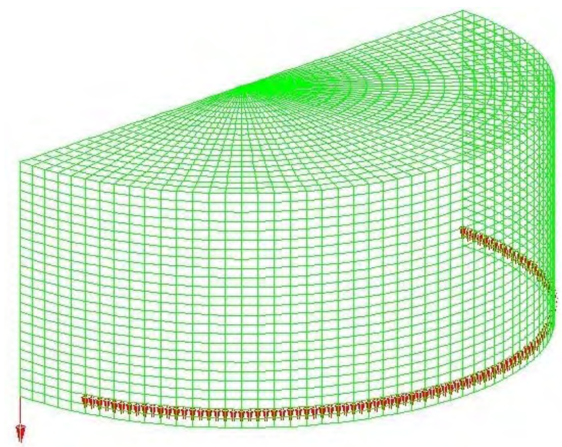

Figure 3.15. Finite element mesh for the small-scale model.

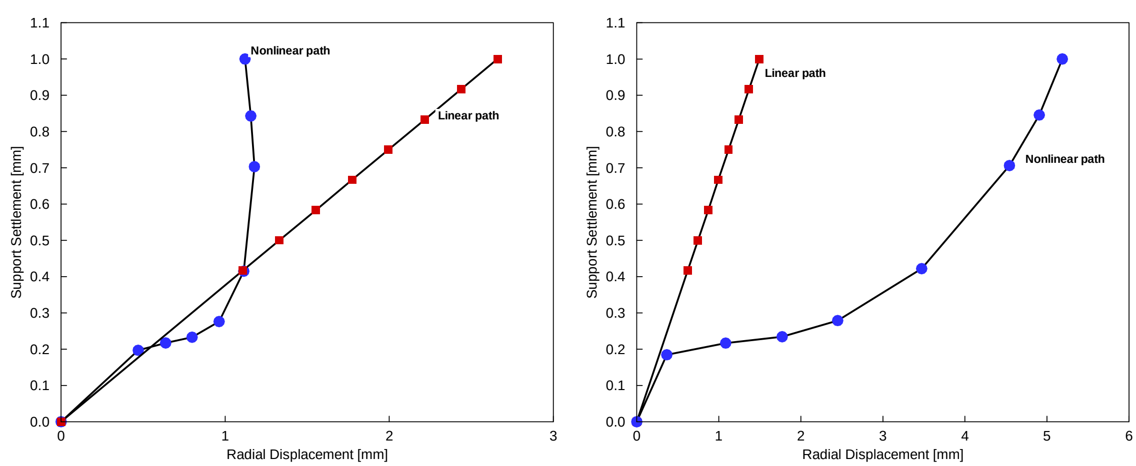

(a) (b)

Figure 3.16. Equilibrium paths at: a) θ = 0º and b) θ = 18°.

The pattern of radial displacement w is compared with experimental values in Figures 3.14(a), (b) and (c). A good agreement is found at the meridian θ = 0º, for u_{max} =

1 mm, and larger differences are found at θ = 30º. However, if one considers the profile of maximum radial displacement in both the experiment and the computation, Figure 3.14(c), then the results are in reasonable agreement.

A sequence of deflected shapes as the control parameter u_{max} is increased is shown in Figure 3.17 and the complete pattern of deflections computed using ABAQUS (2002) is shown in Figure 3.18, for u_{max} = 1 mm. The deflected shape is very similar to what was obtained in the experiments, as shown in Figure 3.13.

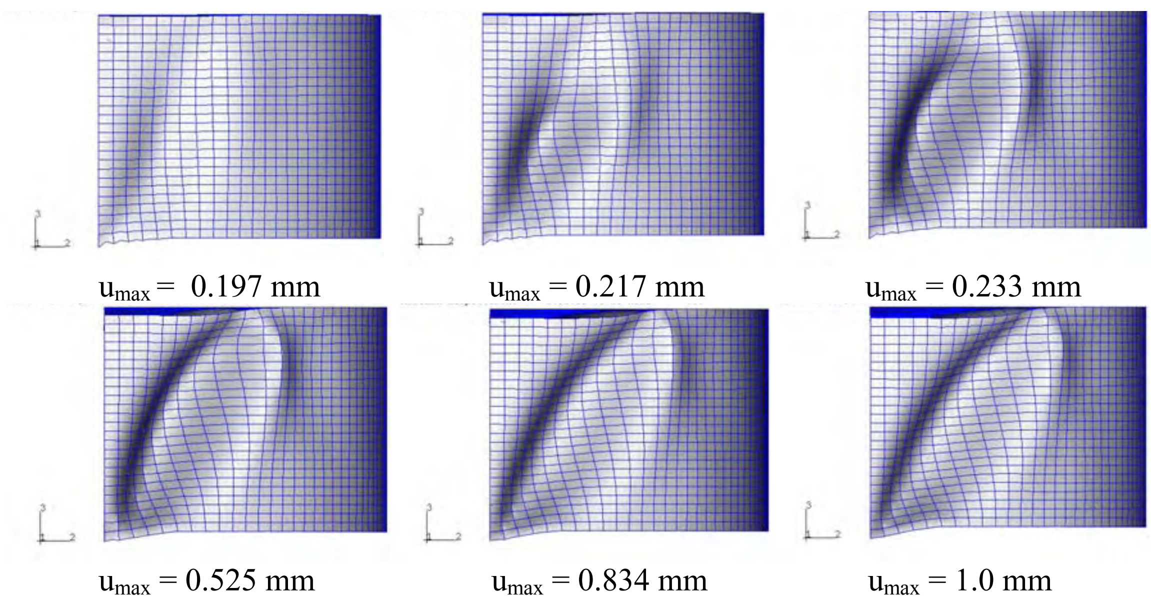

Figure 3.17. Sequence of deflected shapes.

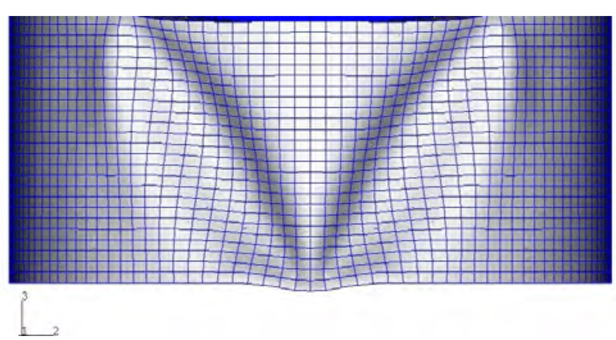

Figure 3.18. Complete deflected shape for the computational model with a settlement of u_{max} = 1 mm.

3.7 CONCLUSIONS

The computer analysis carried out in this research, as well as the tests performed on a small scale model reported in Sections 3.5 and 3.6, show that the deflection patterns in thin-walled shells due to localized settlements of the foundation are due to a highly non-linear behavior of the shell. The patterns of displacements in the shell are identified, and they are different from those found in buckling of the same shells under wind load or internal vacuum. See for example Godoy and Méndez, (2001) and Godoy, *et al*. (2002). Also, the results for one tank configuration show that the buckling displacements are almost independent of the central angle of the zone affected by settlement as depicted in Figure 3.10.

The equilibrium paths showed in Figures 3.5 to 3.8 display a non-linear behavior with a plateau, which is a clear sign of instability. The tangent to the equilibrium path becomes zero for approximately u_{max} / t_3 = 0.5 for the cone roof tank and u / t = 1 for the small-scale model, then it increases for higher values of u_{max} / t_3 or u / t.

For the small-scale model of a cylindrical tank with a flat roof as well as for the cone roof tank model, the behavior seems to be similar to a stable symmetric bifurcation, but with only one branch. The results suggest that the shell buckles for a small value of the control parameter, and then deflects into a post-buckling mode.

Based in the results obtained, notice that in the non-linear analysis it is not necessary to include imperfections. This is due to the fact that the non-linear equilibrium paths, for the cone roof model as well as for the small-scale model are stable. In other words, paths after a small linear behavior have a transition plateau in which begins a constantly raising non-linear path. In the new stable configuration, the shell can withstand further vertical displacements with an increase in the amplitude of the post-buckling mode.

Bifurcation analysis has been shown to give a reasonable approximation to the problem. A linear fundamental equilibrium path is seen to occur, before buckling develops into a new shape for the shell. Modes obtained with bifurcation analysis are in close agreement with those obtained in non-linear analyses.

Regarding the engineering importance of this effect, one has to look at the displacement amplitudes: the out-of-plane displacements computed using a geometric non-linear theory of shells are much larger than the linear values, so that it does not seem wise to establish tolerance criteria for settlements based on linear shell models. Thus, it seems that one should question the results obtained by many authors in the past, which are restricted to a linear analysis and would thus reflect unstable states along a linear fundamental path.

CHAPTER 4

COMPUTATION OF LOWER-BOUND BUCKLING LOADS USING GENERAL-PURPOSE FINITE ELEMENT CODES

4.1 INTRODUCTION

Buckling is a non-linear phenomenon, in which the structure cannot take further load with the same geometry and changes its shape in order to find alternative equilibrium positions (Godoy, 2000). The usual computational tools in the buckling of shells are eigenvalue analysis to identify bifurcation of equilibrium paths, and non-linear analysis to follow equilibrium paths up to (and beyond) a critical state. For complex problems, such as those of interest in this thesis, both types of analysis should be employed. Furthermore, the buckling behavior of shells may be sensitive to initial imperfections, which produce a drop in the critical load (Koiter, 1945). This drop may be moderate, as in laterally loaded cylinders and cylindrical panels, or severe, as in axially loaded cylinders and pressurized spherical shells.

There are alternative ways to account for imperfection-sensitivity, and one of the most interesting approaches oriented to shell design has been the lower bound theory based on a reduced-energy model of the shell (also known as reduced-stiffness model) developed by Croll and collaborators (Croll, 1975 and 1995). In the reduced energy approach it is important to identify the energy components of the shell in the classical eigenmodes, including membrane and bending components as well as load potentials. Depending on the shell and load system, some of the contributions to the second variation of the total potential energy are positive and others are negative, which means that they are stabilizing or de-stabilizing components. The main hypothesis is that stabilizing (positive) components may be lost in the shell due the presence of imperfections. Thus, the reduced energy approach uses a simplified energy version in which some stabilizing components are eliminated from the initial post critical condition. This lower bound theory has been validated extensively for many shell forms; see for example Croll and Batista, (1981), Yamada and Croll, (1989, 1993 and 1999), Croll and Ellinas, (1983) and others.

This chapter is restricted to cylindrical shells under uniform lateral pressure, for which previous studies have shown that the membrane energy contributes to the stability of the shell, and that this energy may be lost due to imperfection sensitivity, so that it is eliminated in a lower bound analysis (Batista, 1979).

In most problems investigated in the literature, an analytical solution has been implemented or else a special purpose program was written; however, a more extensive application of the approach by engineers will only be possible if general purpose finite element codes may be used without any need to develop special computer subroutines.

The motivation of this research is triggered by this need to generalize ways to implement a lower bound approach.

The outline of the chapter is as follows: A review of previous work is presented in Section 4.2. Classical and modified ways to perform buckling analysis are described in Section 4.3. The main shell elements available in ABAQUS (2002) are presented in Section 4.4. Results of the implementation of the proposed reduced energy analysis for a benchmark cylinder are presented in Section 4.5. Results for an open top cylindrical tank are presented in Section 4.6 and for a cone roof tank in Section 4.7. Finally, some conclusions are presented in Section 4.8.

4.2 LITERATURE REVIEW

Since the pioneering work of Koiter (1945), studies on the elastic stability of structures have shown that shells can be highly sensitive to even small deviations from the as-designed geometry. This imperfection sensitivity has the consequence that a bifurcation analysis of the shell, carried out with a perfect geometry, leads to higher buckling loads than a more realistic non-linear analysis of the shell with imperfections.

At the end of the sixties there was a great interest in understanding the buckling of shells due to wind loads, perhaps stimulated by the collapse of three reinforced concrete cooling towers in Ferrybridge, England, during a storm. Since that time, there had been numerous studies dedicated to calculate the critical lateral pressure in cooling towers and in other axi-symmetric structures, like the tanks described in previous chapters. Essentially, most research efforts were oriented to develop analytical and experimental models in order to reach a better understanding of the behavior of shell structures.

However, the discrepancies between experimental and analytical results motivated that researchers attempted to incorporate the physics of the problem to explain the differences in the results (Croll, 1975, 1995).

The classical bifurcation models soon were confirmed not to be accurate in predicting the critical load. In most cases, the load predicted by the bifurcation model was higher than the loads obtained experimentally, so that the eigenvalues were an upper limit and were not safe for design purposes.

Batista and Croll (1979) proposed a method based on the observation that the buckling process of shell structures is a function of the changes in the membrane resistance of the shell. If the shell has small initial imperfections, then there is interaction of modes in post-critical equilibrium states with the consequence that a fraction or all the membrane resistance used by the shell to carry the external load can be eroded in the critical state. This leads to a reduction in the buckling load. This conceptualization of the behavior is known as the “reduced stiffness” or “reduced energy” model and has been used by several authors to find what is known as a “lower limit” of the buckling loads. The reason why this was called a lower limit is because the model can predict a lower envelope of the loads obtained experimentally.

Under this concept, many analytical tests were developed since 1979 in order to validate the methodology. For example, Croll and Batista (1981) used this concept to find the lower limit in the buckling load of isotropic cylinders under axial loads. The goal of that research was to find the minimum safe load used for the design as a function of the geometric characteristics of the models grouped in only one parameter, known as the Batdorf parameter. Similarly, Croll and Ellinas (1983) studied the behavior of axially loaded orthotropic cylinders. In both studies, the analyses were based in energy formulations in which the membrane stiffness components, or their equivalent in terms of energy, were identified and eroded in the critical state to produce a drop in the buckling load. In both cases, the results obtained using this concept were in good agreement compared with non-linear analysis and with available experiments.

Zintilis and Croll (1982) investigated toroidal and hyperbolical geometries with different Gauss curvatures representatives of cooling towers under lateral pressure. The authors only considered uniform external pressure, but expected that their results should also be valid for wind pressures, which are non-uniform in the circumferential direction of the shell. They used one-dimensional shell finite elements to model just a meridian of an axial-symmetric model under an axi-symmetric load. They also analyzed the influence of different curvatures and boundary conditions, and compared the results with non-linear analysis including imperfections finding good agreement between them. In other study, the same authors (Zintilis and Croll, 1983), analyzed similar models under the combined action of axial and lateral load. Again, there was good agreement with the non-linear results.

Yamada and Croll (1989) applied the lower bound concept to cylindrical panels under uniform lateral pressure. Although the behavior of these panels is different from the behavior of a complete cylinder, the model of reduced stiffness can predict a lower limit of buckling load reasonably closer to those calculated using geometrically non-linear models with imperfections. The same authors analyzed cylinders under uniform lateral pressure (Yamada and Croll, 1993), and axially loaded cylinders (Yamada and Croll, 1999, Gavrilenko and Croll, 2001) using a Ritz approximation to compute non-linear paths. The minimum levels of loads obtained were quite similar to those found with the reduced energy concept. From the different cases analyzed by Yamada and Croll, it is possible to conclude that the reduced energy or reduced stiffness methods derived from the classical buckling theory provide a simple and safe tool to find the design elastic buckling load. Additionally, the comparison between the results obtained from the modified classical analysis and the non-linear results, allows one to reach a better understanding of the phenomenon than considering each one separately.

Pandey and Sherbourne (1991) used the concept of reduced energy in cylinders constructed with composite materials. Specifically, they analyzed axially loaded cylinders formed by laminated shells modeled using the classic laminate theory. The reduced energy concept was introduced, and the computations could be performed without the need of sophisticated analytical tools.

The concept of reduced energy or reduced stiffness is nowadays acknowledged as a useful tool to determine lower bound buckling loads. This concept has been validated several shell forms under typical loads, and the results were confirmed using non-linear analysis and experimental tests. However, up to now there are no reports of using this method with conventional computational tools, like general-purpose finite element programs. This is a limitation for the analyst, because the development of non-linear models requires advanced technical skills and additional resources, not always necessary or available at the preliminary stages of the design.

4.3 BUCKLING ANALYSIS

4.3.1 CLASSICAL BIFURCATION ANALYSIS

Let us consider the steps in a bifurcation analysis using a general purpose finite element code. First, the fundamental equilibrium path is computed using linear geometric behavior, in the form:

$$\mathbf{K}\ \mathbf{a}^{F} + \lambda\ \mathbf{P} = 0 \tag{4.1}$$

where $\mathbf{K}$ is the linear stiffness matrix of the shell, which can be written as the sum of two contributions from membrane $\mathbf{K}^{m}$ and bending $\mathbf{K}^{b}$ mechanisms in the shell:

$$\mathbf{K} = \mathbf{K}^{m} + \mathbf{K}^{b} \tag{4.2}$$

The solution $\mathbf{a}^{F}$ is the displacement response along the fundamental equilibrium path, for a load system defined by a load vector $\mathbf{P}$ and scaled by a load parameter λ. We take here $\lambda = 1$ for the fundamental state. This value of $\mathbf{a}^{F}$ is then used to compute the initial membrane stress resultants in the shell along the fundamental path, denoted as $\mathbf{N}^{F}$.

The initial stresses are used in the second step to construct the initial stress or geometric matrix at an element level, given by (Brush and Almorth, 1975):

$$\mathbf{k}^{G} = \int \beta^{T}\ \mathbf{N}^{F}\ \beta\ dA \tag{4.3}$$

where β is the vector of rotations. Finally, the following eigenvalue problem is solved:

$$[\mathbf{K} - \lambda^{C}\ \mathbf{K}^{G}(\mathbf{N}^{F})]\Phi = 0 \tag{4.4}$$

where the initial-stress or geometric matrix $\mathbf{K}^{G}$ is assembled from element contributions containing the initial stresses and rotations (equation 4.3). The scalar parameter λ^{C} is the eigenvalue (the critical load of the problem) and vector Φ is the eigenvector (the critical mode or deflected shape associated to λ^C).

4.3.2 REDUCED STIFFNESS ANALYSIS

The three main postulates of the lower bound approach to elastic buckling of imperfection-sensitive shells under lateral loads have been summarized by Croll (1995) as:

(a) The non-linear geometric behavior of the shells is associated to changes in the membrane energy and membrane resistance.

(b) For a shell to exhibit imperfection-sensitivity, it must have a membrane contribution to the energy in the initial post-buckling behavior.

(c) This membrane energy may be eroded due the presence of imperfections and leads to a lower buckling load. Thus, the reduced energy approach uses an eigenvalue analysis but eliminates the membrane contribution to the eigenproblem.

To account for the reduced contribution of membrane stiffness in the initial post buckling behavior, the same linear problem in equation 4.1 should be solved, but changes need to be introduced in the eigenproblem of equation 4.4. The second term in equation 4.4 remains the same, but considering equation 4.2, the problem is here written in the form:

$$[(\frac{1}{\alpha}\mathbf{K}^{m}+\mathbf{K}^{b})-\lambda'\mathbf{K}^{G}(\mathbf{N}^{F})]\Phi'=0 \tag{4.5}$$

Here α is the reduction factor applied to the membrane stiffness $\mathbf{K}^m$ (dimensionless value > 1), λ' and Φ' are the new eigenvalue and eigenvector of the reduced stiffness system. In order to have a more systematic control of the numerical process, the membrane stiffness in equation 4.5 has not been initially eliminated, but notice that α should be a large number. As $\alpha \to \infty$, then the contribution of $\mathbf{K}^m$ tends to zero and the lower bound, characterized by λ^* and Φ^*, is obtained:

$$[\mathbf{K}^b - \lambda^* \mathbf{K}^G(\mathbf{N}^F)]\Phi^* = 0 \qquad (4.6)$$

Figure 4.1 illustrates the process along the fundamental equilibrium path $\mathcal{P}_1$, in which the shell is assumed to respond with its complete stiffness and leads to λ^C in equation 4.4. For the reduced stiffness, a lower value λ' is obtained, and in the limit for $\alpha \to \infty$ then $\alpha \to \lambda^*$.

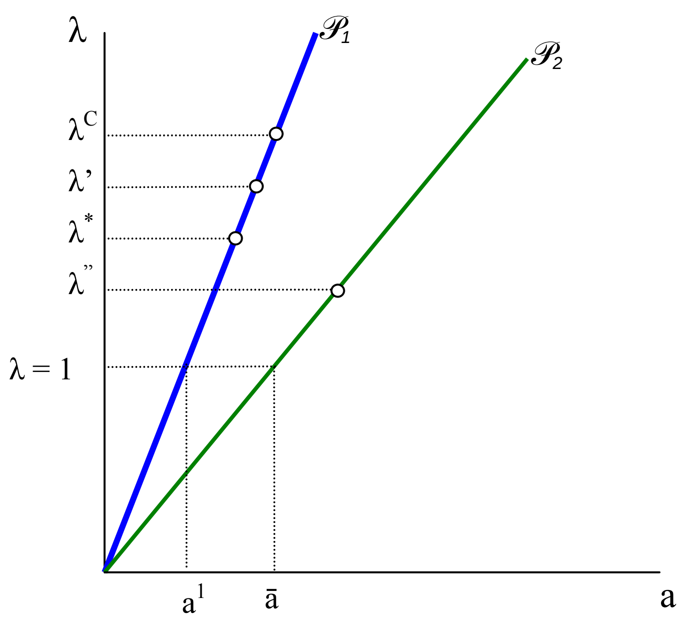

Figure 4.1. Critical load for different load paths.

Notice that if the eigenvalue problem was solved with the reduced membrane stiffness since the beginning (equations 4.1 and 4.4), then an eigenvalue λ" along another path $\mathcal{P}_2$ would be obtained, and this would be an unjustified conservative estimate. Thus, one needs to separate both steps in the analysis and compute each one with different values of $\mathbf{K}^m$.

4.3.3 REDUCED ENERGY ANALYSIS

An alternative computation of the lower bound is to use a knock-down factor η (Croll, 1995) in which:

$$\lambda^* = \eta\,\lambda^C \quad \text{and} \quad \eta = \frac{U^{2b}}{U^{2b} + U^{2m}} \tag{4.7}$$

Here, U^{2b} is the bending strain energy in the critical mode and U^{2m} is the membrane strain energy. To show the equivalence between the reduced stiffness and reduced energy approaches, we may compute the energy in the form:

$$\Phi^T[(\mathbf{K}^m + \mathbf{K}^b) - \lambda^C\,\mathbf{K}^G(\mathbf{N}^F)]\Phi = 0 \tag{4.8}$$

for the classical eigenproblem. For the reduced energy, we writes:

$$\Phi'^T[(\frac{1}{\alpha}\mathbf{K}^m + \mathbf{K}^b) - \lambda'\mathbf{K}^G(\mathbf{N}^F)]\Phi' = 0 \tag{4.9}$$

In the limit, as $\alpha \to \infty$, we get:

$$\Phi^{*T}[\mathbf{K}^b - \lambda^*\mathbf{K}^G(\mathbf{N}^F)]\Phi^* = 0 \tag{4.10}$$

Equations 4.8 and 4.10 may be written as:

$$\Phi^T[(\mathbf{K}^m + \mathbf{K}^b)]\Phi = \lambda^C \Phi^T[\mathbf{K}^G(\mathbf{N}^F)]\Phi \tag{4.11}$$

$$\Phi^{*T}[\mathbf{K}^b]\Phi^* = \lambda^* \Phi^{*T}[\mathbf{K}^G(\mathbf{N}^F)]\Phi^* \tag{4.12}$$

For cases in which the eigenmodes are almost the same as the buckling mode found in experiments or in a geometrically non-linear analysis, then we can assume that $\Phi^* = \Phi$. If $\alpha \rightarrow \infty$, then $\mathbf{K}^m$ vanishes. Dividing equations 4.12 by 4.11 we get:

$$\frac{\Phi^{*T}[\mathbf{K}^b]\Phi^*}{\Phi^T[\mathbf{K}^m + \mathbf{K}^b]\Phi} = \frac{\lambda^*}{\lambda^C} = \eta \tag{4.13}$$

where:

$$U^{2m} = \Phi^T \mathbf{K}^m \Phi \tag{4.14}$$

$$U^{2b} = \Phi^T \mathbf{K}^b \Phi \tag{4.15}$$

Clearly, equation 4.13 is the same as equation 4.7.

4.3.4 PROPOSED METHODOLOGY FOR LOWER BOUND ANALYSIS

The implementation of this procedure can be done as follows: First, the classical eigenvalue problem is solved using the complete equation 4.4, in order to obtain the classical eigenmode Φ and λ^C. Second, the eigenmode Φ is used as an initial displacement field, instead of the external load defined in equation 4.1, and the strain energy is computed as:

$$\Phi^T[(\mathbf{K}^m + \mathbf{K}^b)]\Phi = U^{2m} + U^{2b} \tag{4.16}$$

This is the complete energy mobilized by the shell in displacing to the shape of the eigenmode Φ. Third, the eigenmode Φ is used as an initial displacement in equation 4.16, but with the reduction factor α affecting the membrane stiffness:

$$\Phi^{T}[(\frac{1}{\alpha}\mathbf{K}^{m}+\mathbf{K}^{b})]\Phi=\frac{1}{\alpha}U^{2m}+U^{2b} \tag{4.17}$$

As α increase, the membrane contribution tends to vanish and the remaining bending contribution is used to compute the knock-down factor with equation 4.7. One may tray several increasing values of α in equation 4.17 until the knock-down factor computed with equation 4.7 converge to a constant value, which is used to find the reduced critical load.

Notice that these indirect computations are necessary because all general purpose programs, such as ABAQUS (2002), do not allow for separate computations of membrane and bending energies.

4.4 SHELL ELEMENTS AVAILABLE IN ABAQUS

A key feature in the reduced energy approach is that it needs to model a structural type which is not quite a shell with its complete energy, but deals with an equivalent shell in which part of the energy is only lost at the initial post-buckling state. A finite element model of this approach is a difficult test for any finite element code because it takes the shell well outside the conditions for which it was formulated, and considers a deflected shape that would not be present in the linear analysis. In this research, we employ ABAQUS (2002) to model the proposed approach using the shell elements available in the program. A brief description of the shell elements in ABAQUS (2002) is presented next.

ABAQUS/Standard identifies shell elements using the following nomenclature: S indicates shell element; TRI indicates triangular element; 3 o 4 indicate the number of nodes per element; R after the number of nodes indicates reduced integration; and 6 or 5 indicate the degrees of freedom per node available in the element. The program has a library of shell elements divided in three main categories: general-purpose elements, thin and thick elements. We are here interested only in three dimensional general-purpose and thin elements. From those, general-purpose elements include elements S3, S4, S3R, and S4R. All of them include transverse shear deformation. They use thick shell theory as the shell thickness increases and become discrete Kirchhoff thin shell elements as the thickness decreases. The transverse shear deformation becomes very small as the shell thickness decreases.

Thin shell elements are identified as: S4R5, S8R5, S9R5, STRI3 and STRI65. These elements are in turn classified as those that solve thin shell theory (the Kirchhoff constraint is satisfied analytically), such as the STRI3 element; and those that should converge to thin shell theory as the thickness decreases (the Kirchhoff constraint are satisfied numerically), such as elements S4R5, STRI65, S8R5, and S9R5.

For our analysis, it is convenient to separate quadratic elements (S8R5, S9R5 and STRI65) from linear elements (S3, S3R, STRI3, S4, S4R and S4R5). All those shell elements use bending strain measures that are approximations to the Koiter-Sanders shell theory (Budiansky and Sanders, 1963).

4.5 RESULTS FOR A CYLINDRICAL SHELL SIMPLY SUPPORTED AT THE ENDS UNDER UNIFORM PRESSURE

To illustrate the computational procedure proposed in Section 4.3.4, a case similar to one solved by Batista and Croll (1979) and Yamada and Croll (1999) has been considered in this section. This is a cylindrical shell with radius R = 100 mm, height H = 200 mm, and thickness t = 0.247 mm, thus having R/t = 405 and R/L = 0.5. The Batdorf parameter given by:

$$Z = \frac{H^2}{R\,t}\sqrt{(1-\nu^2)} \tag{4.18}$$

For this shell, Z = 1545. The boundaries conditions at the ends are: radial displacements restrained allowing only axial displacements. The load is a uniform external pressure with unit amplitude.

4.5.1 ANALYTICAL RESULTS

To validate the computational results, an analytical solution was obtained as in Batista and Croll (1979), but using a reduction factor α on the membrane energy contribution to the eigenproblem, rather than eliminating it at once. The results are shown in Figure 4.2. From the results, it may be seen that the solution becomes independent of α for a value of α = 100. The energy contributions for each mode considered in the reduced energy analysis and for several values of α, are shown in Figure 4.3. As α increases, the total energy shows a minimum until it gets close to the curve of bending energy;

however, such minimum has no interest. Following Croll (1995), the analysis here assumes that the eigenmode in the classical analysis with the full energy Φ is the same as the mode Φ^* associated to the lower bound λ^*.

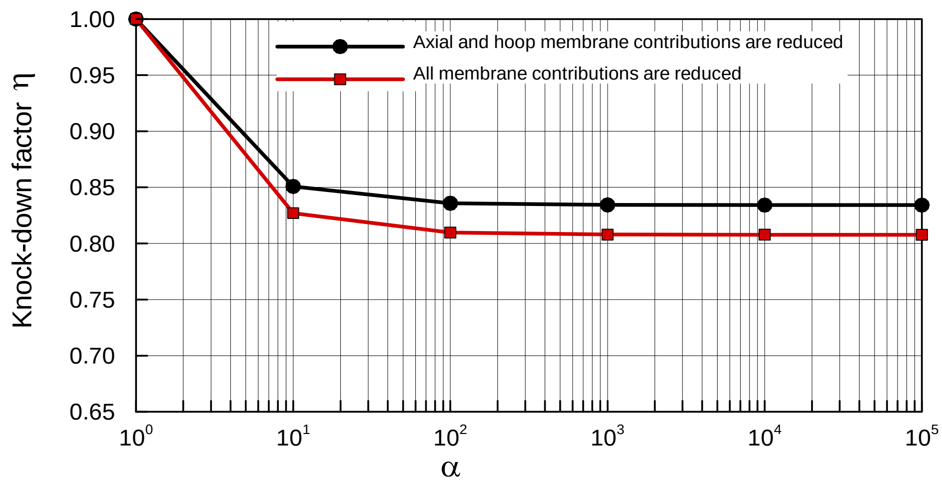

Figure 4.2. Analytical results for a cylindrical shell under uniform pressure.

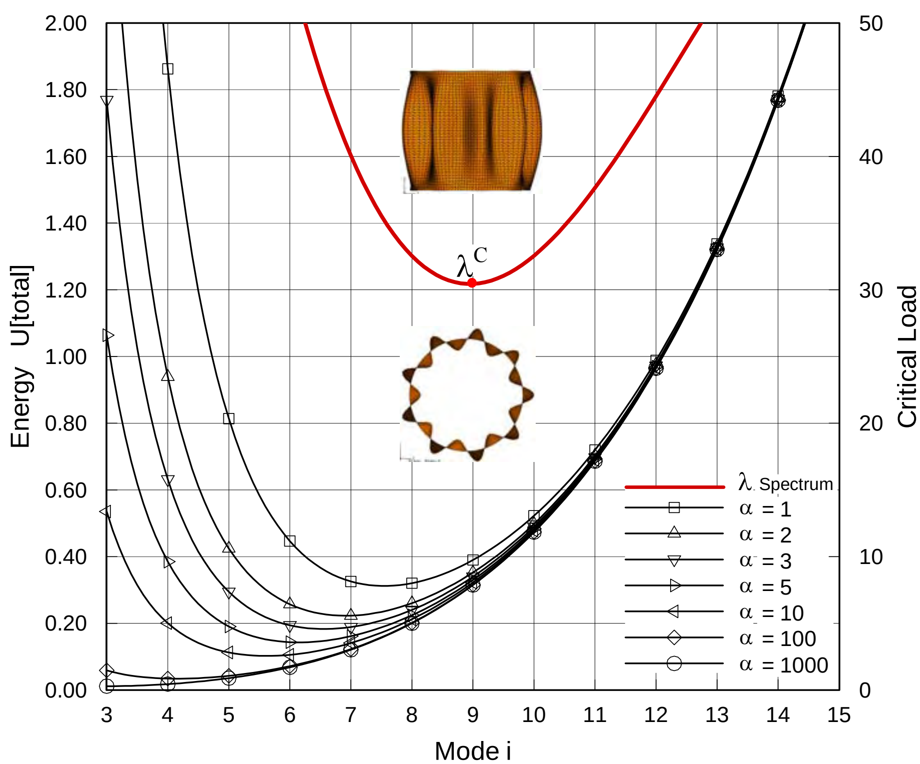

Figure 4.3. Energy spectrum $U_{[Total]} = U^{2m} + U^{2b}$ for different values of α

4.5.2 COMPUTATIONAL RESULTS

Our main interest here is to obtain the knock-down factor η shown in Figure 4.2 using ABAQUS/Standard (ABAQUS, 2002). The first part of the analysis is the classical eigenproblem to compute the buckling mode Φ and λ^C. Next, a linear static analysis is carried out using the eigenmode Φ as a prescribed displacement field, in order to compute the strain energy. This second part is carried out with a discretization of the shell as a composite laminate.

The constitutive matrix for each element is given by:

$$\begin{Bmatrix} \mathbf{N} \\ \mathbf{M} \end{Bmatrix} = \begin{bmatrix} \mathbf{A} & \mathbf{B} \\ \mathbf{B}^T & \mathbf{D} \end{bmatrix} \begin{Bmatrix} \boldsymbol{\varepsilon} \\ \boldsymbol{\kappa} \end{Bmatrix} \tag{4.19}$$

where **A** is a 3×3 membrane sub-matrix given by:

$$\mathbf{A} = \begin{bmatrix} A_{11} & A_{12} & 0 \\ A_{21} & A_{22} & 0 \\ 0 & 0 & A_{33} \end{bmatrix} \tag{4.20}$$

and **D** is the 3×3 bending sub-matrix given by:

$$\mathbf{D} = \begin{bmatrix} D_{11} & D_{12} & 0 \\ D_{21} & D_{22} & 0 \\ 0 & 0 & D_{33} \end{bmatrix} \tag{4.21}$$

B is the bending-extension coupling matrix, which is a null matrix for symmetric laminates, as assumed in the present case. Just one orthotropic lamina is employed in the analysis. A detailed description of the properties of the orthotropic single lamina used here is presented in Appendix A. The membrane reduction is applied in the form:

$$\mathbf{A}' = \frac{1}{\alpha}\mathbf{A} \tag{4.22}$$

where all the coefficients in **A** are affected by α. Computation of the energy in the eigenmode, with $\alpha = 1$, leads to ($U^{2m} + U^{2b}$), while for $\alpha > 1$, we get ($U^{2m} / \alpha + U^{2b}$).

The finite element mesh employed in the eigenvalue analyses use different available quadrilateral and triangular elements in order to analyze the behavior of the proposed procedure as the type of element and mesh density change. Convergence studies show that the solution tends to the theoretical eigenvalue with a mesh of 128×40 = 5120 quadrilateral elements and 128×40×2 = 10240 triangular elements. Appendix B contains detailed information on the input files used in the proposed reduced energy approach.

The results in terms of knock-down factors η are shown in Figure 4.4 for different values of α. Two families of curves are initially obtained, say for $\alpha < 100$, linear elements initially converge to $\eta = 0.668$, while quadratic elements converge to $\eta = 0.809$. But for $\alpha > 500$, a decreasing trend is observed and the results are not independent of α (as in the analytical solution). This shows that the convergence to the correct solution is not attained with most elements as α increase. The only exception in Figure 4.4 is the result for the triangular element STRI3 (a fully integrated and linear element), which follows the quadratic elements up to $\alpha = 100$ and then continues with the same value of η even for very large values of α. The conclusion at this point is that the only element that passes the test is the three-node faceted triangle based in the formulation originally developed by Batoz *et al.* (1980).

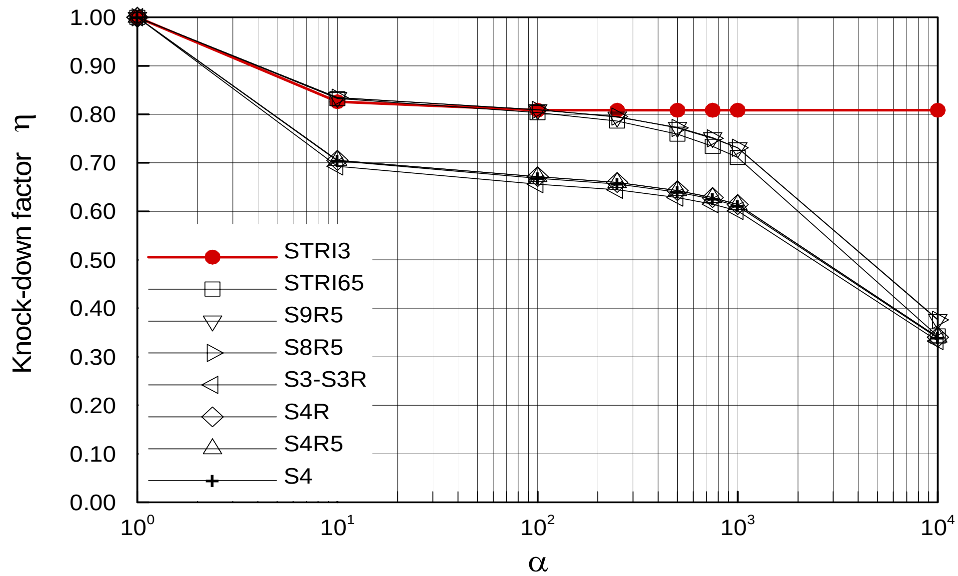

Figure 4.4. Variation of η for different shell elements.

Figure 4.5 compares analytical and numerical results obtained with STRI3. For the analytical model, with all the membrane contributions reduced, the knock-down factor tends to $\eta = 0.808$; while the computational model with the same reduction in the membrane contributions, the knock-down tends to $\eta = 0.803$. The difference between both models is less than 1%.

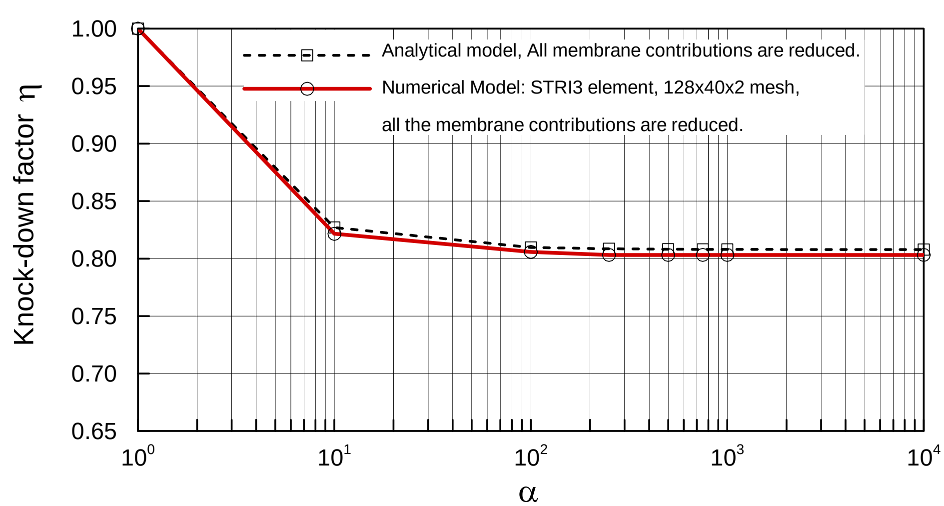

Figure 4.5. Comparison of η for analytical and numerical model.

The reasons why all elements diverge from the correct solution may be associated to membrane locking of the elements, but the full description of this effect is outside the scope of this research. A key difference between the successful element STRI3 and all the others is the Discrete Kirchhoff Constraint. In element STRI3 this is imposed analytically, while in the other elements it is imposed numerically. Similar problems were encountered using equivalent elements available in SAP2000 (Computer and Structures, 2002).

4.6 RESULTS FOR A CYLINDRICAL TANK CLAMPED AT THE BASE AND FREE AT THE TOP UNDER UNIFORM PRESSURE

As a second case of analysis, an open top cylindrical tank was considered. This type of tank is typically found in the Caribbean islands (Portela and Godoy, 2005) and the specific structure investigated has a diameter D = 30.48 m, height H_T = 13.10 m (H_T/D = 0.43), and variable thickness as indicated in Figure 4.6. The model is considered as opened at the top and clamped at the base. The entire cylinder is subjected to uniform pressure. The material of the cylinder is steel, with an elastic modulus E = 206 GPa and a Poisson ratio ν = 0.3.

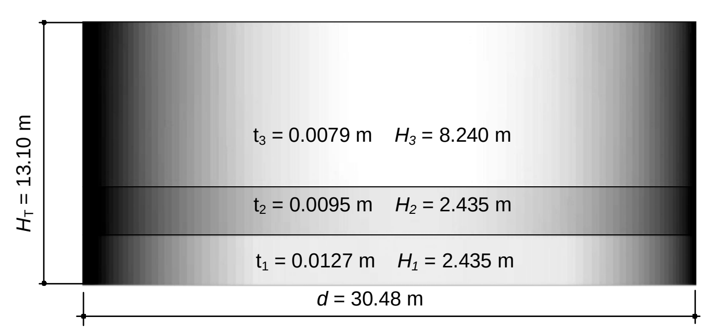

Figure 4.6. Geometric properties of the open tank.

At the present, there is no analytical solution to calculate the knock-down factor for this class of very short cantilever shell. Non-linear analyses including imperfections were performed to validate the results obtained with the proposed approach of eliminating the membrane resistance using α. The finite element mesh used in this case was constructed with STRI3 elements with a high mesh density (26,880 elements) required to achieve convergence in the classical critical load.

Figure 4.7(a) shows the deflected first eigenmode and Figure 4.7(b) shows the expanded modes at the top of the tank for the first eigenmode, the non-linear mode corresponding to the maximum load found by means of a geometrically non-linear analysis using ABAQUS (2002) and the mode for an advanced deflected shape for which the post-critical loads reach a minimum. Although there is a slight difference in the normalized amplitude, the number and distribution of waves are similar for the modes calculated from the eigenvalue analysis and from the geometrically non-linear analysis including imperfections. Thus, the assumption of similarity of the modes in the pre-critical and post-critical states ($\Phi = \Phi^*$) for the proposed approach is fully justified.

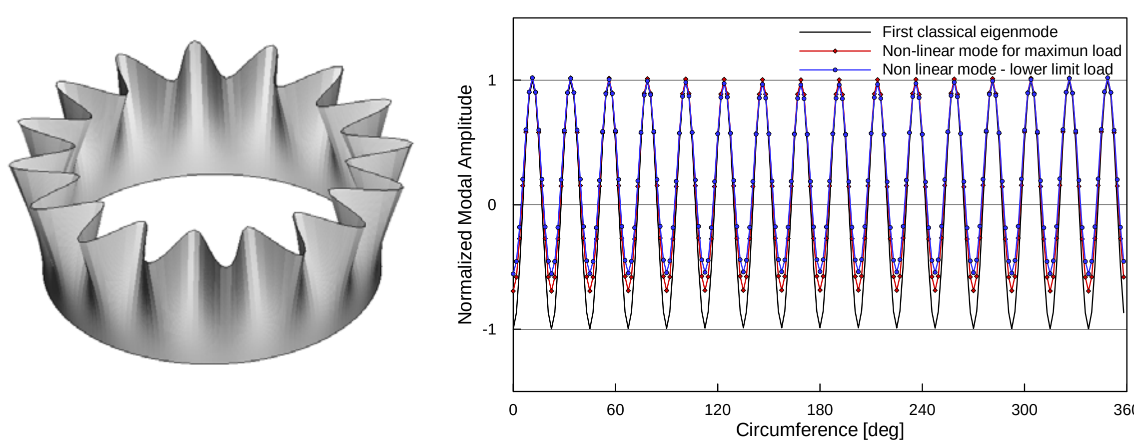

(a) (b)

Figure 4.7. (a) Deflected shape from classical eigenvalue analysis; (b) Expanded modes at the top of the open tank model.

The knock-down factors η for this case are shown in Figure 4.8 for different values of α. For α > 100 the solution converges to a constant value η = 0.77. Figure 4.9(a) shows equilibrium paths computed for different amplitudes of imperfections. For those analyses, the imperfection was generated by adding to the initial geometry of the tank, the first eigenmode calculated in the classical eigenvalue analysis scaled by the factor ξ to represent the amplitude of the imperfection in terms of the minimum thickness of the tank. The imperfection analysis shows that the critical load tends to decrease to a constant value of approximately λ = 0.76 as the imperfection amplitudes increase. Thus, there is good agreement between the non-linear and lower bound analyses, with differences in the order of 1%.

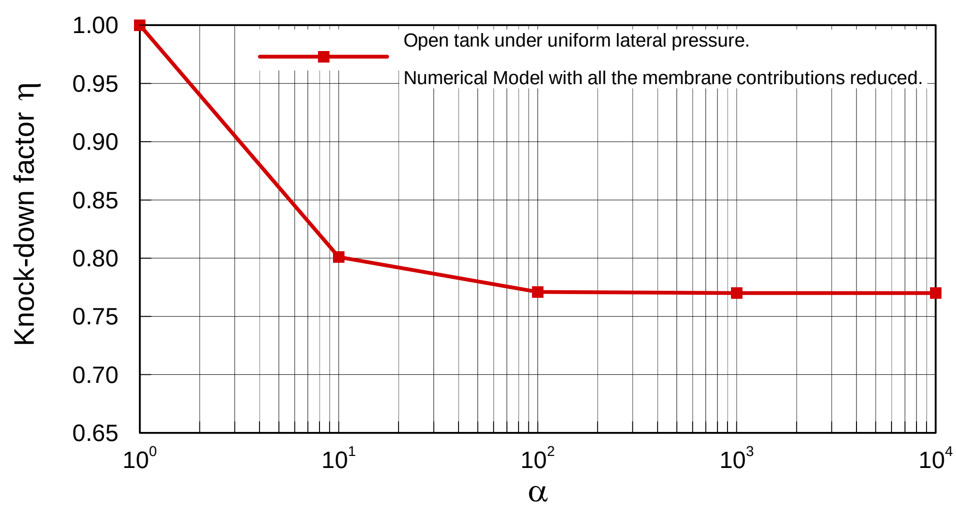

Figure 4.8. Open tank model: knock-down factors η for different values of α.

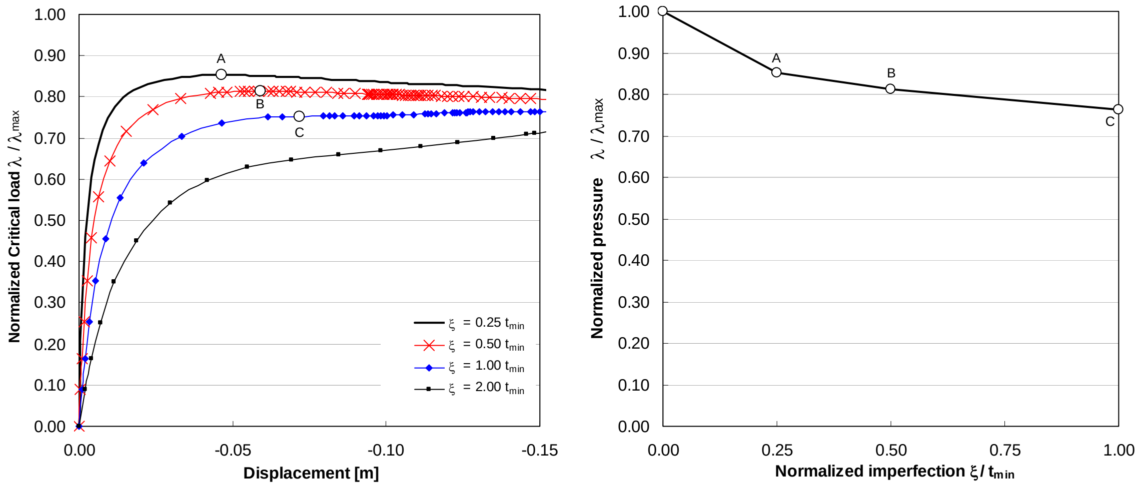

(a) (b)

Figure 4.9. (a) Non-linear paths for different level of imperfections; (b) Imperfection sensitivity curve.

4.7 RESULTS FOR CONICAL ROOF TANKS UNDER UNIFORM PRESSURE

The third case considered is a set of cylindrical tanks with conical roof similar to those analyzed by Virella (2004) under earthquake loads. This set of tanks have a constant diameter D = 30.48 m and variable height and thickness calculated according to the API Standard 650, Section 3.6.3 (API-650, 1988). Table 4.1 summarizes the dimensions and H/D ratios, and Table 4.2 shows the thicknesses adopted in the design for different models. The material properties are the same as those used in the open tank. The conical roof is supported by rafters and at the center of the cone there are boundary conditions that simulate the presence of a central column. Here again, the finite element models were constructed using STRI3 elements. The models were loaded with uniform unit pressure (1 KPa) in the cylindrical part as well as in the cone roof. Figure 4.10 shows the relative proportions of the three models analyzed.

The computations are divided in three stages. First, the critical load is calculated by solving the classical eigenproblem. Second, the proposed methodology of reduced energy described in Section 4.3.4 is implemented for the models specified here. Finally, non-linear analyses with geometric imperfections are carried out to compare the results with those obtained in stage two.

Results from the classical eigenvalue problem show that the eigenvalues are almost the same for all the models studied. The buckled zone for Model 1 covers almost all the cylindrical part of the tank. But, as the ratio H/D increases, as in Model 3, the deflected mode displays large deflections in the zone of small thicknesses. In all cases the cone roof stands almost undistorted. This feature is depicted in Figure 4.11.

Table 4.1. Dimensions adopted of the cylindrical part of the model.

Dimensions	Model 1	Model 2	Model 3
H [m]	12.19	19.20	28.96
D [m]	30.48	30.48	30.48
H/D	0.40	0.63	0.95

Table 4.2. Thickness adopted for each model.

Course	Model 1	Model 2	Model 3
	t_{design} [m]	t_{design} [m]	t_{design} [m]
1	0.0127	0.0206	0.0286
2	0.0111	0.0175	0.0254
3	0.0079	0.0159	0.0254
4	0.0079	0.0127	0.0222
5	0.0079	0.0111	0.0206
6		0.0079	0.0191
7		0.0079	0.0159
8		0.0079	0.0127
9			0.0111
10			0.0079
11			0.0079
12			0.0079

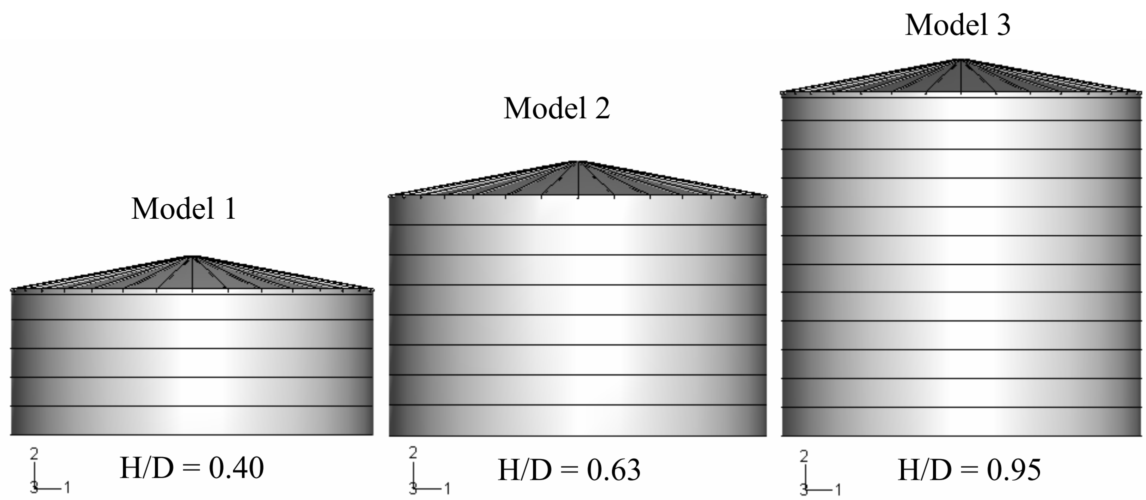

Figure 4.10. Relative proportions of the models with conical roof.

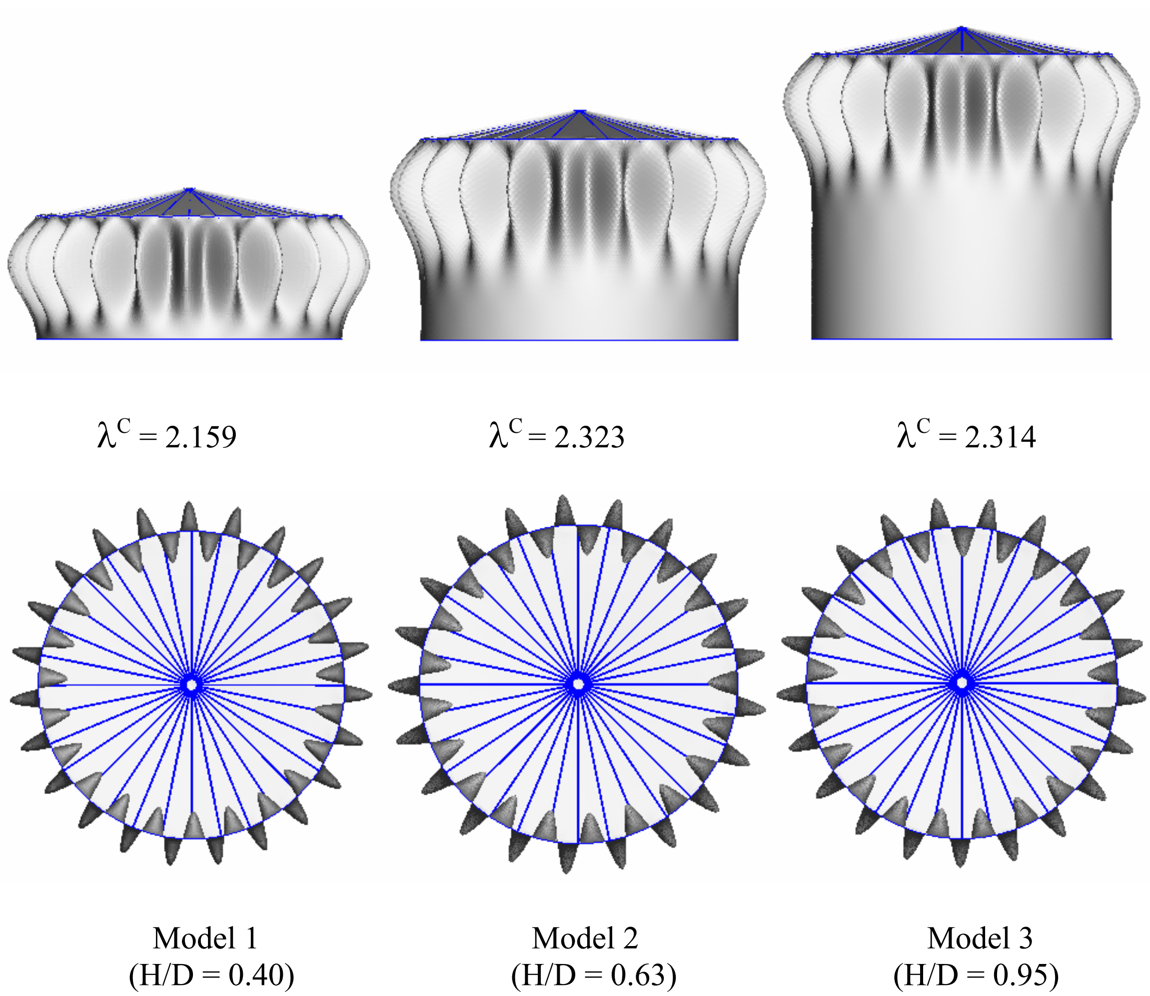

Figure 4.11. First classical eigenmodes for all the models considered.

In the next stage of the computations, the knock-down factor η was estimated. The variation of η was obtained using the first eigenmode given in the previous step and computing the energy for different levels of reduction of the membrane stiffness. For each relation H/D and for α > 100 the solution converges to a constant value of the knock-down factor. For Model 1, this value is η = 0.774, for Model 2, η = 0.739, and finally, for Model 3, η = 0.744. Figure 4.12 shows the variation of the knock-down factor as the reduction factor of membrane stiffness α increases.

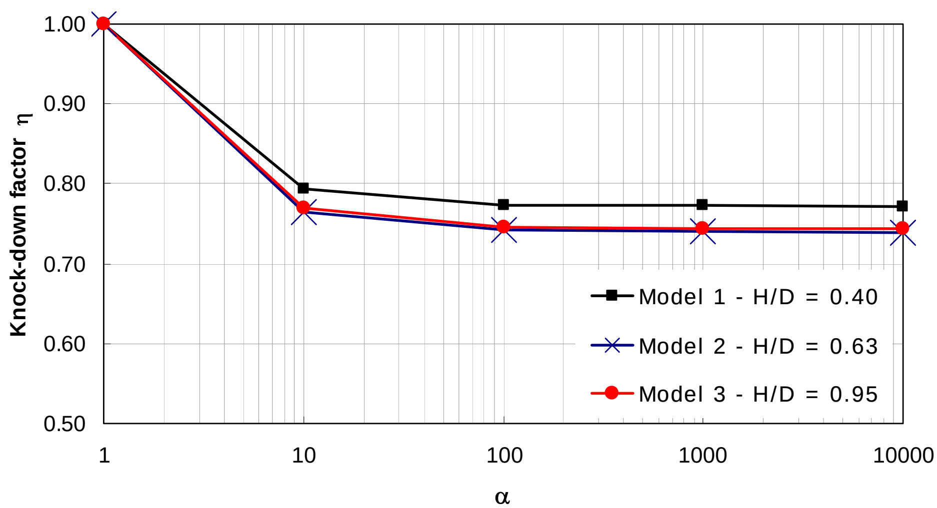

Figure 4.12. Knock-down factor calculated using the first eigenmode in the reduced energy method.

To compare the lower bound results with those obtained in the previous classical analysis, extensive non-linear imperfection sensitivity analyses were carried out. For these analyses, all the models were analyzed including small amplitude imperfections following the shape of the first eigenmode. The amplitudes of the imperfections vary from 0.10 t_{min} to 1.0 t_{min}, where t_{min} is the smallest shell thickness of each cylinder. Typical non-linear equilibrium paths for the mentioned levels of imperfections are shown for all the models at the left side of Figure 4.13. The imperfection sensitivity curves shown at the right side in Figure 4.13 were generated by plotting the normalized critical load λ / λ_{max} for each imperfection level, versus the dimensionless imperfection amplitude ξ / t_{min}. From this graph it is possible to observe that for imperfection amplitudes larger than 0.5 t_{min}, the non-linear equilibrium paths tend to be stable, so the imperfection sensitive curves are plotted up to the maximum for such level of imperfection. In this way, the lower bound obtained via non-linear analysis tends to η = 0.73, which is close to the results computed using the reduced energy approach. This behavior is similar for the three models, so that it seems that the proposed method is able to predict reasonably well the lower bound for this kind of tanks under uniform pressure. Figure 4.14 summarizes the imperfection sensitivity curves for all the models.

Notice that the non-linear modes at the maximum load are quite similar to those corresponding to the classical eigenvalue analysis and here again, the assumption that the modes in the pre-critical and post-critical states are similar is also well satisfied, as shown in Figure 4.15.

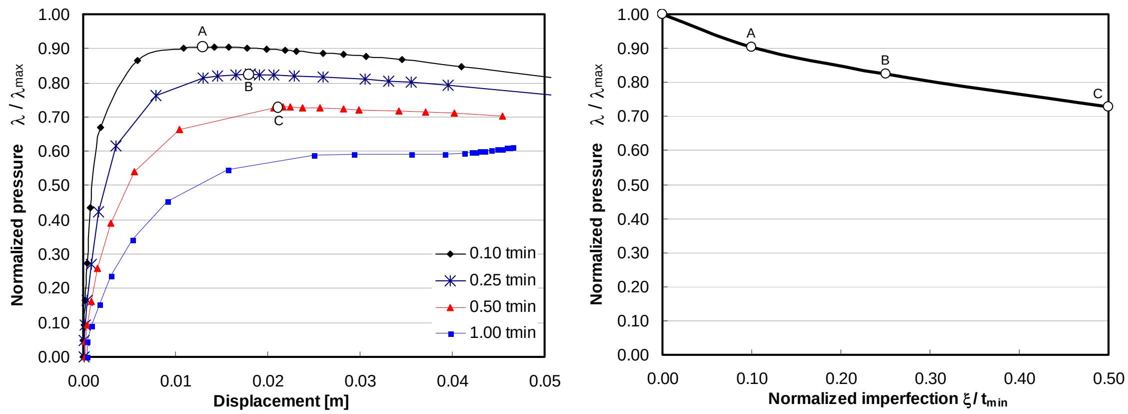

(a) Model 1 (H/D = 0.40)

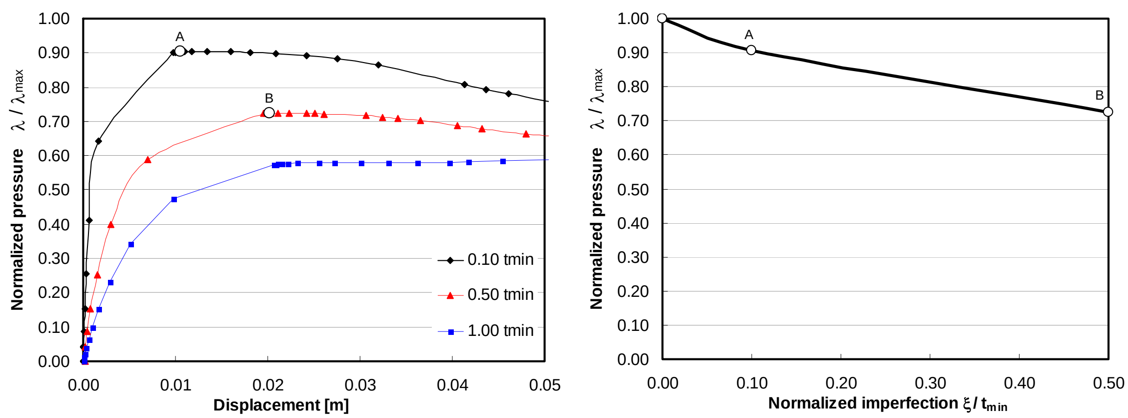

(b) Model 2 (H/D = 0.63)

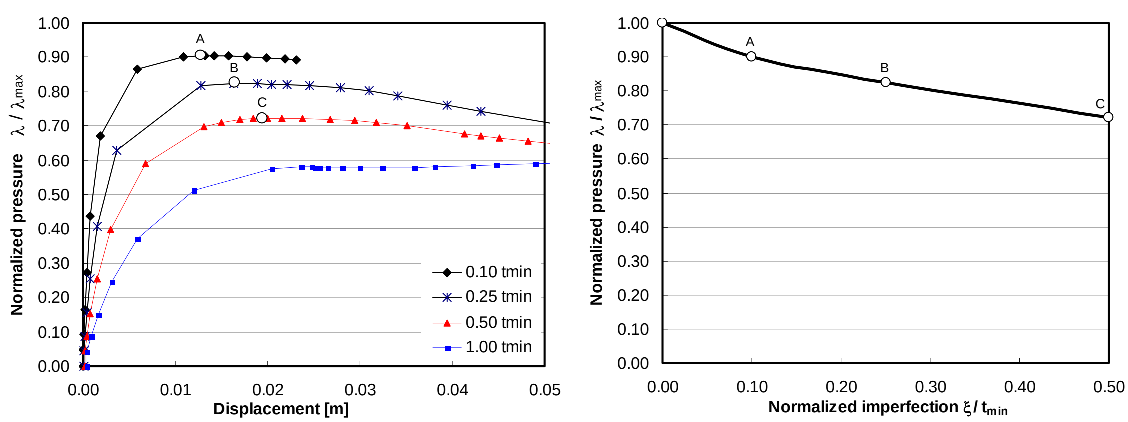

(c) Model 3 (H/D = 0.63)

Figure 4.13. Non-linear equilibrium paths and imperfection sensitivity curves for all models.

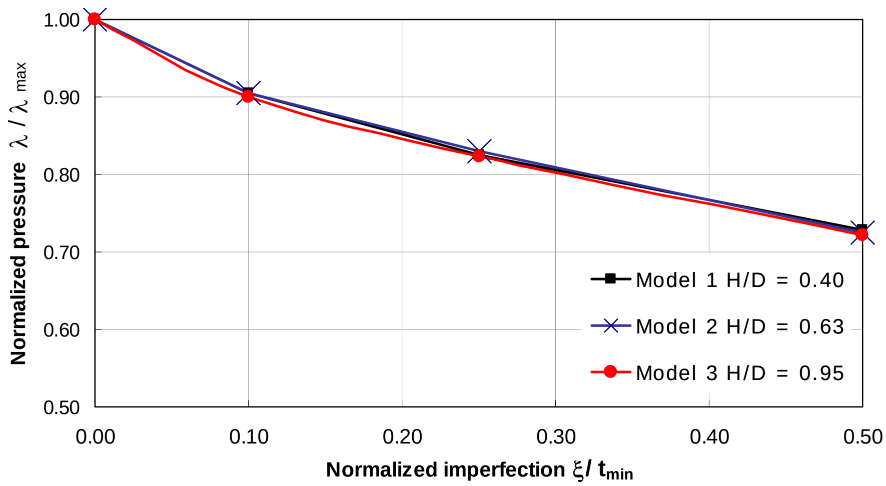

Figure 4.14. Imperfection sensitivity curves for all models.

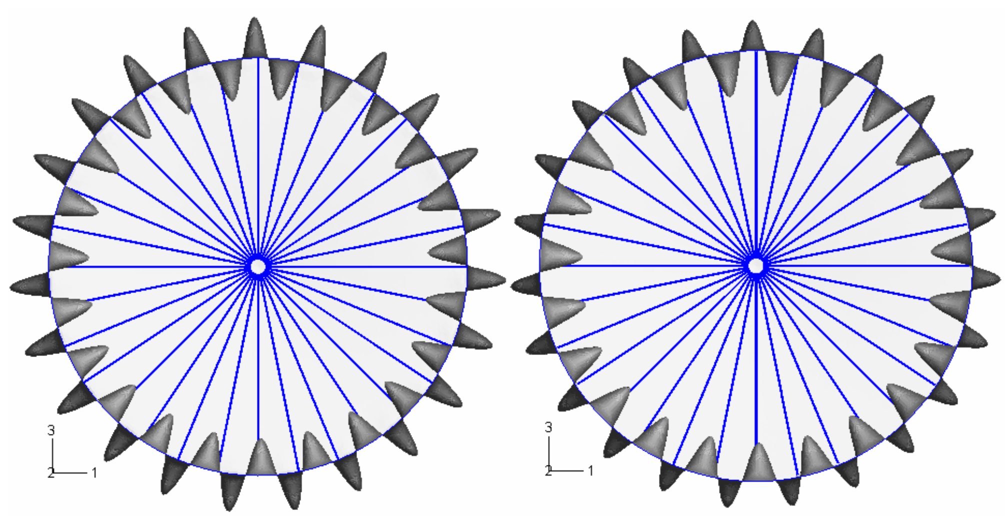

(a) (b)

Figure 4.15. Eigenmodes of Model 1 for: (a) classical buckling analysis; (b) imperfection sensitivity analysis for $\xi / t_{min} = 0.5$ at maximum load.

4.8 CONCLUSIONS

In this chapter a numerical procedure to calculate the knock-down factor for cylindrical shells under uniform lateral pressure has been proposed. This procedure has been implemented to estimate the lower bound pressures with standard tools available in the general purpose finite element code ABAQUS (2002).

First, a test case was considered for which an analytical solution of the knock-down factor has been used and compared with the proposed numerical solution. The results show that the proposed procedure can approximate reasonably well the analytical solution satisfying all the assumptions with a small error.

The open top cylindrical tank analyzed as a second case shows that the reduced energy approach is also able to predict the lower bound pressure with a small error compared with the non-linear imperfection sensitivity results. Finally, the proposed reduced energy approach has been implemented for three conical roof tanks, and the results display very good agreement with those obtained by using non-linear analysis. In all cases, the error is less than 5%. Here, if one compares the computational cost of performing non-linear analysis versus implementing the proposed approach, evidently there is a significant advantage in the second procedure. This is so because the computation of classical static buckling analysis and energies for prescribed displacements are computationally less costly than performing incremental non-linear analysis to obtain the drop in the buckling load due to imperfection sensitivity.

The next step is the implementation of this reduced energy approach for other important loading conditions, such as wind, and this is the subject of Chapter 5.

CHAPTER 5

COMPUTATION OF LOWER-BOUND BUCKLING LOADS FOR TANKS UNDER WIND PRESSURES

5.1 INTRODUCTION

The studies in this chapter deal with two tank configurations: conical roof tanks and open top tanks. For both tank configurations, several geometric relations were considered in order to cover a range of typical tanks found in the field. Six conical roof tank models are studied, of which three are similar to those analyzed by Virella (2004). The tank walls are designed according to the API-650 code (API-650, 1988) and loaded with a non uniform wind load around the cylinder and on the roof. The open tank models considered in this chapter were selected because there are useful geometrically non-linear results obtained by Godoy and Flores (2002), which allow direct comparison with the results obtained in the current study.

In both tank configurations, the proposed reduced energy method has been implemented to compute a lower bound for critical wind pressures. Some of the results are compared with static non-linear analysis carried out on the same models.

Section 5.2 deals with conical roof tank models, while Section 5.3 describes the results for open top tank models. An analysis and discussion of the results are presented in Section 5.4 and finally, some conclusions are addressed in Section 5.5.

5.2 CONICAL ROOF TANKS UNDER WIND PRESSURE

5.2.1 GEOMETRY AND LOAD DESCRIPTION

This section describes the conical roof tanks considered to compute lower bound buckling loads under wind pressures. The six models (here identified as MC1, MC2, MC3, MC4, MC5 and MC6) chosen for the analysis have in common the diameter of 30.48 m (100 ft) and are built using 2.438 m (8 ft) steel courses. The cylindrical part of the models has variable height, ranging from H/D = 0.24 to H/D = 0.95, with tapered thickness calculated according the 1-foot method specified in the API Standard 650, Section 3.6.3 (API-650, 1988). Models MC2, MC4 and MC6 are the same as those analyzed by Virella (2004) under earthquake loads.

All the models have a conical fixed roof supported by 32 rafters with a roof slope of 3/16. The cylinder is assumed to be fixed at the base and it is assumed that each model is isolated, so that the pressures applied on the shell and on the roof are not perturbed by other surrounding tanks. Table 5.1 and Table 5.2 summarize all the information regarding the dimensions adopted for the models. Figure 5.2 shows the geometry of all the models considered in this section.

The space variation of pressures in the cylindrical part of the tank is taken in this section as constant in elevation and variable around the circumference, as in other research works in the field. For the pressures acting on the roof, this chapter considers the wind-tunnel pressures obtained by Mac Donald *et al*. (1988) which are similar to those reported by Portela and Godoy (2005). The maximum pressure in the reference case is taken as 1 KPa acting on the windward meridian on the cylindrical part of the shell. For the stability analysis, the values of the pressures acting on the complete shell are scaled using the load parameter λ. The circumferential pressure distribution is assumed in the form (Rish, 1967):

$$p = \lambda \sum_{i=0}^{6} c_i \cos(i\theta) \tag{5.1}$$

where the Fourier coefficients are: c_0 = 0.387, c_1 = -0.338, c_2 = -0.533, c_3 = -0.471, c_4 = -0.166, c_5 = 0.066, c_6 = 0.055. Figure 5.1(a) shows the pressure distribution used in the conical roof and Figure 5.1(b) shows the wind pressure distribution assumed around the circumference.

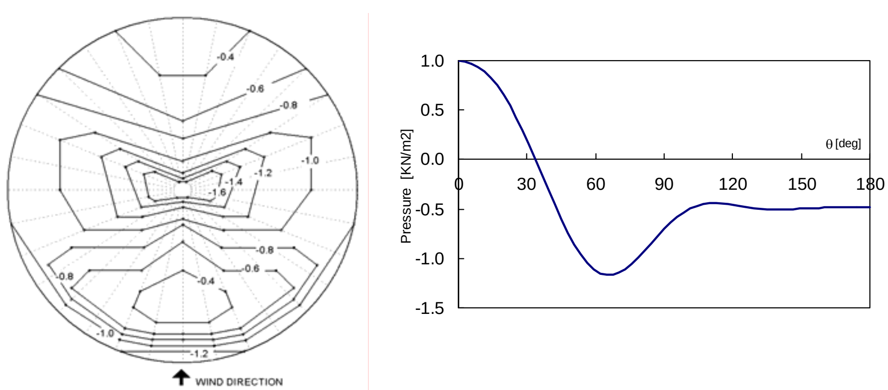

(a) (b)

Figure 5.1. (a) Pressure distribution used in the conical roof. (b) Wind pressure distribution assumed around the circumference.

Table 5.1. Dimensions adopted of the cylindrical part of the model.

	MC1	MC2	MC3	MC4	MC5	MC6
H [m]	7.32	12.19	17.07	19.20	24.08	28.96
D [m]	30.48	30.48	30.48	30.48	30.48	30.48
H/D	0.24	0.40	0.56	0.63	0.79	0.95

Table 5.2. Thickness adopted for each model.

Course	MC1	MC2	MC3	MC4	MC5	MC6
	t_{design} [m]	t_{design} [m]	t_{design} [m]	t_{design} [m]	t_{design} [m]	t_{design} [m]
1	0.0095	0.0127	0.0175	0.0206	0.0254	0.0286
2	0.0079	0.0111	0.0159	0.0175	0.0222	0.0254
3	0.0079	0.0079	0.0127	0.0159	0.0206	0.0254
4		0.0079	0.0111	0.0127	0.0175	0.0222
5		0.0079	0.0095	0.0111	0.0159	0.0206
6			0.0079	0.0079	0.0127	0.0191
7			0.0079	0.0079	0.0111	0.0159
8				0.0079	0.0079	0.0127
9					0.0079	0.0111
10					0.0079	0.0079
11						0.0079
12						0.0079

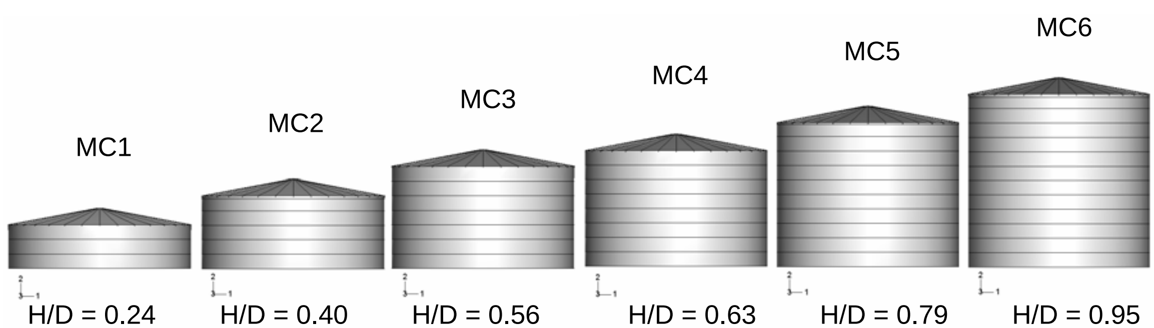

Figure 5.2. Relative proportions of the models with conical roof.

5.2.2 COMPUTATIONAL MODEL FOR CLASSICAL BUCKLING ANALYSIS

All the tanks investigated were modeled using triangular finite elements STRI3 with adequate mesh density to obtain convergence. The computations were divided in three stages: First, the critical load was calculated by solving the classical buckling eigenproblem. Second, the proposed methodology of reduced energy described in Chapter 4 was implemented for the models specified here. Third, non-linear analyses with geometric imperfections were carried out to compare the results with those obtained in stage two. The applicability of the reduced energy method in the models described above, will be discussed by comparing the results with those predicted using imperfection-sensitivity analysis.

Results for the classical eigenvalue problem show that the eigenvalues for the first and second modes are almost the same for all the models studied. The shortest model seems to be more rigid and the classical critical loads in the other models tend to a constant value as the relation H/D increases. However, the classical critical loads for these tanks are highly dependent on the set of thicknesses adopted in the design. A change in the thickness, especially in the zone of the buckling mode or in the transition to the thicker thickness, produces a change in the eigenvalue. Table 5.3 summarizes the eigenvalues for the modes 1 and 2, and the variation in the eigenvalues for all the models is depicted in Figure 5.3 for the set of thickness specified in Table 5.2.

Table 5.3. Critical pressures for wind loaded tanks.

Model		Critical pressure [kN/m^2]		Critical wind gust speed [Km/h] (mph)
		Mode 1	Mode 2	
MC1	H/D = 0.24	3.854	3.881	294 (183)
MC2	H/D = 0.40	2.480	2.481	236 (147)
MC3	H/D = 0.56	2.916	2.926	256 (159)
MC4	H/D = 0.63	2.537	2.547	239 (148)
MC5	H/D = 0.79	2.558	2.568	240 (149)
MC6	H/D = 0.95	2.478	2.485	236 (147)

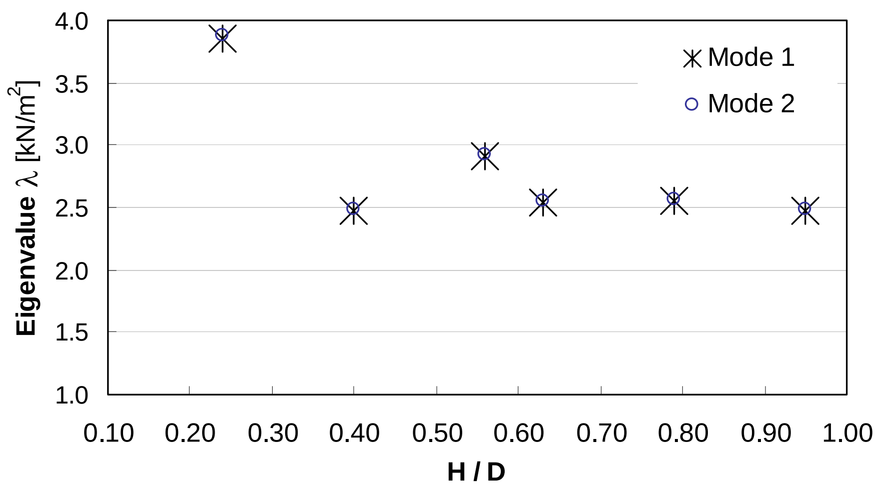

Figure 5.3. Eigenvalues for the geometric configurations of Figure 5.2.

In order to relate the critical pressures indicated in Table 5.3 with the wind speed, it is possible to use ASCE-7-02 (2002) to calculate wind speed for the critical pressures obtained:

$$p = 0.613\ K_z\ K_{zt}\ K_d\ I\ \mathrm{V}^2 \tag{5.2}$$

where p is the pressure of the wind in (N/m^2), V is the basic wind speed (m/s), K_z is the exposition factor, K_{zt} is the topographic factor, K_d is the directionality factor and I is the importance factor. It is assumed that the tanks are placed in flat terrain, so K_{zt} = 1. Category II structure gives the importance factor I = 1, the directionality factor is K_d = 1 and K_z = 0.94, then equation 5.2 becomes:

$$p = 0.576\,\mathrm{V}^2 \tag{5.3}$$

The wind speeds in Table 5.3 were calculated using Equation 5.3.

From the analysis of the modes it may be seen that the buckled shape has displacements which are concentrated in the zone of windward positive pressures. It seems that the suctions (negative pressures) in the leeward zone and in the conical roof do not have strong influence on the mode shape. The first and second modes are almost identical in shape in all the models investigated. The difference between the modes is that the first mode is asymmetrical and the second is symmetrical with respect to a vertical axis. In all the models, the buckled zone is concentrated in the thinner courses of the cylinder. Furthermore, the negative pressures (suctions) acting on the conical roof do not play an important role in the buckling process. The negative pressures of the loads do not seem to affect the load and mode of buckling. Numerical tests performed without including suction pressures predict almost the same buckling results. However, in order to be consistent, all the results presented in this section are computed for pressures acting on over the complete cylindrical shell and on the cone roof. Figure 5.4 and Figure 5.6 show the first mode and Figure 5.5 and Figure 5.7 illustrate the second mode for all the models considered.

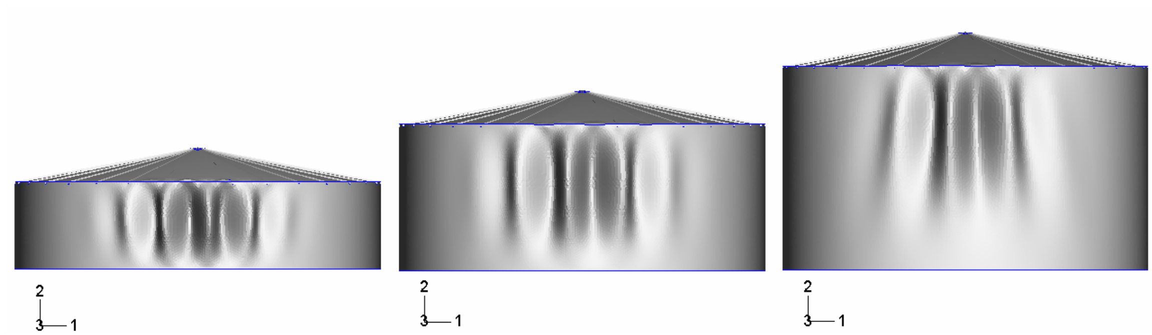

MC1 $\lambda^C = 3.854$

MC2 $\lambda^C = 2.480$

MC3 $\lambda^C = 2.916$

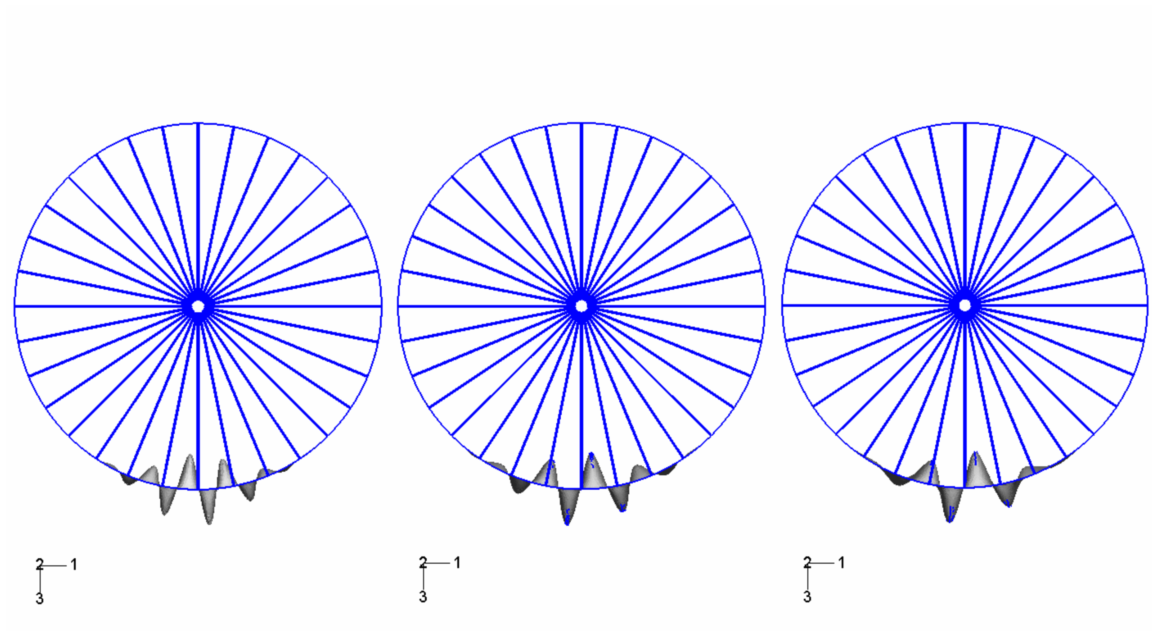

MC1 (H/D = 0.24) MC2 (H/D = 0.40) MC3 (H/D = 0.56)

Figure 5.4. First classical buckling mode, models MC1, MC2, MC3.

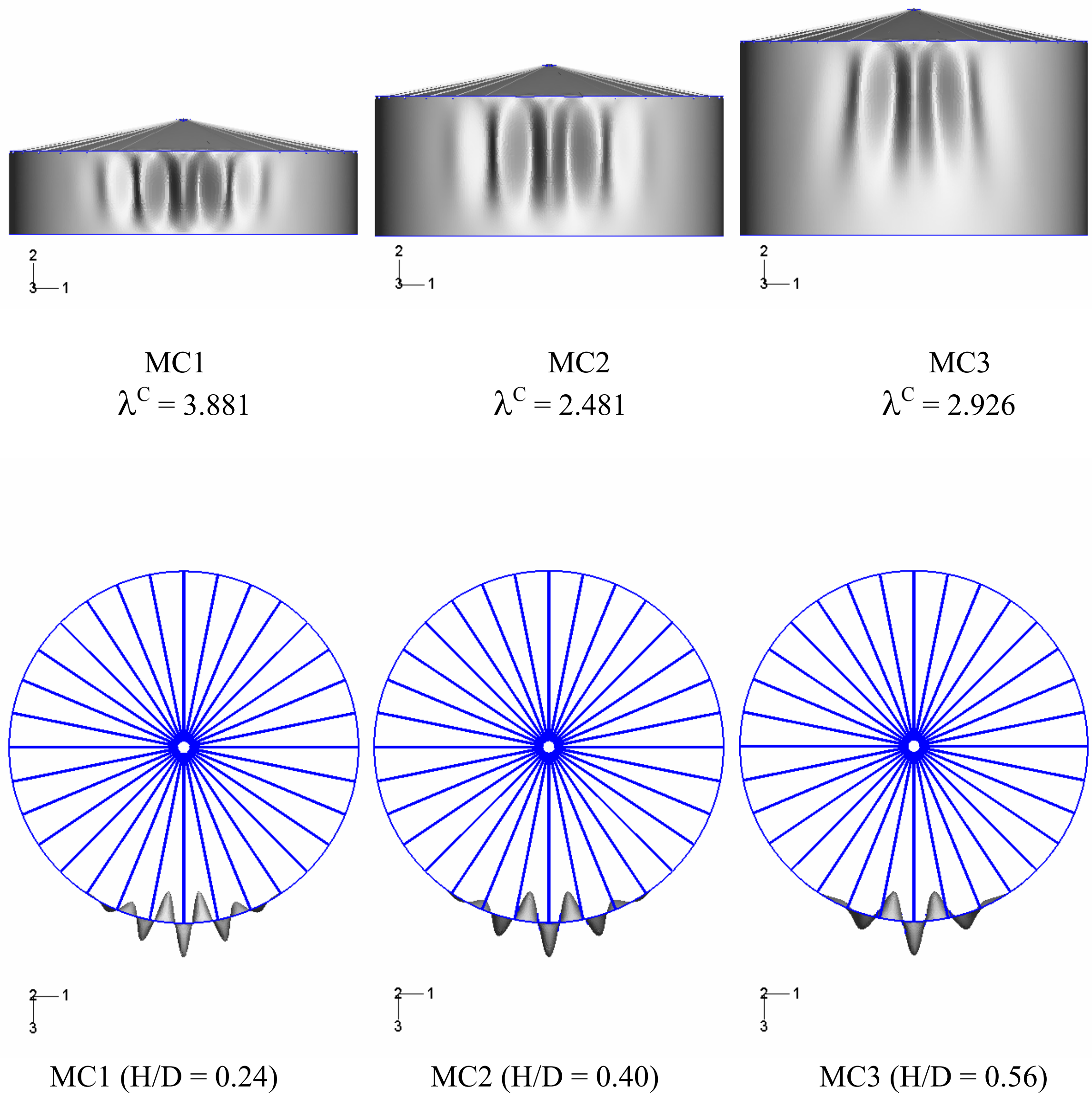

Figure 5.5. Second classical buckling mode, models MC1, MC2, MC3.

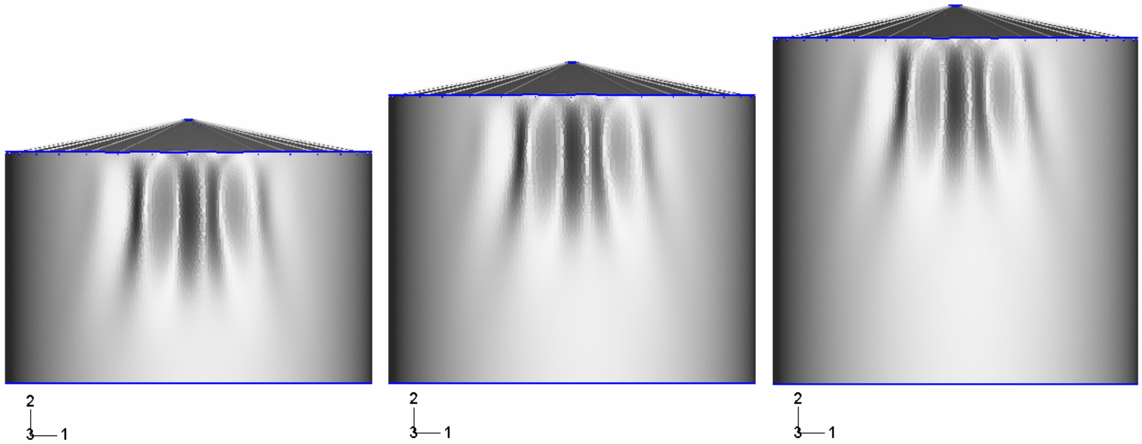

MC4 $\lambda^{C} = 2.537$

MC5 $\lambda^{C} = 2.558$

MC6 $\lambda^{C} = 2.478$

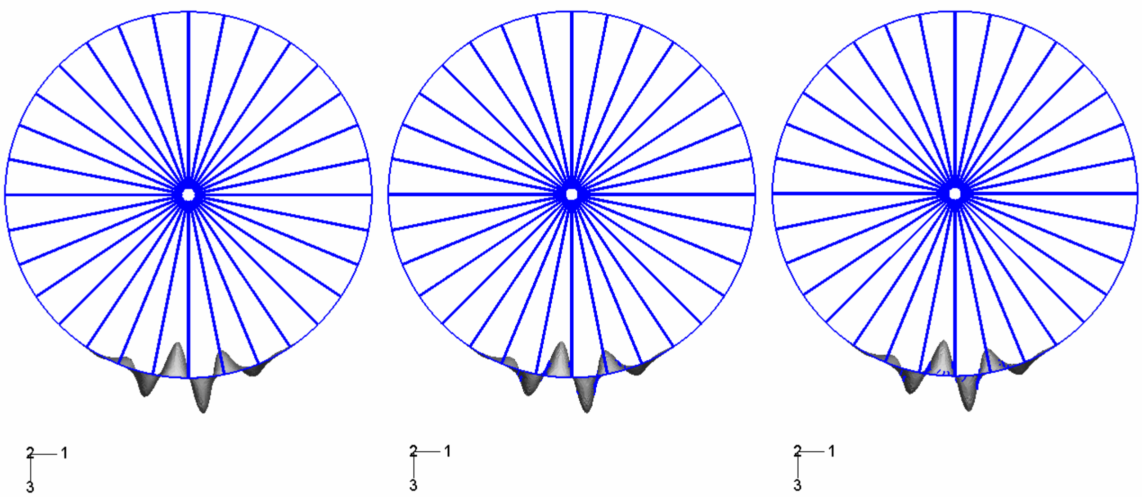

MC4 (H/D = 0.63)

MC5 (H/D = 0.79)

MC6 (H/D = 0.95)

Figure 5.6. First classical buckling mode, models MC4, MC5, MC6.

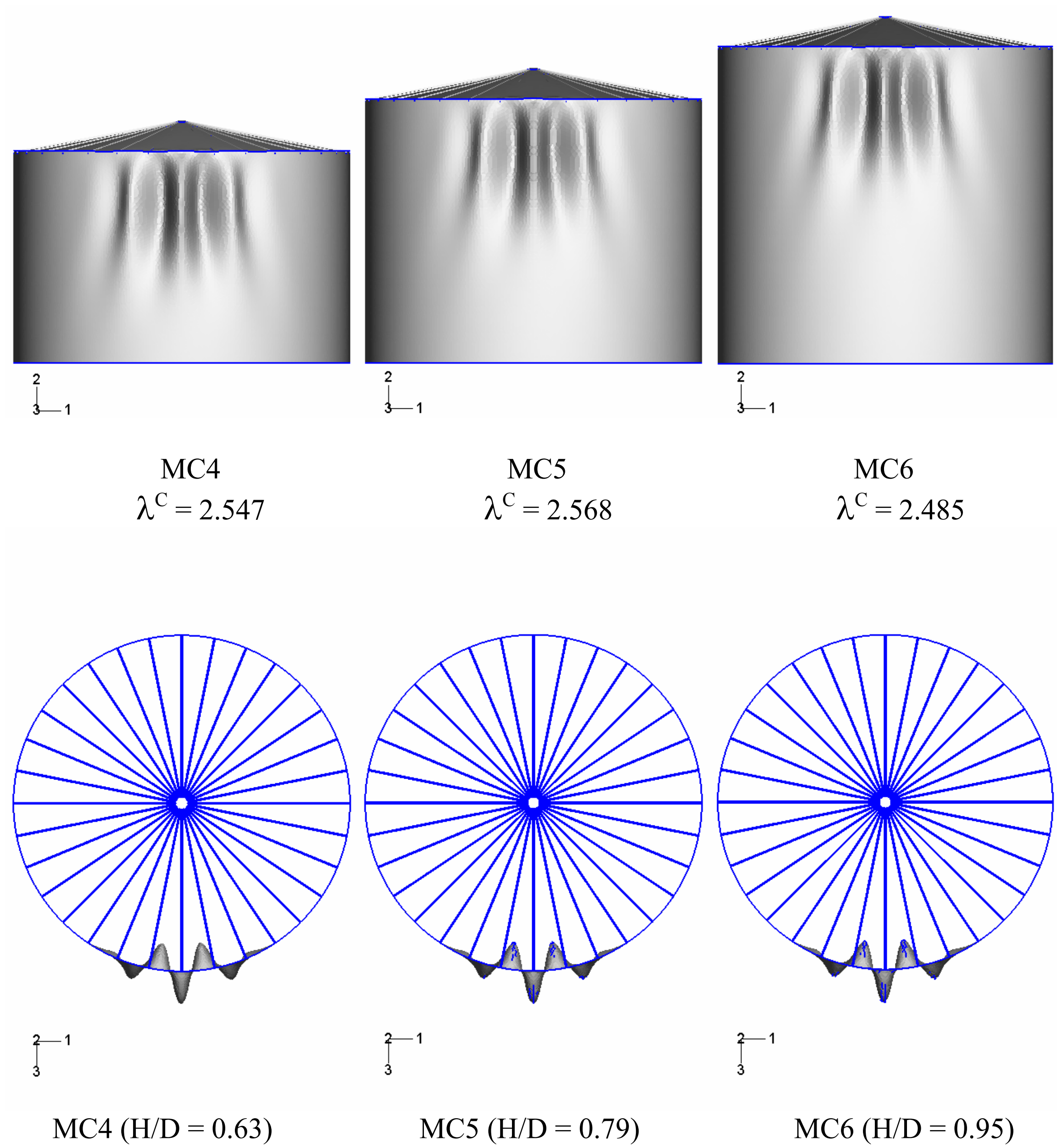

Figure 5.7. Second classical buckling mode, models MC4, MC5, MC6.

5.2.3 COMPUTATIONAL MODEL FOR REDUCED ENERGY ANALYSIS

The next stage in the computations is the implementation of the reduced energy method. In this step, the lower bound wind pressure is calculated using the first mode of the eigenvalue analysis as an imposed displacement pattern. Additionally, the second mode is also used to compute the lower bound. Every part of the shell that forms the whole cylinder (all courses) undergoes simultaneous reductions in the membrane stiffness while the scaled mode is imposed as a prescribed initial displacement. In that configuration, the energy used by the structure to reach that deflected configuration is calculated. With the calculated energy for each reduction factor α eroding the membrane stiffness, and having calculated the energy without reduction in its stiffness for the same load conditions, we are able to determine the loss in the buckling capacity to support additional load. The knock-down factor η, as previously defined, is the relation between the energy computed for different levels of reduction in the membrane stiffness and the energy computed with all the membrane stiffness, say $\eta = U^b / (U^m + U^b)$.

It is found that the knock-down factor η tends to a constant value as the reduction factor α increase. The results of these computations are illustrated in Figure 5.8(a) for the first eigenmode and in Figure 5.8(b) for the second eigenmode. From these plots, it seems that the knock-down factor has a small dependence on the H/D relations. All the models show a similar trend and the differences in η between the shortest and the tallest models are of only 4%.

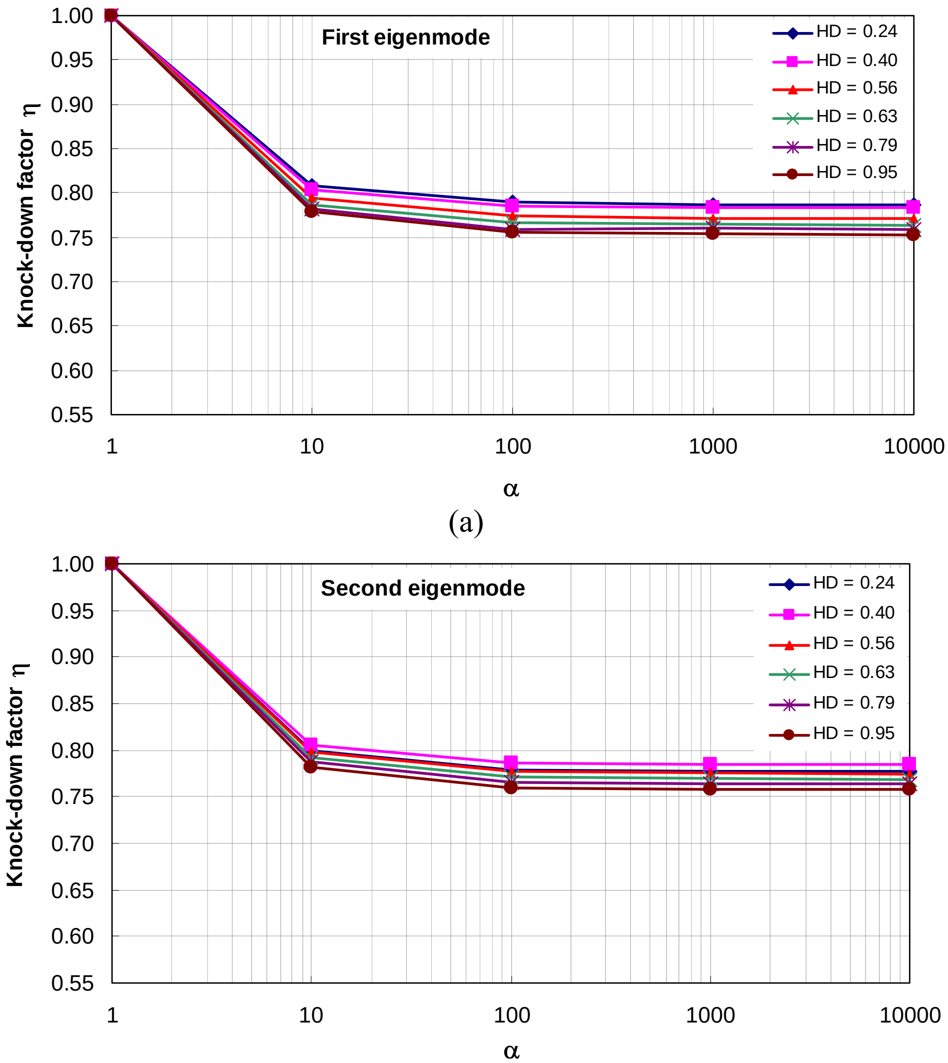

(a)

(b)

Figure 5.8. Knock-down factors calculated using the reduced energy method for: (a) first eigenmode, and (b) second eigenmode.

5.2.4 LOWER BOUND VIA NON-LINEAR ANALYSIS

To compare the lower bound results with those obtained in the previous classical analysis, non-linear imperfection sensitivity analyses were carried out. For these analyses, all the models were analyzed including small amplitude imperfections following the shape of the first and the second eigenmodes. The amplitudes of the imperfections vary from 0.10 t_{min} to 1.0 t_{min}, where t_{min} is the smallest shell thickness of each cylinder. For each imperfection level, non-linear equilibrium paths are computed using the Riks technique (Riks, 1972 and 1979), so that the structure may display its post-critical behavior. For small amplitude imperfections, the non-linear post-critical path is unstable. This means that the shell can withstand a maximum load for a relatively small displacement. Beyond that maximum, the shell cannot take additional loads and it has large deflections.

For imperfection amplitudes larger than 1.0 t_{min}, the equilibrium path has very large deflections, becomes stable and constantly raising. This is an indication that the shape of the shell has changed so much that the behavior is quite different from the behavior of the original perfect shell. This level of imperfection settles on the lower limit of load that the structure is able to support with small deviations from the original form. After that limit, the deflected structure behaves in a different way.

Typical non-linear equilibrium paths for the mentioned levels of imperfections are shown for the models MC2, MC4 and MC6 in Figure 5.9. The imperfection sensitivity curves shown in the right side in Figure 5.9 were generated by plotting the normalized critical load λ / λ_{max} for each imperfection level versus the dimensionless imperfection amplitude ξ / t_{min}. Figure 5.10 summarizes all those curves for all the models analyzed and they show the lower limit to which the pressure loads tend as the imperfection levels increase. In this way, the knock-down factor $\eta = \lambda / \lambda_{max}$ is directly comparable with the results obtained using the reduced energy method.

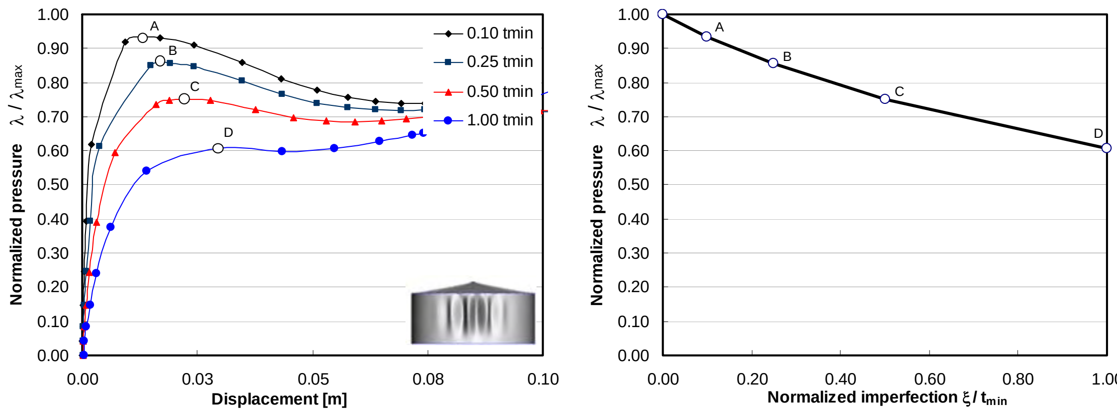

(a) MC2 (H/D = 0.40); Imperfection shape: first mode.

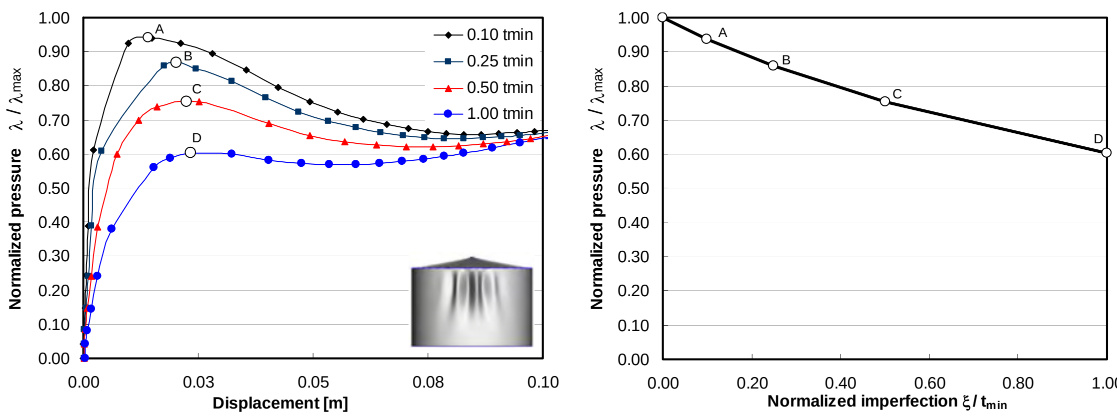

(b) MC4 (H/D = 0.63); Imperfection shape: first mode.

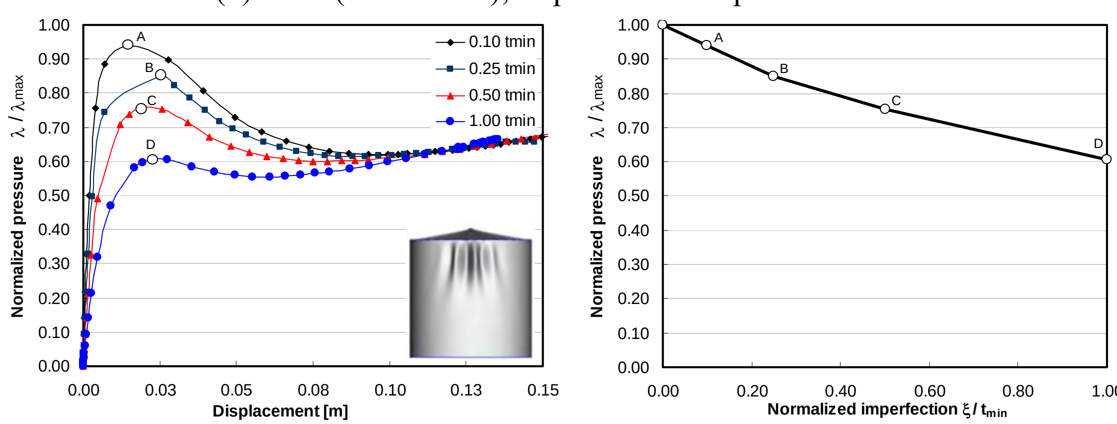

(c) MC6 (H/D = 0.95); Imperfection shape: first mode.

Figure 5.9. Non-linear equilibrium paths and imperfection sensitivity curves for selected models.

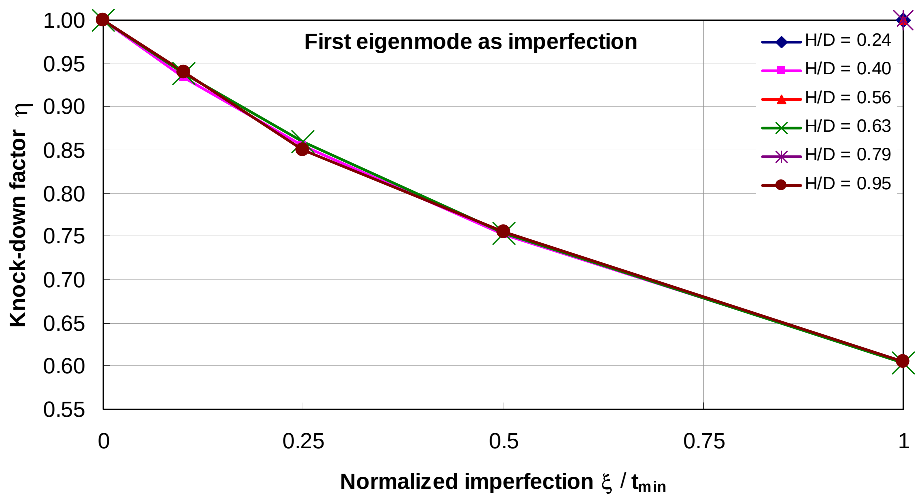

(a)

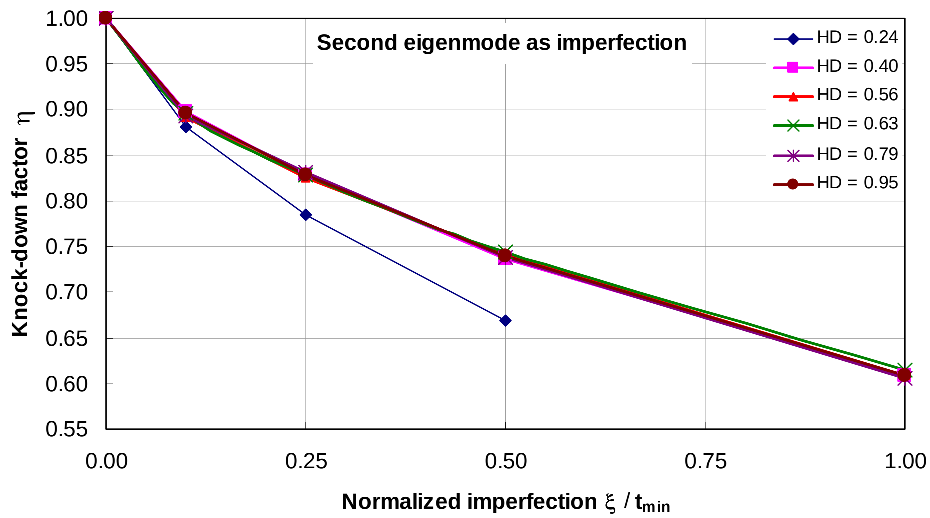

(b)

Figure 5.10. Knock-down factor calculated with non-linear imperfection sensitivity analysis using as imperfection shape: (a) First eigenmode, and (b) Second eigenmode.

From Figure 5.9 it is possible to see that the imperfection-sensitivity is practically the same for all the models. This feature may be justified by the fact that in all the models the buckling mode deflections are concentrated in the zone of lower shell thickness. That thickness is the minimum required by the design in all models and at least the last three courses at the top of the cylinder have the minimum thickness. Probably, that is why the classic eigenvalues indicated in Figure 5.3 have small variations as the H/D ratio increases.

5.2.5 DISCUSSION

Notice that the knock-down factor in Figure 5.10 does not approach clearly a plateau, as obtained in the reduced energy method. The first mode shows more a slight tendency to a plateau than the second mode. Comparing the results displayed in Figures 5.8 and 5.10, the reduced energy method predicts a higher limit than the actual imperfection sensitivity analysis. In the reduced energy method, the curves tend to values of η ranging from $\eta = 0.758$ to $\eta = 0.785$, while in the non-linear analysis method, for the maximum imperfection amplitude considered ($\xi / t_{min} = 1.00$), the lower limit considering both modes, seems to be between $\eta = 0.6$ and $\eta = 0.7$.

Clearly, the values predicted by the proposed reduced energy method for wind pressures cannot be considered a safe lower limit. The main reason for the discrepancy seems to be associated to the different deflection modes obtained in the classical eigenvalue and the non-linear analyses. The mode obtained in the classical eigenvalue computations (and then used in the reduced energy method) is not quite the same as the mode found in the non-linear analysis with an imperfection. This difference affects the assumptions made previously and consequently the accuracy in the computations. The following sections deal with open tank models, where the discrepancies are even more evident.

5.3 OPEN TANKS UNDER WIND PRESSURE

5.3.1 GEOMETRY AND LOAD DESCRIPTION

The models analyzed in this section are the same as those considered by Godoy and Flores (2002). They are four cantilever cylinders with different geometric relations studied in order to emphasize the differences in the behavior according to changes in their geometric relations. These models represent tanks clamped at the base and free at the upper edge without any reinforcing ring and with constant thickness. The material is steel, with elastic modulus E = 206 GPa and Poisson ratio ν = 0.3. The main geometric properties for the models are summarized in Table 5.4.

Table 5.4. Geometric properties.

Model	Diameter	Height	Thickness	Non-dimensional parameters		
	D [m]	H [m]	t [m]	H/D	R/t	Z
M1	24.0	4.0	0.006	0.17	2000	212
M2	14.0	3.5	0.004	0.25	1750	417
M3	9.0	4.5	0.003	0.50	1500	1431
M4	5.0	5.0	0.002	1.00	1250	4770

In Table 5.4, Z is the Batdorf parameter given by:

$$Z = \frac{H^2}{R\,t}\sqrt{(1-\nu^2)} \qquad (5.4)$$

where H is the height, R the radius, t the thickness and ν the Poisson coefficient. The Batdorf parameter is a measure of the slenderness of the cylindrical shell and as its value increases, the slenderness of the shell increases. From Table 5.4, note the significant changes in the radius and the thickness, keeping the height with relatively small variations. Figure 5.11 provides a graphical representation of the geometries. The discretization of the shells is carried out using STRI3 finite elements and the load distribution in the cylindrical shell is the same as that used for the conical roof tanks.

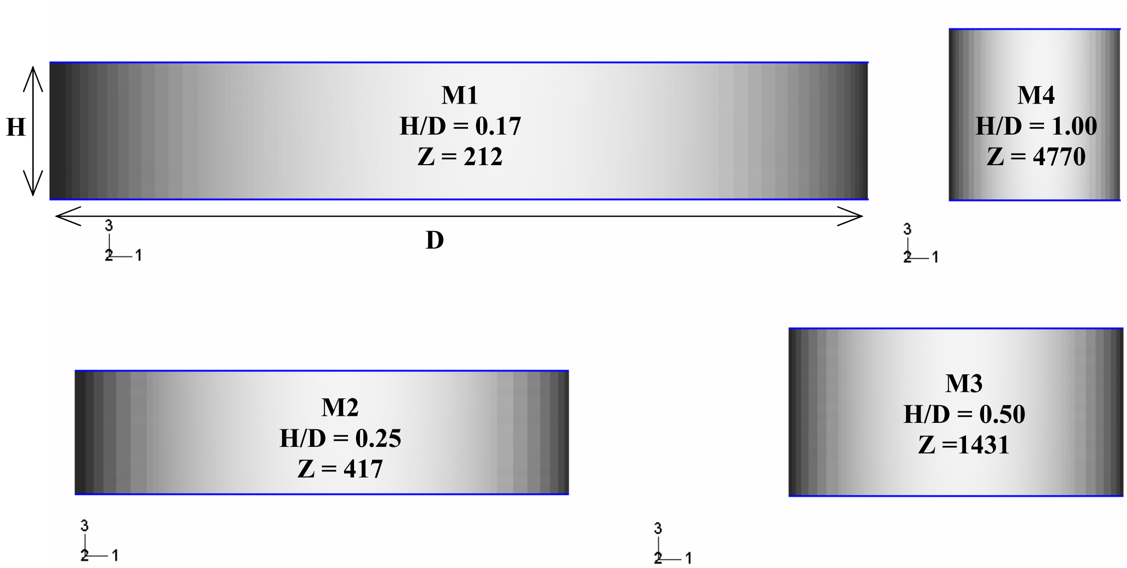

Figure 5.11. Comparison between the model geometries investigated.

5.3.2 COMPUTATIONAL MODEL FOR CLASSICAL BUCKLING ANALYSIS

This section reports the results for classical linear buckling analysis for each model. Then, the first eigenmode obtained is imposed as a prescribed initial displacements field to calculate the lower bound load according to the reduced energy method. These results are compared with those reported by Godoy and Flores (2002), based on non-linear analysis with imperfections. However, here it was necessary to repeat the non-linear analysis for reasons that will be explained in the following paragraphs.

For the wind pressures given by equation 5.1, the classical critical pressures were calculated and contrasted with the results reported by Godoy and Flores (2002). To understand the influence of the specific finite element employed, the critical values were also calculated using S8R5 elements. The results obtained with the proposed discretization using STRI3 elements predict values which are close to those calculated with S8R5 elements, and they are in good agreement with the previously reported results. Table 5.5 summarizes this part of the study. Here again, the critical wind speeds for the same conditions described in Section 5.2.2, and corresponding to the first mode for the STRI3 discretization, are calculated in Table 5.5.

Table 5.5. Classical critical loads (eigenvalue analysis).

Model	Non-dimensional parameters			λ^c [kN/m2]			Critical Wind Gust Speed [Km/h] (miles/h)
	H/D	R/t	Z	Godoy-Flores (2002)	S8R5	STRI3	
M1	0.17	2000	212	2.282	2.201	2.225	225 (139)
M2	0.25	1750	417	-	2.107	2.137	220 (136)
M3	0.50	1500	1431	-	1.683	1.694	196 (121)
M4	1.00	1250	4770	1.558	1.500	1.518	186 (115)

5.3.3 LOWER BOUND USING REDUCED ENERGY METHOD

Let us consider the buckled mode for each model using element STRI3. First, as in the conical roof models, the deflections in the buckled mode are concentrated in the windward zone and the suction has almost no effect on the deflected shape. As the slenderness increases, the number of waves decreases and the deflected shape concentrates in the upper zone of the cylinder. ABAQUS (2002) normalizes the mode using the maximum displacement, so that the maximum normalized displacement is equal to one. Figure 5.12 illustrates the first mode for all the models.

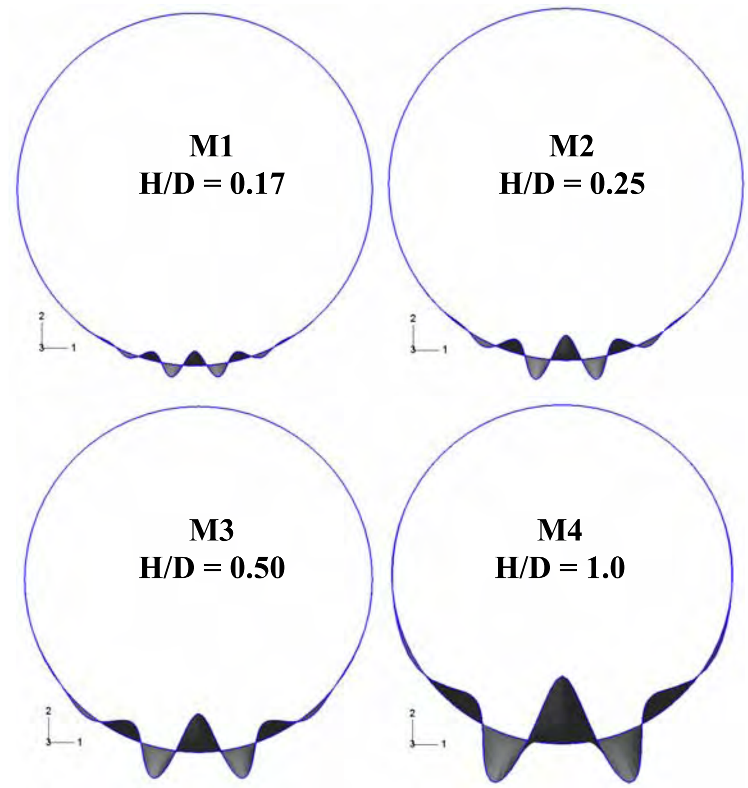

Figure 5.12. First classical buckling modes for all models. The amplification factor is one for all four cases.

Those normalized first modes were used to calculate the lower bound pressures using the reduced energy method. For convenience, a scaling factor 1/1000 was used for the modes, although using other scaling factors leads to identical results. The reduction in the membrane stiffness is done according to the procedure detailed in Appendix A. The knock-down factor $\eta = U^b / (U^m + U^b)$ calculated for each model is illustrated in Figure 5.13. In that figure, the knock-down factor converges to a constant value for α larger than 100, and is almost independent of the model geometry.

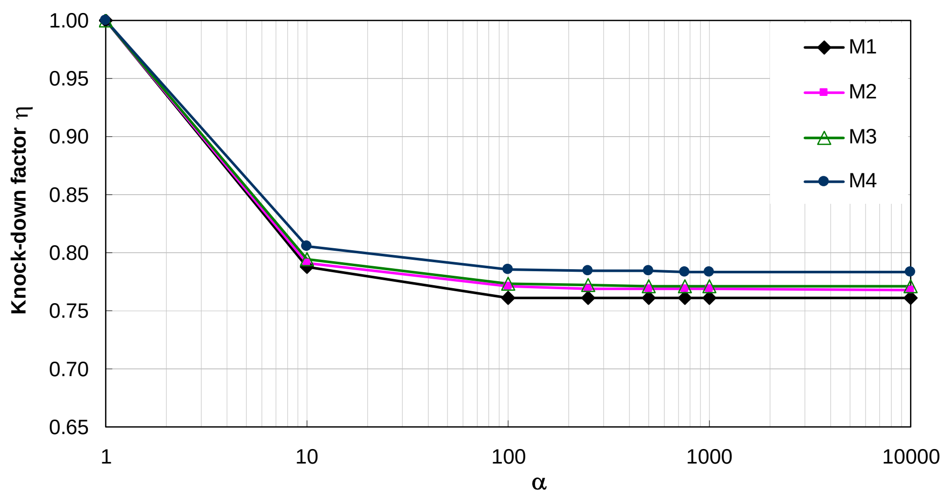

Figure 5.13. Lower bound estimate for open tank models.

5.3.4 LOWER BOUND VIA NON-LINEAR ANALYSIS

According to the results reported by Godoy and Flores (2002), the knock-down factor should lead to different lower bounds as the geometry of the tank changes. However, Figure 5.13 shows that all the models tend to approximately the same lower limit. For example, consider just two extreme cases, model M1 (H/D = 0.17) and model M4 (H/D = 1.00): the reduction factors according to results reported by Godoy and Flores (2002) are approximately $\eta^{M1} = 0.60$ and $\eta^{M4} = 0.95$. Those results have been reproduced with the models used here (see Figure 5.14), using element STRI3 and geometrically non-linear analysis. Clearly, the lower bound estimates shown in the previous section are not in good agreement with the non-linear results. Alternatives for overcoming such differences are proposed in the next sections.

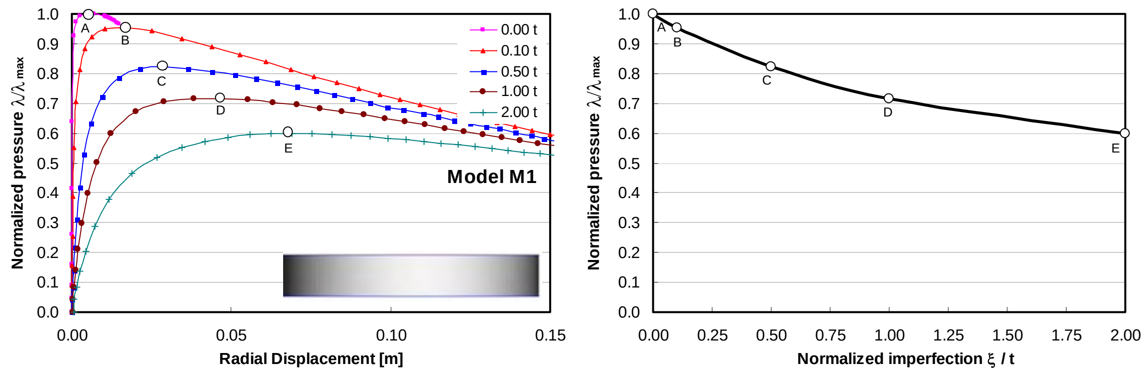

(a) M1 (H/D = 0.17); Imperfection shape: first mode.

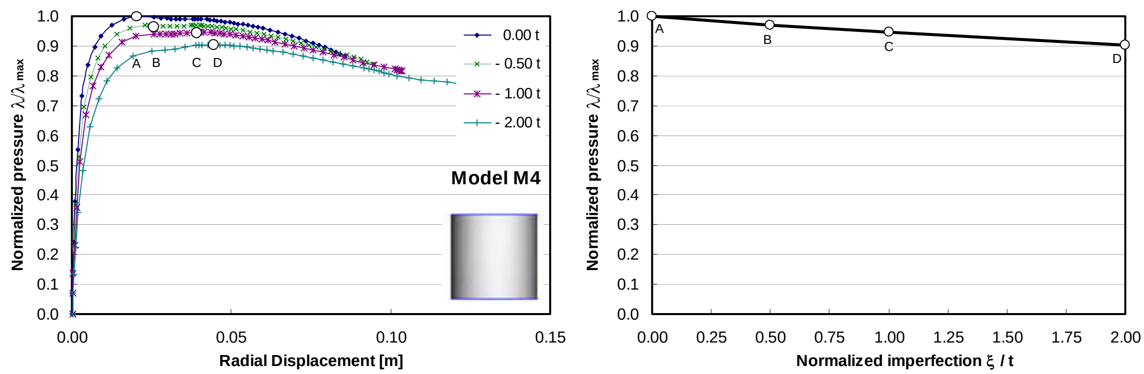

(b) M4 (H/D = 1.00); Imperfection shape: first mode.

Figure 5.14. Results of non-linear imperfection sensitivity analysis.

5.4 ALTERNATIVES FOR IMPROVING THE LOWER BOUND COMPUTATIONS

5.4.1 CHANGE IN THE BUCKLING MODE

In sight of the results described in the previous sections, it is apparent that the traditional lower bound approach has not been able to capture the expected behavior displayed in the non-linear analysis; thus it is necessary to explain the differences. An attempt to find an answer to the discrepancies is to reconsider the mode used as prescribed displacements in the energy computations. Looking the non-linear equilibrium paths (Figure 5.14), for imperfections of the order of twice the shell thickness, it is possible to see that the non-linear paths are unstable and there are relatively small differences between the maximum load and the loads reached in the post-critical path. This means that, for that level of imperfection, the shell is close to reaching the lower load without changing the configuration dramatically. For imperfections larger than twice the thickness (not shown in Figure 5.14), the non-linear equilibrium paths become stable, but in such case, the shell behavior is different due to the very large deflections.

It seems appropriate to use the mode corresponding to the maximum load reached in the non-linear analysis for the mentioned level of imperfection, and use that mode to compute the energy U^b in the reduced energy method. However, the mode extracted from the non-linear analysis to compute U^b needs to be normalized in the same way as in mode used to compute $U^m + U^b$. Notice that, the non-linear mode has small displacement components associated to the leeward pressures, which are almost inexistent in the mode calculated in the classical buckling analysis.

With these considerations, the reduced energy method was implemented in the models M1 and M4 using the new mode to compute U^b. Figure 5.15 shows the results for this case. Both models show similar trends, but with an even small lower bound compared with the previous results. Evidently, the discrepancies between both attempts using different modes and the non-linear results, makes one to think again about the implementation of the proposed method for wind loads.

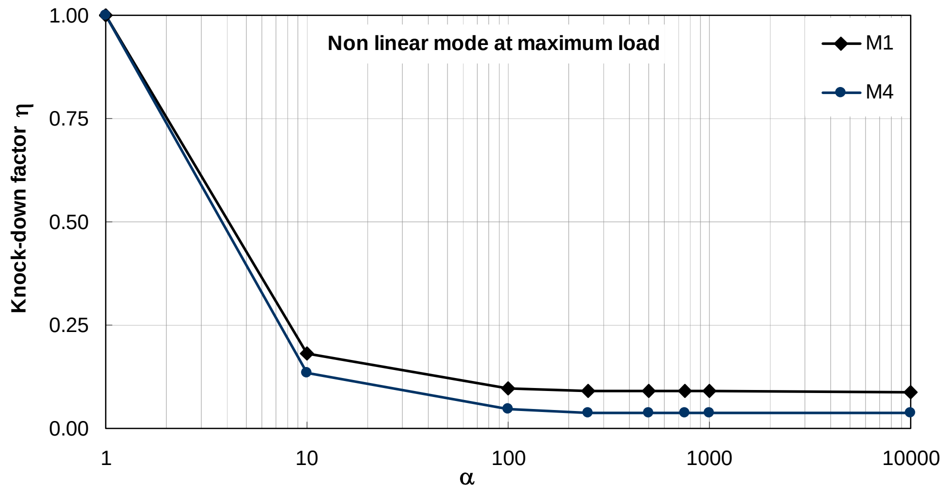

Figure 5.15. Lower bound calculated using non-linear mode.

Figure 5.16(a) compares modes obtained in the classical buckling analysis and in the non-linear analysis, clearly they are not exactly the same mode. That difference is not only in the amplitudes, even normalized, but also in the wave configuration for each model. This difference in the modes is more clearly visualized by superposing the deflected shape for both modes at the free top of the shell as in Figure 5.16(b). From Figure 5.16(b), the waves in the non-linear modes for the maximum load and for an advanced buckled state are not in phase with waves in the classical mode. In addition, the amplitude even using the same criteria in the normalization is dominated by the classical mode, which implies that the energies computed for each case would be different.

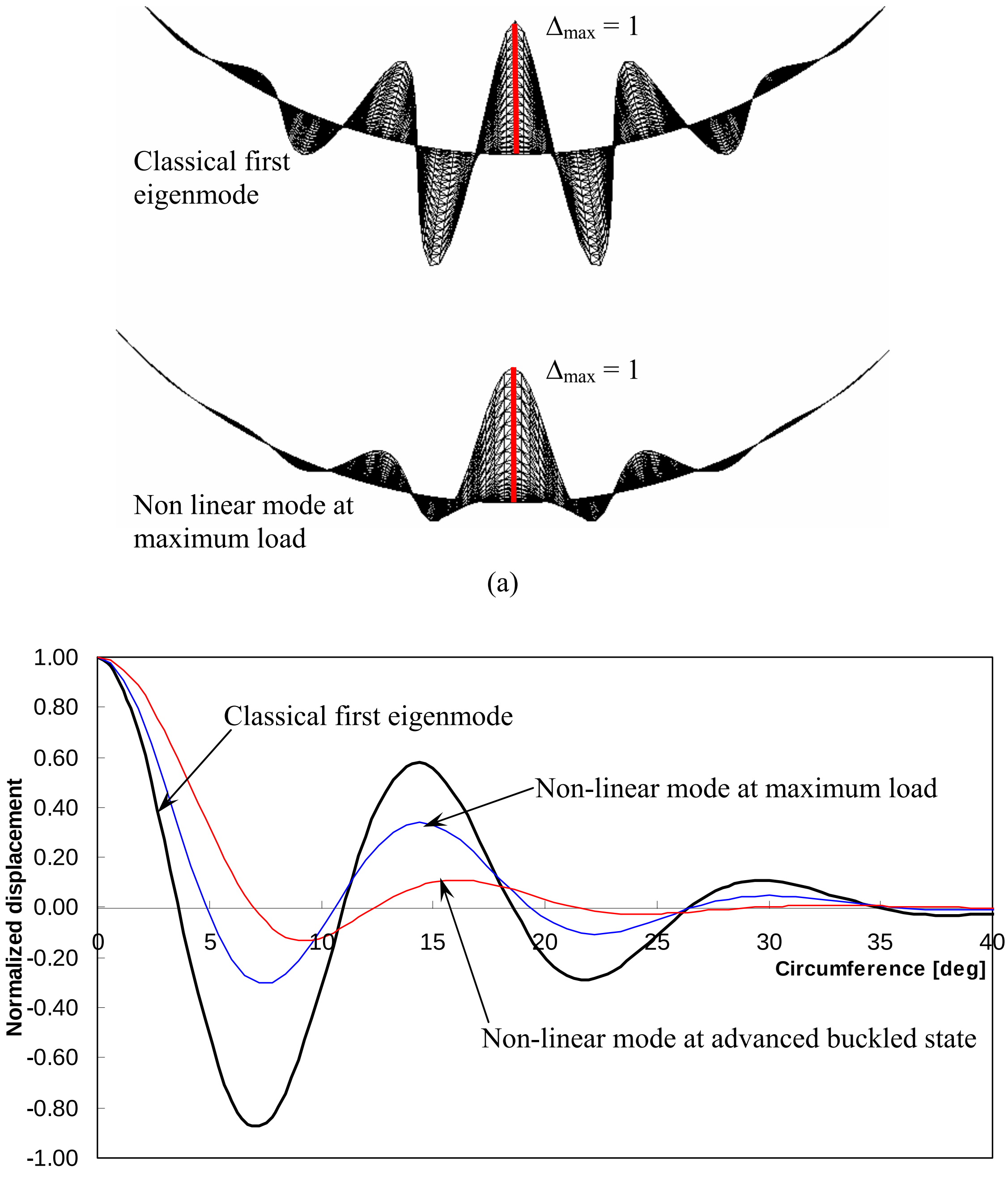

(b)

Figure 5.16. Mode comparison for model M1.

5.4.2 CHANGE IN THE MODE NORMALIZATION TO COMPUTE THE ENERGY

To understand the reasons of the discrepancies in the results, we write the classic eigenvalue problem as:

$$\Phi_1^T[\mathbf{K} - \lambda^C \mathbf{K}^G(N^F)]\Phi_1 = 0 \tag{5.5}$$

where $\Phi_1{}^T$ is the first eigenmode in the classic eigenvalue analysis, K is the stiffness matrix, K^G is the geometric matrix assembled with the contributions of the initial stresses N^F in the fundamental state; λ^C is the classical critical load. Matrix K has a membrane (K^m) and a bending (K^b) component, thus:

$$\Phi_1^T[(\mathbf{K}^m + \mathbf{K}^b) - \lambda^C \mathbf{K}^G(N^F)]\Phi_1 = 0 \tag{5.6}$$

Next, the membrane stiffness is eroded in the reduced eigenproblem, so that the lower bound should be computed as:

$$\Phi^{*T}[(\mathbf{K}^b) + \lambda^* \mathbf{K}^G(N^F)]\Phi^* = 0 \tag{5.7}$$

where Φ^{*T} is the mode in the lower bound state and λ^* is the reduced critical load. Both expressions can be written in terms of computable energies as:

$$\Phi_1^T\ [\mathbf{K}^m + \mathbf{K}^b]\ \Phi_1 = \lambda^C\, \Phi_1^T\ [\mathbf{K}^G(N^F)]\ \Phi_1 \tag{5.8}$$

$$\Phi^{*T}[\mathbf{K}^b]\ \Phi^* = \lambda^*\, \Phi^{*T}[\mathbf{K}^G(N^F)]\Phi^* \tag{5.9}$$

It is possible to compute the left term in equation 5.8, which is the energy with the complete membrane and bending stiffness. For the same equation, but in the right term, it is possible to obtain the classical eigenvalue λ^C by solving the eigenproblem. The energy term involving the geometric matrix is not easy to compute because, although the modes are known from the classical eigenproblem, the geometric matrix K^G is not explicitly available in ABAQUS (2002). In this case, a different normalization of the eigenvector, similar to what is used in structural dynamics, is to let Φ_1^T $[K^G (N^F)]$ $\Phi_1 = 1$. Before the normalization the scalar

$$\Phi_1^T [\mathbf{K}^G (N^F)]\ \Phi_1 = \psi \tag{5.10}$$

is used to normalize this term in a way that the energy involving the geometric matrix becomes one. Thus, equation 5.8 takes the following form:

$$\Phi_1^T [\mathbf{K}^m + \mathbf{K}^b]\ \Phi_1 = \lambda^C \psi \tag{5.11}$$

After normalization, we get a mode $\bar{\Phi}_1 = \Phi_1 / \sqrt{\psi}$, and:

$$\frac{\Phi_1^T}{\sqrt{\psi}} [\mathbf{K}^m + \mathbf{K}^b]\ \frac{\Phi_1}{\sqrt{\psi}} = \lambda^C \tag{5.12}$$

From equation 5.12, ABAQUS (2002) can compute the energy Φ_1^T $[K^m + K^b]$ Φ_1, as well as λ^C; then, the normalization factor ψ is calculated from those values as:

$$\psi = \frac{\Phi_1^T [\mathbf{K}^m + \mathbf{K}^b]\ \Phi_1}{\lambda^C} \tag{5.13}$$

Repeating the same procedure in equation 5.9, we get:

$$\Phi^{*T}\ [\mathbf{K}^G (N^F)]\ \Phi^* = \rho \tag{5.14}$$

Then, the reduced eigenproblem in equation 5.9 becomes:

$$\Phi^{*T} [\mathbf{K}^b]\ \Phi^* = \lambda^* \rho \tag{5.15}$$

or else:

$$\frac{\Phi^{*T}}{\sqrt{\rho}}[\mathbf{K}^{b}]\frac{\Phi^{*}}{\sqrt{\rho}} = \lambda^{*} \tag{5.16}$$

Notice that the normalization factors ρ and ψ are quite different ($\rho \neq \psi$), as will be shown in Figures 5.17 and 5.18. There are two unknowns in equation 5.15: The reduced eigenvalue λ^*, which is the lower bound and the mode Φ^* for such reduced eigenvalue. Notice that the main objective of this proposed procedure is to find λ^* as well as Φ^* without using non-linear imperfection analysis. Then, with these unknowns it is not possible to find the energy in both sides of equation 5.15.

First, let us assume that the reduced eigenmode Φ^* is available from the non-linear analysis. Then, the left side of equation 5.15 can be computed. However, in the other side, even with the assumed Φ^*, ρ is also a function of matrix $\mathbf{K}^G$. This matrix is the same as that used in equation 5.8 because the lower bound must occur along the same fundamental path as the classical critical load, so that the initial stresses in both states must be the same (See Figure 4.1 in Chapter 4). But, as mentioned before, $\mathbf{K}^G$ is not directly available, thus becoming an obstacle to the computations and keeping the value of ρ as an unknown.

The most important unknown is still the reduced eigenvalue λ^* and although the term Φ^{*T} [K^b] Φ^* in equation 5.15 can be computed, the absence of λ^* or ρ does not allow to proceed with the computations. An additional condition is needed to overcome that restrictive situation. The key limitation is that ABAQUS (2002) does not allow the user to compute K^G individually and extract that result separately. Regardless of this limitation, the knock-down factor can be expressed in the form:

$$\eta = \frac{\lambda^*}{\lambda^C} = \frac{\psi}{\rho} \frac{\Phi^{*T}[\mathbf{K}^b]\,\Phi^*}{\Phi_1^T[\mathbf{K}^m + \mathbf{K}^b]\,\Phi_1} \tag{5.17}$$

From this last equation, except for ρ, it is possible to compute all the other terms and the reduction factor would be only a function of a constant multiplied by the inverse of ρ, that is:

$$\eta = \frac{\lambda^*}{\lambda^C} = \frac{1}{\rho} C \tag{5.18}$$

where the constant C is:

$$C = \psi \frac{\Phi^{*T}[\mathbf{K}^b]\,\Phi^*}{\Phi_1^T[\mathbf{K}^m + \mathbf{K}^b]\,\Phi_1} \tag{5.19}$$

Graphically, equation 5.18 is an hyperbola and contains the values of the normalization factors ψ and ρ. If we rewrite the constant C remembering that:

$$\left(\frac{1}{\alpha}\mathbf{K}^m + \mathbf{K}^b\right) \rightarrow \mathbf{K}^b \text{ as } \alpha \rightarrow \infty \tag{5.20}$$

Substituting equation 5.20 into 5.19, we get:

$$C = \psi \frac{\Phi^{*T}\,[\frac{1}{\alpha}\mathbf{K}^m + \mathbf{K}^b]\;\Phi^*}{\Phi_1^T\;\;[\mathbf{K}^m + \mathbf{K}^b]\;\;\Phi_1} \tag{5.21}$$

Equation 5.21 substituted into equation 5.18 leads to a family of hyperbolas for different values of the reduction factor α, which are illustrated in Figures 5.17 and Figure 5.18 for models M1 and M4 respectively. For our purposes, it is interesting to find the limiting values of ψ and ρ to predict accurate values of η as geometry changes. In the graphs, ψ^C indicates the value for which C is computed with α equal to one, say with no membrane stiffness reduction. ρ^C indicates the value of C for a large reduction in the membrane stiffness, say $\alpha \rightarrow \infty$. Then, ρ^* must be between these two values, which is the value that satisfies equation 5.18 for a correct lower bound critical load.

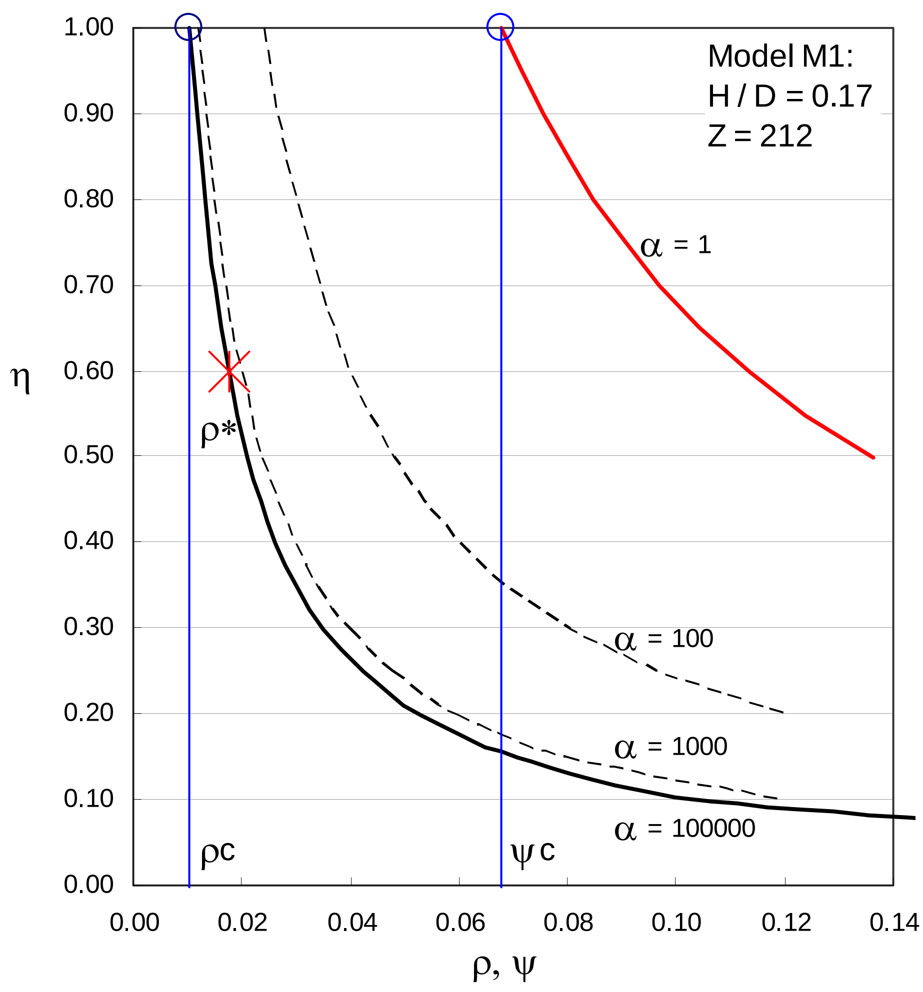

Figure 5.17. Variation of η as a function of ψ, ρ and the membrane reduction coefficient α, for model M1.

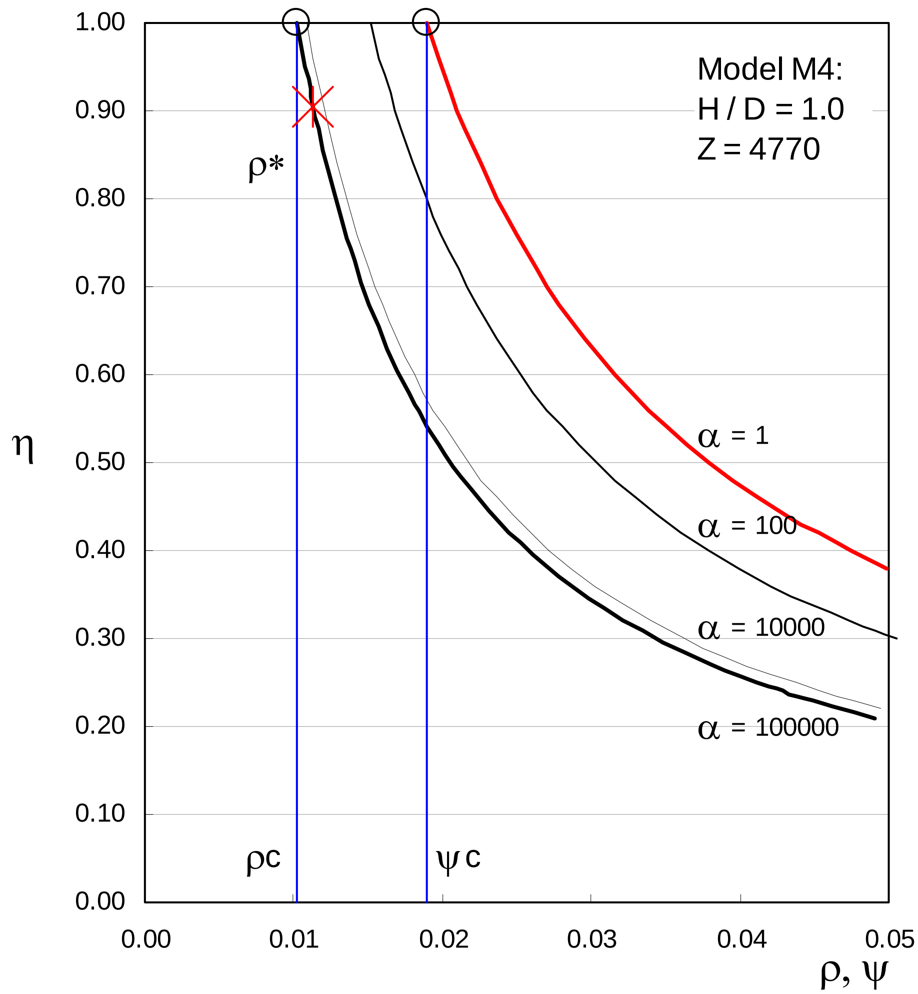

Figure 5.18. Variation of η as a function of *ψ, ρ* and the membrane reduction coefficient α, for model M4.

As previously mentioned, an additional condition is needed to find that value in absence of the capability of computing using $\mathbf{K}^G$ and the assumed mode Φ^*, but this condition is not available from the formulation. However, from Figures 5.17 and 5.18, in the range $\psi^C - \rho^C$, every value of ρ can be normalized as:

$$\bar{\rho} = \frac{\rho - \rho^C}{\psi^C - \rho^C} \tag{5.22}$$

Particularly, for ρ^* there is a normalized value $\overline{\rho}*$, given by:

$$\overline{\rho}* = \frac{\rho * - \rho^C}{\psi^C - \rho^C} \tag{5.23}$$

This normalized coefficient indicates how distant is ρ^* from ρ^C according the model and it is computed for open tank models in order to see if it changes as the geometry and the knock-down factor change.

For open tank models, from Table 5.6 and Figure 5.19(a), it is seen that $\overline{\rho}*$ is about 0.13 and seems to be almost constant for different geometries (described by Z or H/D) and for expected values of η obtained from the geometric non-linear analysis. Normalized hyperbolas for all the open tank models are depicted in Figure 5.19(b), where each model is characterized by a different curve and a different knock-down factor. However, for all the curves, the normalizing factor is defined by an almost constant value of $\overline{\rho}*$.

The same normalization was implemented in three models of cone roof tanks. Particularly, for models MC2, MC4 and MC6, Table 5.7 and Figure 5.20(a) summarize the computed values of $\overline{\rho}*$ which remain almost constant at about 0.32 for all models. Different from the case of the open tanks models, notice that in Table 5.7, the knock-down factor η is practically the same. Additionally, the normalized hyperbolas shown in Figure 5.15(b) are almost coincident. The cause may be that the models considered have similar deflected patterns in the buckled zone, which in turns has the same thickness configuration and lead to almost identical classical eigenvalues. Also, the non-linear behavior is similar for the three models as illustrated previously in Figure 5.6

Table 5.6. Normalized factor for open tank models.

Model	H/D	Z	η	$\bar{\rho}^*$
M1	0.17	212	0.598	0.1228
M2	0.25	417	0.647	0.1324
M3	0.50	1431	0.718	0.1379
M4	1.00	4770	0.904	0.1248

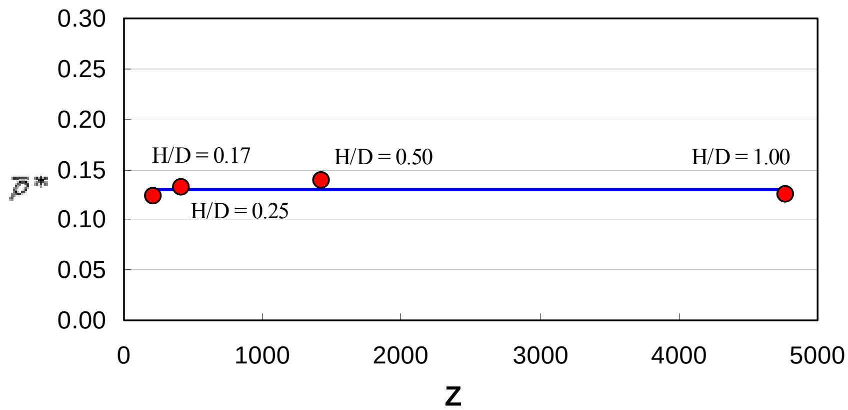

(a)

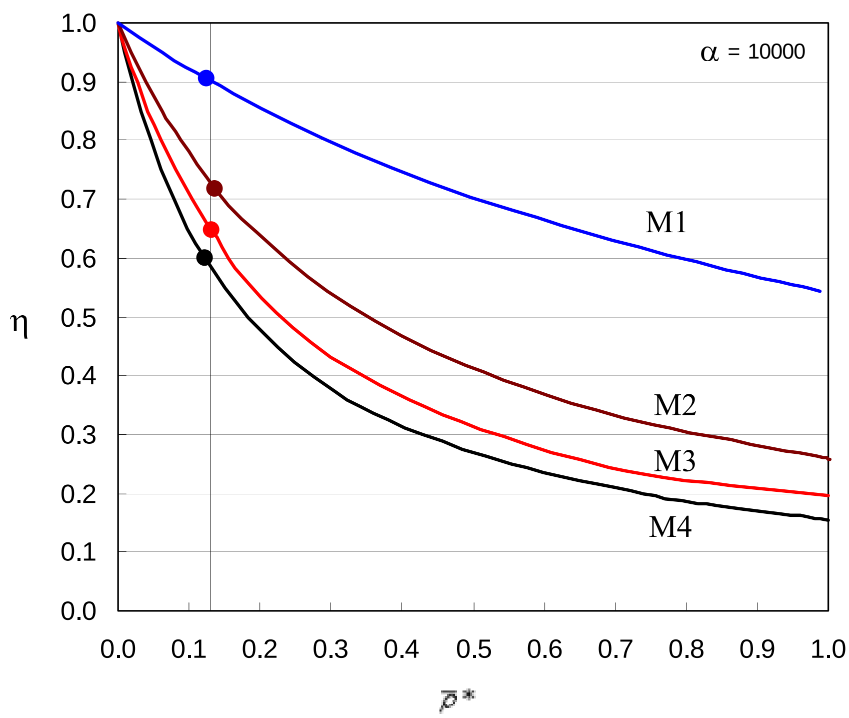

(b)

Figure 5.19. (a) Variation of $\bar{\rho}^*$ as a function of H/D and Z. (b) Variation of η as a function of $\bar{\rho}^*$, for all open tank models.

Table 5.7. Normalized factor for cone roof tank models.

Model	H/D	η	$\bar{\rho}^*$
MC2	0.63	0.606	0.3082
MC4	0.79	0.603	0.3316
MC6	0.95	0.605	0.3205

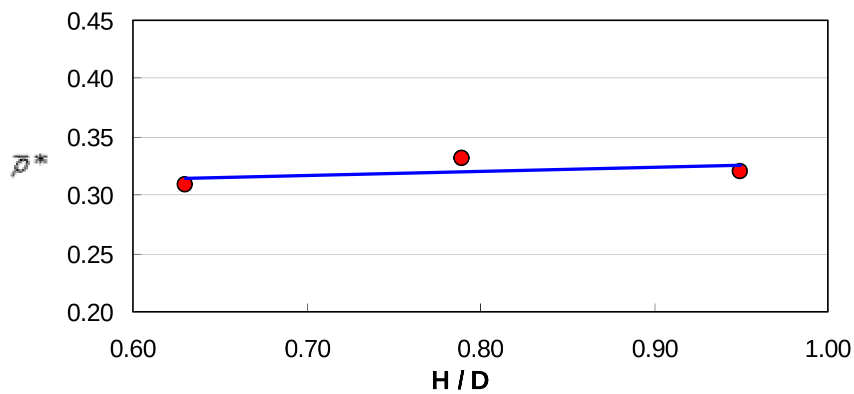

(a)

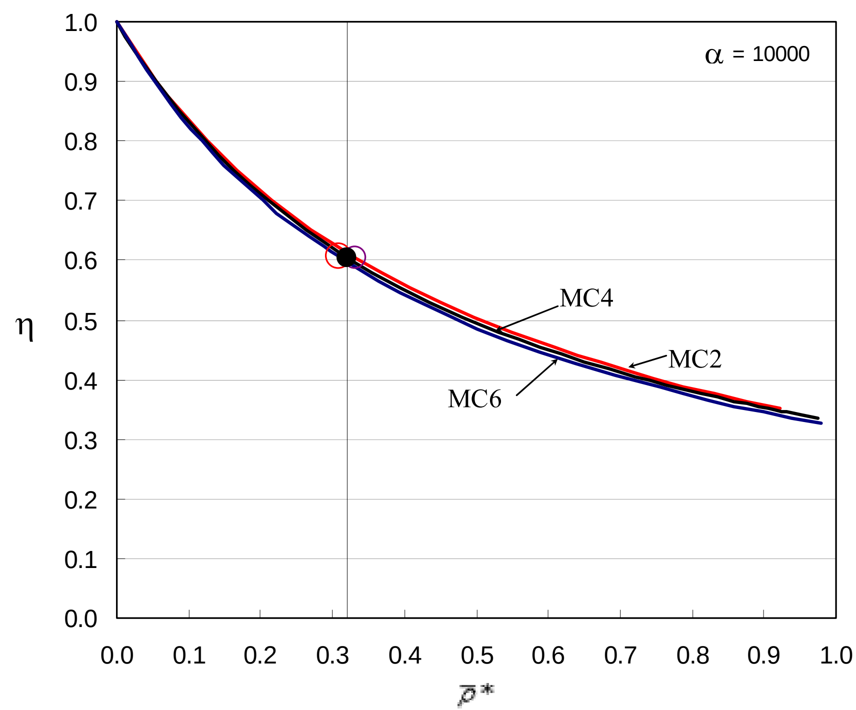

(b)

Figure 5.20. (a) Variation of $\bar{\rho}^*$ as a function of H/D. (b) Variation of η as a function of $\bar{\rho}^*$, for selected cone roof tank models.

From this proposed normalization in the range of $\psi^C - \rho^C$, it is possible to see that the change from the classical eigenmode to the reduced eigenmode (obtained in this case from a geometrically non-linear analysis) follows a uniform pattern described by the uniformity in the values of $\overline{\rho}\,*$. These values indicate the fraction necessary to add to the classical ρ^C to obtain the true ρ^* and consequently the right knock-down factor η for each model.

Clearly, in this alternative procedure to improve the results obtained previously for wind pressures, it is necessary to compute a non-linear path for a high amplitude imperfection (typically ξ / t = 1 or 2) in order to determine the mode and the maximum load reached for that level of imperfection. Furthermore, the procedure requires computing the energy for the reduced membrane stiffness in addition to computing energies using the classical eigenmode. All these operations were done here to understand the reason for the differences in the results on models under wind loads, but they cannot be implemented as a standard simple procedure to find the knock-down factor for the classical buckling load. This is a limitation of the method and it restricts its applicability to those cases in which the classical mode is quite similar to the reduced mode.

5.5 CONCLUSIONS

From the results obtained in the previous sections using a general purpose finite element code and a lower bound buckling formulation, it is possible to obtain a preliminary general conclusion. The proposed reduced energy method is not able to estimate the lower bound for wind pressures. The errors are smaller in the cone roof tank models than in the open top tank models. In the former, the non-linear imperfection-sensitivity analysis shows results that are similar for all models, but with a tendency to estimate a lower critical load than the predicted by the reduced energy method. Although the differences in the knock-down factors are not significant (about 10%), the lower bound predicted by the reduced energy method is unsafe for design.

The differences in the results for open top models are more important. Significant discrepancies were found in comparison with a non-linear analysis, and this suggests that the method is not capable of distinguishing changes in the geometry, and consequently changes in the slenderness. The main source of the discrepancies seems to be the shape of the mode used in the computations of the energy. This feature was verified from the geometrically non-linear analysis, and it is seen that the modal shape changes from the full membrane stiffness configuration to the reduced membrane configuration. This change in the modal shapes invalidates one of the main assumptions made in the formulation of the reduced energy method, as originally formulated by Croll (1975, 1995), namely that the buckling mode in the lower bound is the same as in the unreduced membrane stiffness state. Considering those observations, an attempt to apply an alternative way to improve the method using a code like ABAQUS (2002) requires at least one additional condition to find the correct knock-down factor. However, such condition is not available from the proposed formulation or requires additional computations which are useful to understand the differences in the results, but are beyond of the purpose of implementing the reduced energy method for wind loads in a simple way.

CHAPTER 6

NON-LINEAR DYNAMICS OF ABOVE-GROUND THIN-WALLED TANKS UNDER FLUCTUATING PRESSURES

6.1 INTRODUCTION

This chapter investigates the non-linear dynamic behavior and buckling of thin-walled steel tanks with a fixed conical roof under a deterministic simulation of wind pressures. Typical designs of short tanks make use of very thin shells, with ratios between the radius of the cylinder and the wall thickness (R/t) of the order of 1,500-2,000, and height to diameter ratios (H/D) of less than 0.5. Because of the slenderness of the shell, buckling has been reported under high winds or hurricanes (Flores and Godoy, 1998 and Flores and Godoy, 1999), and it is a major constraint in the design.

Most studies reported in the technical literature of buckling of tanks under wind are restricted to open tanks. In addition, the studies consider a static analysis of the problem and do not account for the possibility of any dynamic effect due to wind. However, wind gusts induce transient vibrations in the shell during short times, which may eventually lead to dynamic buckling.

In the design of tanks in the United States, wind gusts of 3 sec at 10 m above ground surface are considered, with wind velocities of 64 m/s in the Eastern Coast (ASCE-7-02, 2002). Preliminary results using wind pressures in the form of a rectangular impulse with 3 sec duration seem to indicate that the dynamic effects are not significant in terms of the buckling capacity of the shell. However, the question remains if pressure fluctuations within a 3 sec impulse may have a more damaging effect on the stability of the shell, and thus justify an numerical investigation of such fluctuations in wind records. This chapter addresses this question by means of a non-linear dynamic analysis of a specific tank with a conical roof.

The outline of the chapter is as follows: A revision of previous works is described in Section 6.2. The model of fluctuating pressure adopted in this work is described in Section 6.3. Such pressure model is applied to a theme structure described in Section 6.4. Section 6.5 deals with the dynamic response of the structure in the time domain, and in Section 6.6 the analysis is carried out in the frequency domain. Finally, conclusions are presented in Section 6.7.

6.2 LITERATURE REVIEW

There are numerous studies concerning the behavior of cylindrical shells under wind pressures. Most of them are focused in cylindrical tanks, open at the top and fixed at the base and they do not consider any type of conical, spherical or flat roof.

Gopalacharyulu and Johns (1973) developed an analytical model based in the Donell's shell theory to find functions of displacements, stresses and moments acting in the cylindrical shell due wind pressures applied statically. They used the analytical pressure distribution developed by Rish (1967) based on wind tunnels experiments in open cylinders under uniform speed winds, given by the equation:

$$\mathrm{P} = p_0 \sum_n a_n \cos(n\ \theta) \tag{6.1}$$

where p_0 is the pressure amplification factor at the windward meridian (θ = 0º); and a_n are the Fourier decomposition factors for the n terms of the expansion series. This equation is considered valid through the complete height of the cylinder. With this pressure distribution, the author of that work calculated the variation of the top displacement for different radius to thickness (R/t) ratios. They also obtained the variation of stresses and strains along the height for the same radius to thickness ratios.

Kundurpi *et al*. (1975) evaluated the instability in scaled models due to wind pressures generated in a wind tunnel. They developed an analytical tool to find the buckling critical pressure based on the second variation of the potential energy of the system. In this study, as well as in the one mentioned before, the authors did not considered non-linearity, dynamic effects or imperfections in the shell. The results reported are only for critical pressures using different radius to thickness ratios. The values found were slightly higher than the pressures obtained experimentally which results an overestimation of the critical load based in the design criteria at that time.

Other study on instability of cylindrical shells is due to Jerath and Sadid (1985). These authors developed an analytical model to evaluate the static instability of orthotropic cylindrical shells (representative of corrugated steel shells) under lateral wind pressures. They analyzed open and closed at the top tanks using the following wind pressure distribution:

$$P_r = P_0 \sum_m \sum_n \rho_{mn}\, x^n \cos(m\theta) \qquad (6.2)$$

This pressure was assumed to act radially on un-deformed cylinder. P_0 is a reference pressure given by $P_0 = \gamma V^2/ 2g$; V is the wind velocity; x is the axial coordinate and ρ_{mn} are the pressure coefficients taken from the studies of Maderpach and Kamat, (1979) and Purdy *et al*. (1967), for open and closed cylinders, respectively.

Several of the most recent studies on instability of tanks come mainly from Europe, particularly from England and Germany. Among them, Greiner (1998) collected the results on pressures distributions obtained by many researchers for a variety of cylindrical configurations. Such collections included the incidence of conical and spherical roofs, and cover not only the pressure on the cylinder, but also on the roof. Although most of the results reported are for silos, which are higher and slender than the tanks considered in this work, it is interesting to consider the distributions of wind pressures on the roof considering the lack of information available on this feature.

Greiner (1998) also analyzed the difference between the models of instability as a function of the height of the shell and the inclusion or not of the non-linear geometry in the formulations. He concluded that its addition significantly changed the buckling mode in higher cylinders (like silos), but it practically had not a great effect on short cylinders like the typical tanks considered here.

Flores and Godoy (1998) evaluated the instability of open tanks under hurricane wind pressures using finite element models. They considered the deterministic wind distribution given by the equation developed by Rish (1967) with its coefficients and the coefficients given by the code ACI-ASCE (1995), and did not observe significant changes in the results. In that study, the evaluation of the critical pressure using classical bifurcation analysis predicted similar results than those calculated using non-linear static analyses. However, the introduction of imperfections in the non-linear analysis produced a drop in the critical load. They performed non-linear dynamic analyses in order to evaluate the influence of inertia effects for constant amplitude pressure. Considering the studies to be carried out in this chapter, it is interesting the criteria employed by the authors to find the dynamic buckling load. Particularly, they used the criteria proposed by Budiansky and Roth (1962) and obtained the response in the time domain by integrating explicitly the non-linear equations of motion. Through this procedure, they showed that inertial effects do not influence the response of the structure and that the inclusion of imperfections did not significantly change the response.

In other work, Godoy and Flores (2002) reported the results for short open tanks under wind loads. There again, the study was restricted to static analyses, including classical bifurcation and non-linear procedures to find the lowest critical pressure as a function of the shell geometry.

For the work in this chapter, are interesting the results obtained recently by Portela and Godoy (2005). They reported wind tunnel experiments done to find wind pressure distributions on small scale tanks similar to those considered here, as well as the results obtained using the measured distributions in computational models of the same structures.

From this revision arises that the availability of studies on tanks with any type of roof are few or limited in their considerations regarding the influence of the roof on the behavior of the shell, or the behavior of the roof itself as a function of the wind distribution considered. On the other side, there are no results regarding the influence of fluctuations in the pressures due the variations in the wind speed. The few previous studies on this topic are restricted to constant amplitude loads. It is interesting to establish if the conclusions of Flores and Godoy (1998) can be extended to the case of closed tanks under non uniform spatial pressures.

6.3 WIND ACTION

Typical wind records measure wind velocity every 3 sec. Since no information is obtained for intervals of less than 3 sec, any fluctuations in the velocity (and in the consequent pressures on the structure) are eliminated from the data. Such information is not relevant for most types of structures, but for thin-walled tanks, it may be important in order to understand the nature of buckling. From the information provided by wind records, it seems that an adequate load configuration would be an impulsive pressure with 3 sec duration. The only studies reported in the literature including wind as an impulsive pressure on tanks have considered a constant pressure during 3 sec, or else a step variation (see for example Flores and Godoy, 1998 and 1999).

At present, there are no extensive records regarding the values or the nature of pressure fluctuations for periods less than 3 seconds, and the question remains open if it is necessary to obtain such data because it may have a significant influence on the behavior of a tank structure. To investigate the influence of such fluctuations on the dynamic response of the shell one can resort to computer simulations. This chapter reports the result of studies using geometrically non-linear dynamic analysis under impulsive loads with fluctuations in the pressure. The pressure fluctuations within a gust considered in this chapter are shown in Figure 6.1. There are two parameters involved in the definition of such pressures. First, the pressure fluctuation amplitude, P_f, and second, the fluctuation period, T_f. Non-dimensional quantities may be defined as $\tau = T_f / T_3$ and $\varphi = P_f / P_3$, where T_3 = 3 sec and P_3 is the average value of the wind gust pressure.

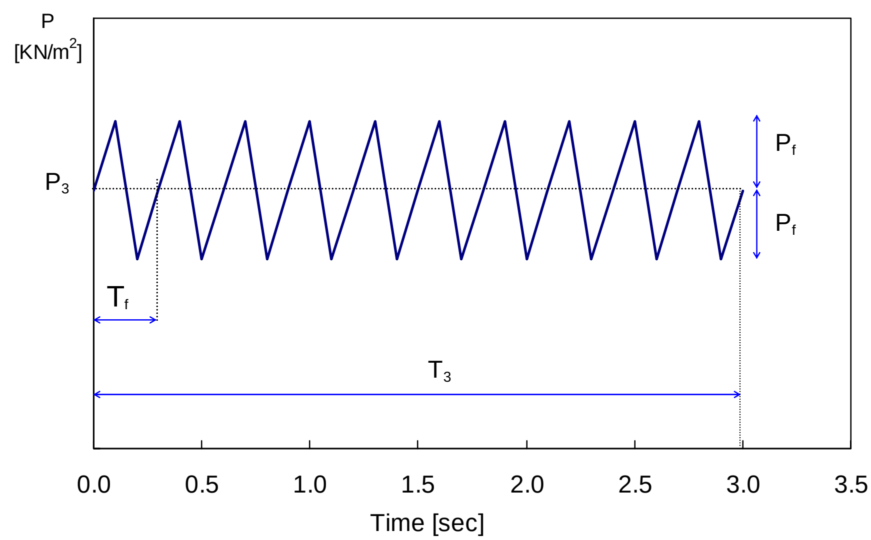

Figure 6.1. Model of pressure variation with time. Rectangular impulse with fluctuations. T_f: period of the fluctuation; T_3: 3 sec interval; P_f: fluctuation amplitude of the; P_3: average amplitude pressure.

To carry out the computations, it is necessary to assume a pressure distribution on the roof and in the cylindrical shell. For the roof, a pressure distribution reported by Macdonald *et al*. (1988), which was obtained from wind-tunnel experiments, has been adopted. Figure 6.2(b) shows the original contours for the pressure distribution on the tank roof and Figure 6.2(d) shows simplified contours of the roof pressures used in the computations. For the cylindrical shell there are several distributions reported by Macdonald *et al*. (1988) and Sabransky and Melbourne (1987), but their pressure distributions are for higher H/D relations than those used in this study. An alternative distribution is given by Rish (1967), and has also been used by Flores and Godoy (1998). This was adopted here for the computations. Portela and Godoy (2005) reported new pressure distributions for cylindrical shell with H/D = 0.43 as well as for the conical roof (Figure 6.2(c)). However, those pressure distributions are less demanding in terms of pressure than those adopted initially here. Figure 6.2(a) shows a comparison between the pressure coefficients (Cp) distributions reported by other researchers and the one used in this study.

The current model assumes that the pressures are applied simultaneously on the complete surface of the structure. This investigation considers pressures on an isolated tank in an open terrain. It is worthwhile to mention that several factors influence wind pressures in real tanks, such as topographic effects, roughness of the terrain, interaction with other tanks, etc. The influences of such factors are topics for future research. Additionally, a more refined model should include the change in pressures as wind flows on the surface of the shell; however, this refinement is outside of the scope of the present investigation.

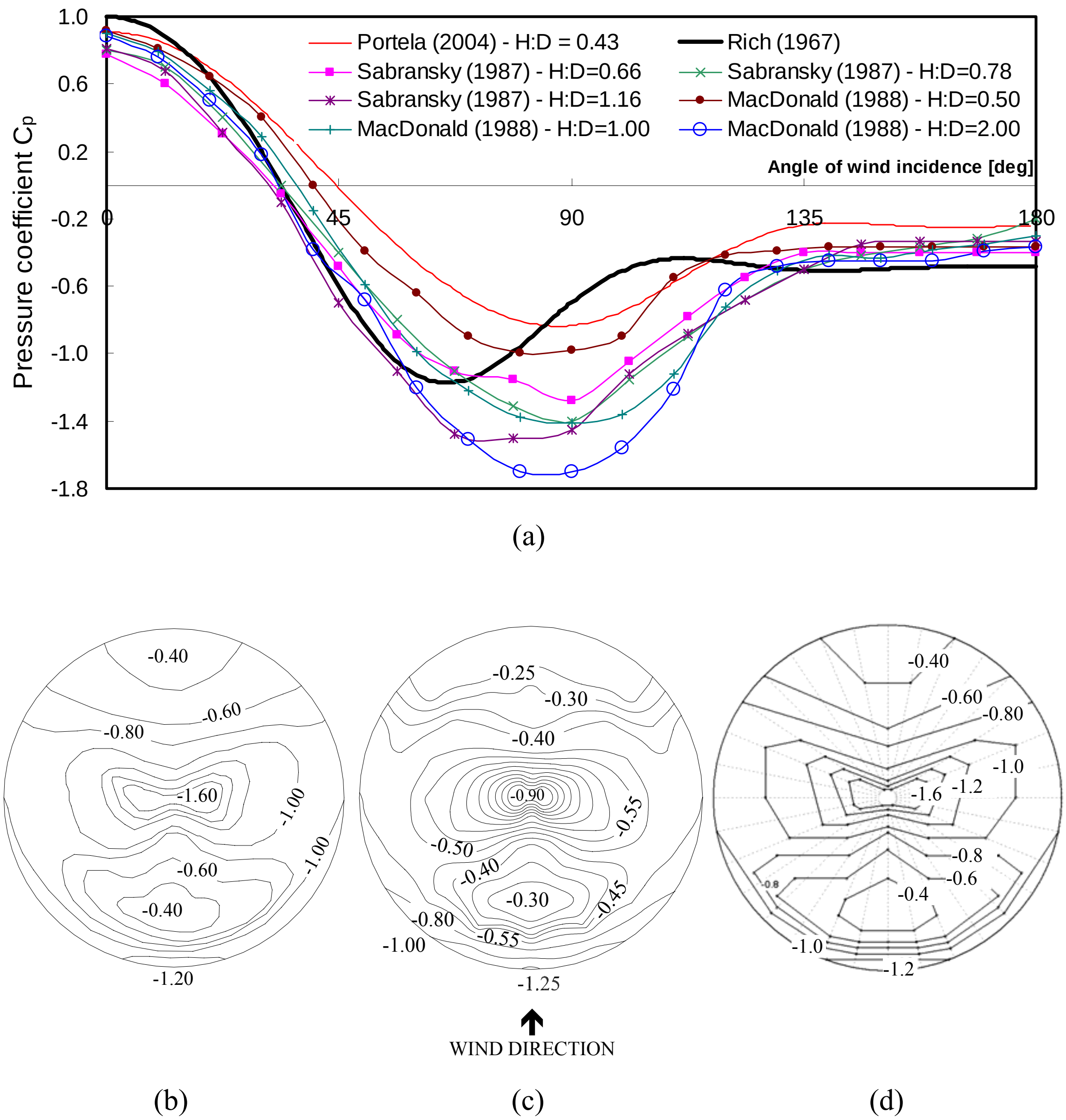

Figure 6.2. (a) Pressure coefficient distributions on the cylindrical shell (b) Contours of pressure coefficient distribution on the conical roof reported by Macdonald *et al*. (1988) (c) Contours of pressure coefficient distribution on the conical roof reported by Portela and Godoy (2005); (d) Contours of wind pressures coefficient used in computations.

6.4 THEME STRUCTURE AND COMPUTATIONAL MODEL

The theme tank investigated in this chapter is representative of typical tanks found in the Caribbean Islands and in the eastern coast of the United States. Their geometry and dimensions are shown in Figure 6.3(a). The same geometry has been employed by Godoy and Sosa (2003) for the analysis of static buckling due to support settlement,.

The tank is modeled by means of a finite element discretization. Approximately 12,000 quadrilateral and triangular linear shell elements are used to model both the cylindrical shell with a tapered wall and the conical roof. Additionally, the rafters that support the conical shell are included in the model; they have the shape and dimensions found in usual real tanks. Specifically, in this research a W8×13 steel section according to AISC (2001) code was used to model the rafters. The rafters were modeled with quadrilateral linear shell elements and placed in a radial configuration supporting the conical roof as shown in Figure 6.3(b). The tank is assumed to be fixed at the base and has additional boundary conditions at the top of the conical roof. To simulate the presence of a central column a series of constraints in the vertical displacements of the rafters are placed, which allow free translations in the horizontal plane and free rotations. The junction between the cylindrical wall and the conical roof is continuous.

Geometrical non-linear dynamics analyses have been carried out to evaluate the response of the tank to spatial and temporal variation of the pressure. For this kind of analysis, explicit integration of the equation of motion is performed using ABAQUS/Explicit (ABAQUS, 2002). Very small time increments are necessary to make the algorithm stable. The constitutive material is elastic with modulus of elasticity E = 206 GPa, Poisson's ratio ν = 0.3, and density ρ = 7800 kg/m^3.

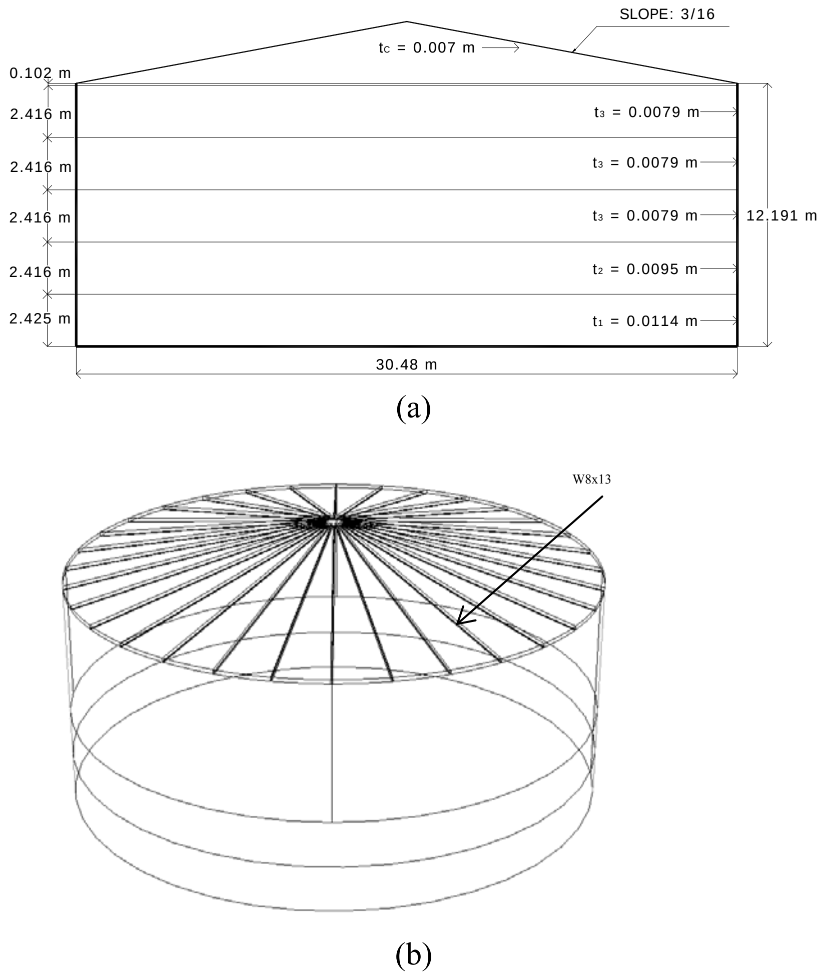

Figure 6.3. Details of the tank considered in the analyses: (a) Dimensions; (b) Overview of conical shell and configuration of the rafters.

6.5 NON-LINEAR DYNAMIC RESPONSE

6.5.1 RESULTS FOR PERFECT GEOMETRY WITHOUT DAMPING

The dynamic buckling criterion employed in this work is due to Budiansky and Roth (1962). This is a qualitative criterion and requires the computation of the transient geometrically non-linear response of the shell for different levels of dynamic pressures. The main variables involved in the criterion are the dynamic pressure and a displacement (or a displacement component). Dynamic buckling occurs if, for a small increment in the load, there is a large increment (at least one order of magnitude) in the transient displacements at a given time. In other words, dynamic buckling occurs at the lowest pressure level that produces a fast transition from small to large transient displacements. This criterion requires expensive computations, i.e. the geometrically non-linear transient response of a system with many degrees of freedom, and many trials are necessary to find the dynamic buckling load. Other publications have adopted this criterion for the evaluation of a dynamic buckling load in tanks (see for example Flores and Godoy, 1998 and 1999, and those cited there).

First, let us consider a pressure distribution without any fluctuation, and with a 3 sec time of application of the load. The space distribution of pressures coefficients is shown in Figure 6.2. To increase the values of pressures at all points, a non-dimensional scalar parameter λ is used. The pressure configuration in Figure 6.2 is for $\lambda = 1$. The relation between velocity and pressure is that given by ASCE-7-04 (2004). Figure 6.4(a) shows the non-linear dynamic response computed numerically. For $\lambda = 2.50$ and $\lambda = 2.51$

the oscillations have small amplitude and will vanish in the presence of material damping. The lowest value of λ for which divergent oscillations are computed is λ = 2.515 (or wind gust velocity of about 64.4 m/s or 144 mph), in which there are small amplitude oscillations up to a time t = 2.16 sec, and then the amplitude increases by two orders of magnitude (increasing from 7mm to 150mm). As the load is increased, i.e. λ = 2.52 or λ = 2.60, the structure becomes unstable at earlier times. According to the criterion of Budiansky and Roth (1962), the dynamic buckling load is λ_D = 2.515 and finding this value involves a sequence of computations for different load levels. The deflected shape of the shell, as it becomes unstable at the load λ_D, is shown in Figure 6.4(b) at the onset of instability (t = 2.16 sec), and at an advanced buckled state (t = 3 sec) in Figure 6.4(c). The practical significance of the wind velocities computed depends on the location of the tank, and these are not uncommon velocities in the Caribbean region and in the eastern coast of the United States where hurricane winds can reach considerable high values.

Second, to examine the influence of the fluctuations in time of the pressure, let us consider the case with φ = 0.1 and τ = 0.25. The procedure to identify dynamic buckling was repeated and yielded a value of λ_D = 2.315 (or wind velocity of about 61.3 m/s or 137 mph), that is, a smaller multiplier than in the first case. For a given value of η, the value of λ_D is seen to be dependent on τ, so that it becomes important to understand the relation between λ_D and τ.

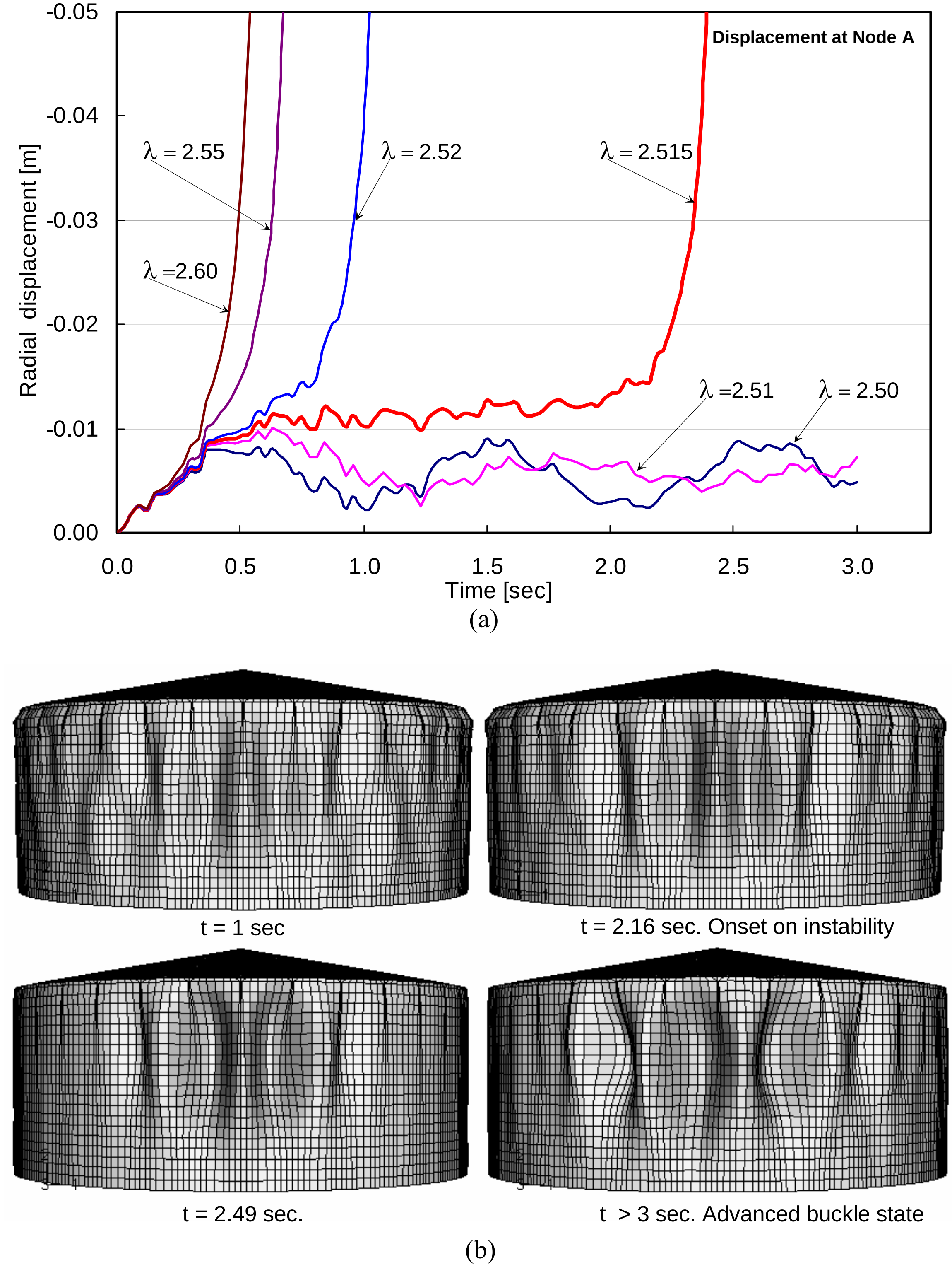

Figure 6.4. Tank under constant impulsive load: (a) Time response for different load levels (b) Deflected shapes at four instant times.

The natural frequencies of the tank were computed with ABAQUS/Standard (ABAQUS, 2002) and are listed in Table 6.1. For the present case, the highest period (lower frequency) is $T_N = 0.3562$ sec, which is smaller than the period of the excitation of both cases considered previously. Thus, a fluctuation having $T_f = T_N$ ($\tau = 0.3562/3 = 0.1187$ and $\varphi = 0.1$) would be an unfavorable load case for the structure, since there is coupling between the frequencies of the load and the structure. The results of transient displacements for $T_f = T_N$ are plotted in Figure 6.5(a). The dynamic buckling modes at the onset of instability and for an advanced buckled state are given in Figure 6.5(b) and 6.5(c) respectively. The dynamic buckling load results in $\lambda_D = 2.34$ (or a wind velocity of about 61.8 m/s or 138 mph), which is smaller than the value obtained for constant amplitude pressure model, but larger than the value for the second model with $\varphi = 0.1$ and $\tau = 0.25$.

Table 6.1. Natural frequencies and periods of the tank model.

Mode	f [Hz]	T [sec]	Mode	f [Hz]	T [sec]	Mode	f [Hz]	T [sec]
1	2.8077	0.3562	11	3.7563	0.2662	21	4.7698	0.2097
2	2.8134	0.3554	12	3.7784	0.2647	22	4.8082	0.208
3	2.9323	0.341	13	3.7801	0.2645	23	4.8694	0.2054
4	2.9349	0.3407	14	3.7853	0.2642	24	4.8974	0.2042
5	2.9642	0.3374	15	4.074	0.2455	25	4.9036	0.2039
6	2.9704	0.3367	16	4.107	0.2435	26	4.904	0.2039
7	3.1703	0.3154	17	4.3774	0.2284	27	4.9177	0.2033
8	3.1808	0.3144	18	4.416	0.2264	28	4.9191	0.2033
9	3.4571	0.2893	19	4.6372	0.2156	29	4.9591	0.2016
10	3.4661	0.2885	20	4.6706	0.2141	30	4.9638	0.2015

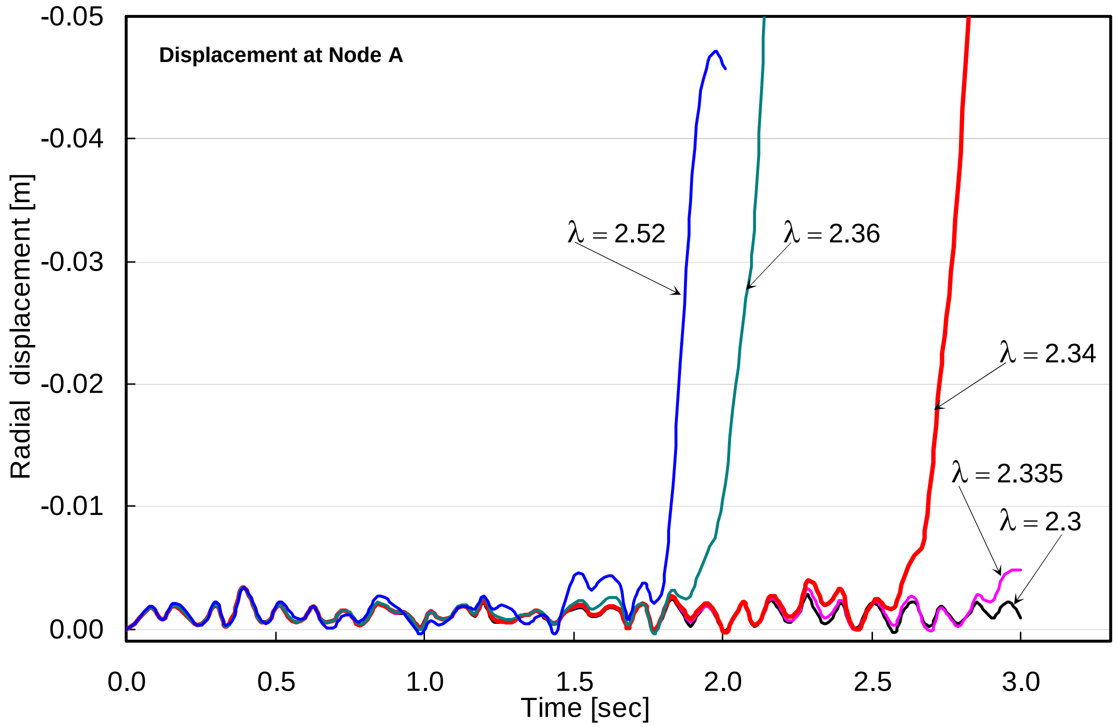

(a)

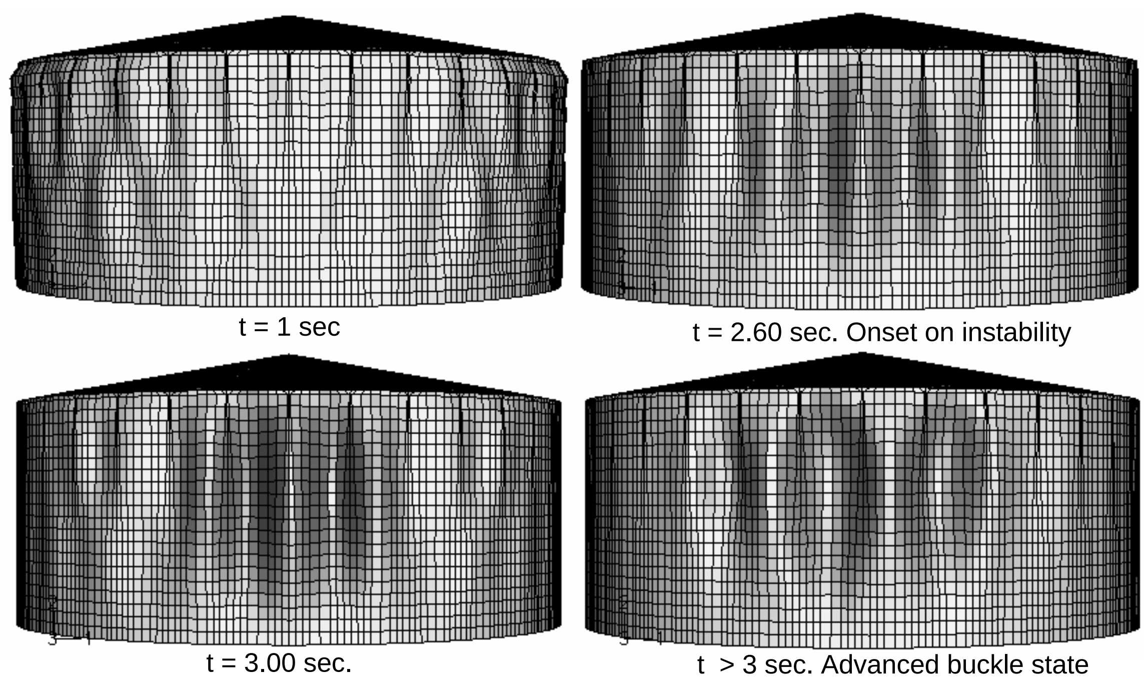

(b)

Figure 6.5. (a) Time response of tank with impulsive load and fluctuation with $T_f = T_N$ and $\varphi = 0.1$; (b) Deflected shapes at four instant times.

A more complete picture of the problem may be obtained from a parametric study in which τ is changed and the transient response is computed. The results are plotted in Figure 6.6 in terms of λ_D versus τ. First, it seems that the changes are not as drastic as one may imagine: the variations in λ_D are of the order of 10% with respect to the value for a rectangular pressure impulse. Second, the lowest values of λ_D are not necessarily associated to the lowest natural frequency of the shell. This is because the pressure pattern applied to the shell yields deflections that are not coincident with the fundamental mode of vibration of the tank.

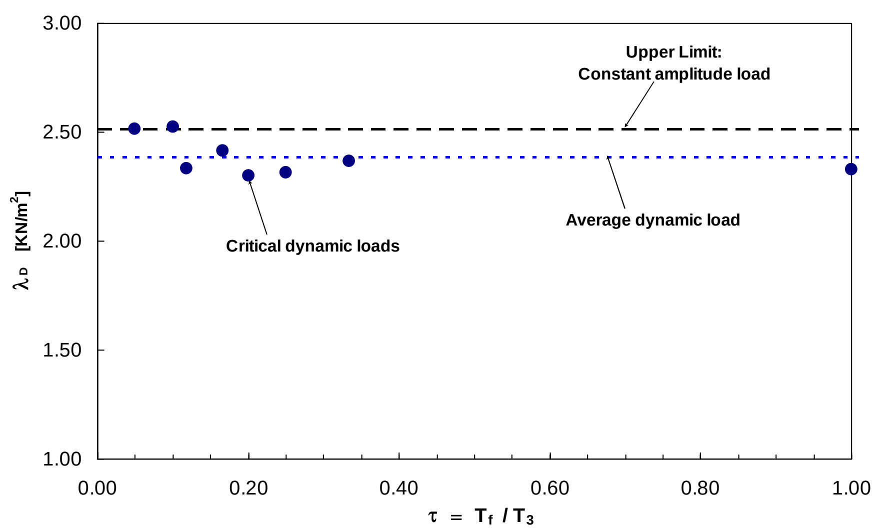

Figure 6.6. Critical dynamic load λ_D for different normalized load periods $\tau = T_f / T_3$ using $\varphi = 0.1$.

6.5.2 RESULTS INCLUDING DAMPING

All previous computations did not include damping. It is important to understand the influence of damping on the response. In the explicit integration of the equations of motion, it is useful to use the Rayleigh damping:

$$\zeta = \frac{\alpha_R}{2\omega_i} + \frac{\beta_R \omega_i}{2} \qquad (6.3)$$

It is usual to assume that the damping in this kind of structures is proportional to the mass matrix. In this case β_R can be considered null and the mass-proportional coefficient is:

$$\alpha_R = 2\omega_i\, \zeta \qquad (6.4)$$

To consider the influence of modes of frequencies up to ω_{25} = 4.9036 Hz (30.81 rad/sec) in a cylinder mode, and assuming the usual damping coefficient for steel structures of ζ = 3 %, the mass proportional coefficient is α_R = 1.848. For the pressure constant in time reported in Figure 6.4, the dynamic buckling load increased from 2.515 to 2.53, or a 0.6% increment. For the fluctuating pressure case shown in Figure 6.5, the effect of damping increased the dynamic buckling load from 2.34 to 2.40 (a 2.78% change). Because the influence is so small, it was decided to perform all the computations using zero damping.

6.5.3 RESULTS INCLUDING IMPERFECTIONS

The imperfection-sensitivity of buckling loads has not been addressed up to now. However, it is well known that imperfections play an important role in reducing the buckling load in static problems of tanks (Godoy and Flores, 2002 and Greiner and Derler, 1995). Small geometric imperfections, with an amplitude of the order of the minimum thickness of the shell (t_{min} = 7.9 mm), have been included in the analysis. The geometry of the imperfections was taken with the shape of the displacement pattern at the onset of dynamic buckling, which is significant only in the buckled region. For the imperfect shells, the non-linear dynamic buckling studies under fluctuating pressures were repeated for the same parameters (T_f = 0.3562 seg or τ = 0.1187 and φ = 0.1) used in Figure 6.5. A summary of the results is presented in Figure 6.7. The reduction in buckling load depends on the maximum amplitude of the imperfect shape, and for an amplitude equal to the top shell thickness (t_{min} = 7.9 mm), the reduction is about 30%. The shell under pressure constant in time and under fluctuating pressures is equally affected by the imperfections.

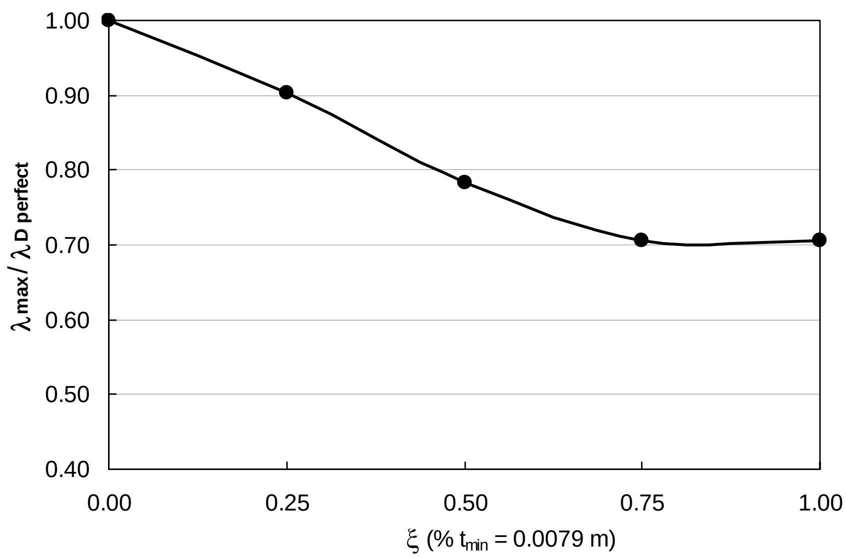

Figure 6.7. Summary of analysis of sensitivity to imperfections of λ_D for φ = 0.1 and T_f = 0.3562 seg.

The influence of the imperfections on the maximum dynamic load can be analyzed using the representation proposed by Budiansky and Roth (1962). This representation consists in taking the maximum displacement at the first cycle for different load levels and plotting such displacement versus the load that produced the maximum value. In this way, for low amplitude pressures, the maximum displacement has small values, but when the load increases, the maximum value increases to a point in which the difference between the maximum displacement produced by one load level compared with the maximum generated with a slightly lower load level is considerable great. One can perform this representation for different imperfections levels as indicated in Figure 6.8 and arrive to the lowest load that the structure is able to support without severe modifications in its original configuration. However, an imperfection of the order of the ¾ of the thickness of the shell is enough to produce an important drop in buckling strength (about 30%, as mentioned before). This is denoted in Figure 6.9 in which at the same time that the imperfection amplitude increases the maximum load decreases.

From Figure 6.9 it is possible to also see that the plateau that defines the dynamic buckling load is broad for small amplitude imperfections and as the imperfections amplitudes increase, the plateau tends to narrow. This feature can be observed in the time domain response for two levels of imperfections. For instance, Figure 6.8(a) shows the response for $\xi / t_{min} = 0.25$ and Figure 6.8(b) for $\xi / t_{min} = 1.00$. From these pictures, it is possible to see that the presence of imperfections modifies the way in which the shell vibrates. In Figure 6.8(a) the identification of the dynamic buckling load is practically evident, however in Figure 6.8(b) that is not possible. This behavior is represented in Figure 6.9 in a compact style.

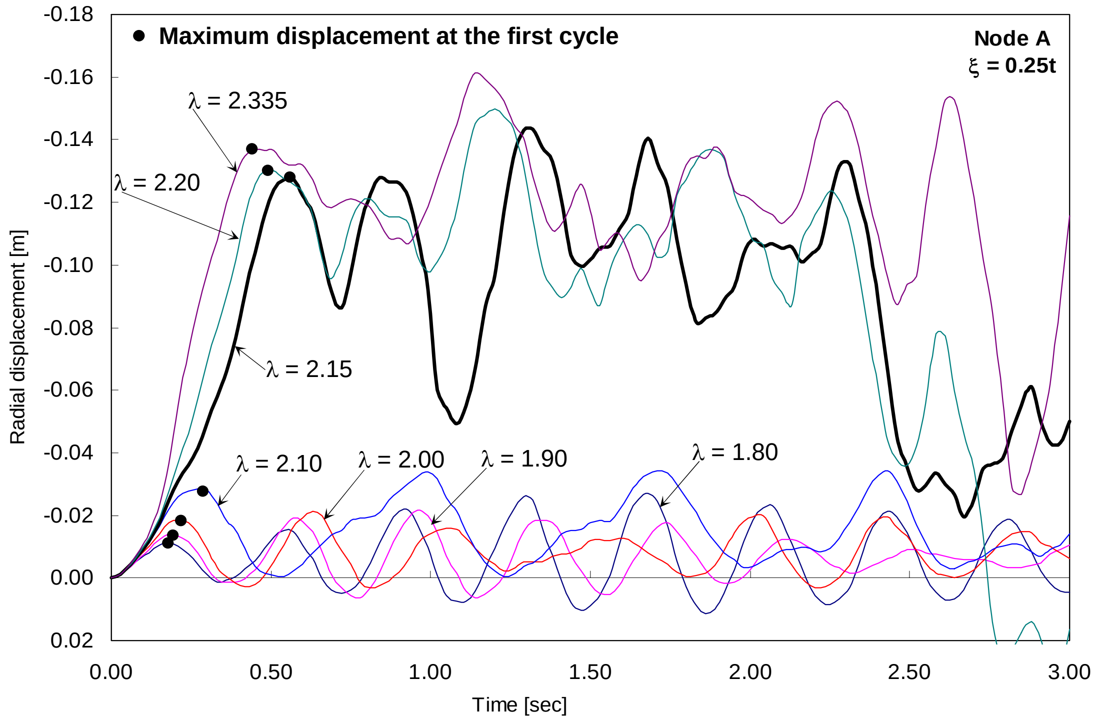

(a)

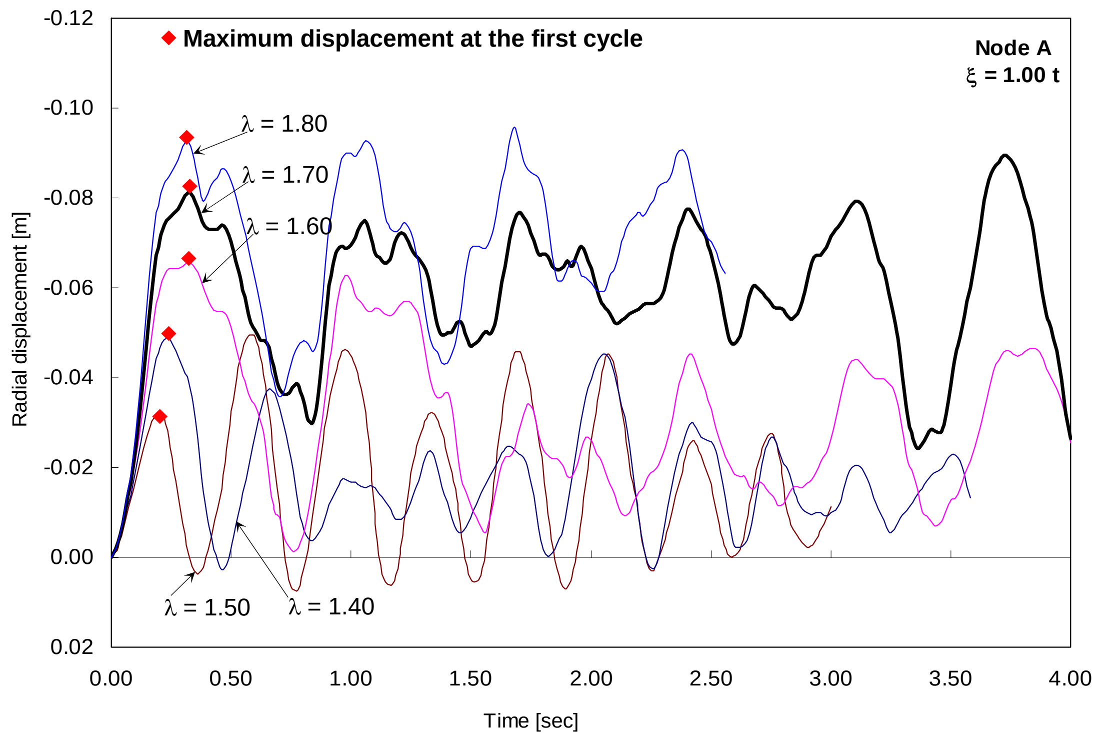

(b)

Figure 6.8. Time response for two levels of imperfections for a tank with impulsive load plus a fluctuation with $T_f = T_N$ and $\varphi = 0.1$.

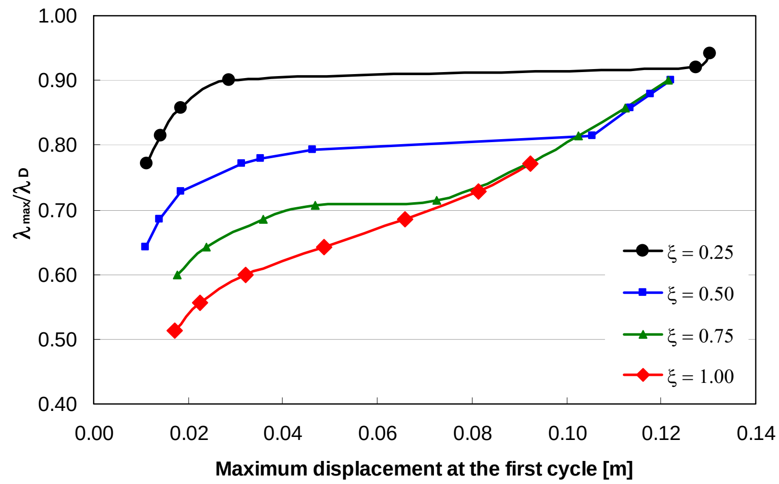

Figure 6.9. Dynamic buckling load for different levels of imperfections.

6.6 FREQUENCY DOMAIN ANALYSIS

A frequency domain analysis of the perfect shell for two time variations of the load has been carried out. They are rectangular impulse of 3 sec and λ = 2.515, and a fluctuating pressure with λ = 2.34 and T_f = 0.3562 sec (equivalent to an excitation frequency of 2.807 Hz, that is, the lowest natural frequency of the tank). These chosen pressures for the analysis made in this section are the lowest values for which the shell buckles before the 3 sec period.

The shell response computed for the duration of 10 sec is shown in Figure 6.10 at the location of maximum radial displacements of the shell. For the rectangular impulse, the shell has large oscillations when the load is removed and the oscillations continue in the absence of damping. Under a fluctuating load, on the other hand, there are two clearly identified stages: small amplitude oscillations when the load is applied until buckling occurs and oscillations about the deflected shape once the load is removed.

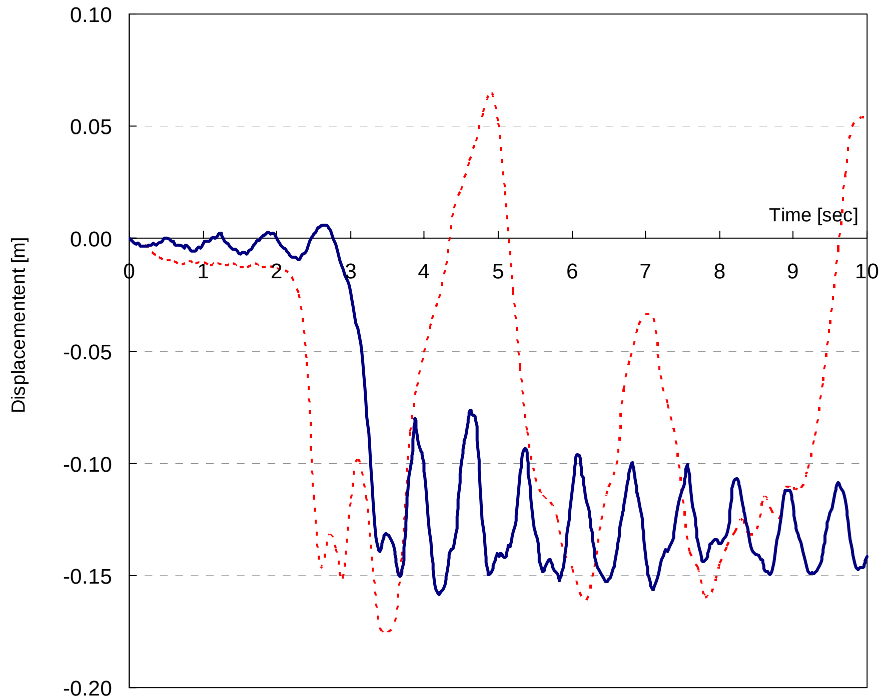

Figure 6.10. Maximum response of Node A recorded during 10 sec for constant load: — λ_D = 2.515 and fluctuating load: – – – λ_D = 2.34 (φ = 0.1, T_f = 0.3562 sec).

The Fast Fourier Transform (FFT) for the complete history of displacements is shown in Figure 6.11 (for rectangular impulse) and in Figure 6.12 (for fluctuating pressure). In the studies reported in this section, the cutting frequency for Δt = 0.03 sec is f_c = 16.66 Hz, so that a broad range of natural frequencies of the tank may be taken into account. The natural frequencies have been computed from an eigenvalue analysis using ABAQUS/Standard (ABAQUS, 2002) and are included in Table 6.1. However, the results have been plotted up to a frequency of 5 Hz because for higher frequencies the amplitudes are negligible and do not provide additional information. Figures 6.11(a) and 6.12(a) show the FFT of the response, while Figure 6.11(b) and Figure 6.12(b) show the FFT of the acting loads. In both loading cases, the highest contribution to the displacement response is at the zero frequency with small peaks occurring for frequencies smaller than 0.5 Hz in Figure 6.11(a)

The FFT of the response for constant pressure with limited duration shows peaks for low frequencies that may be due to the period of the oscillations after the tank has buckled. This period is 2.78 sec (frequency 0.35 Hz) and this is what can be observed for the third peak in Figure 6.11(a). The FFT of the response for the fluctuating pressure is shown in Figure 6.12(a) following buckling, the period of oscillation is 0.85 sec (1.43 Hz), which the FFT shows a small peak.

The possibility of coupling between the excitation and the natural frequency of the structure has been considered, but it seems that only for frequency zero there is a strong coupling and there are only minor effects for higher frequencies. This suggests that even for the case of fluctuating load, resonance does not occur as Figure 6.12(a) and (b) illustrate.

An alternative analysis was to split the response to distinguish between the pre-buckling and the post-buckling transient displacements, and to compute the FFT for each part separately. The results are drawn in Figure 6.13(a) for the rectangular impulse and in Figure 6.13(b) for the fluctuating load. Again, it can be seen that the maximum response occurs at zero frequency and that there are no peaks with large amplitude for higher frequencies.

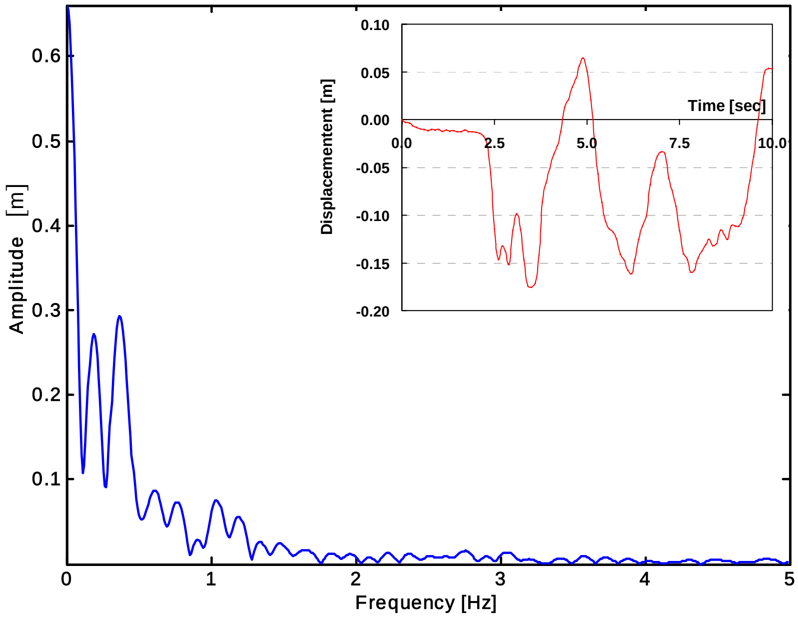

(a)

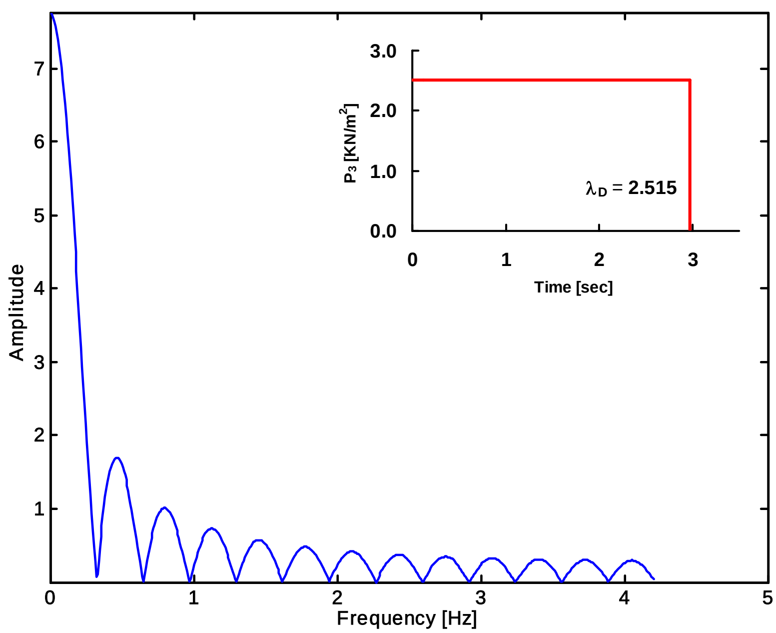

(b)

Figure 6.11. FFT of (a) Response to a constant amplitude pressure in time; (b) Constant amplitude load function.

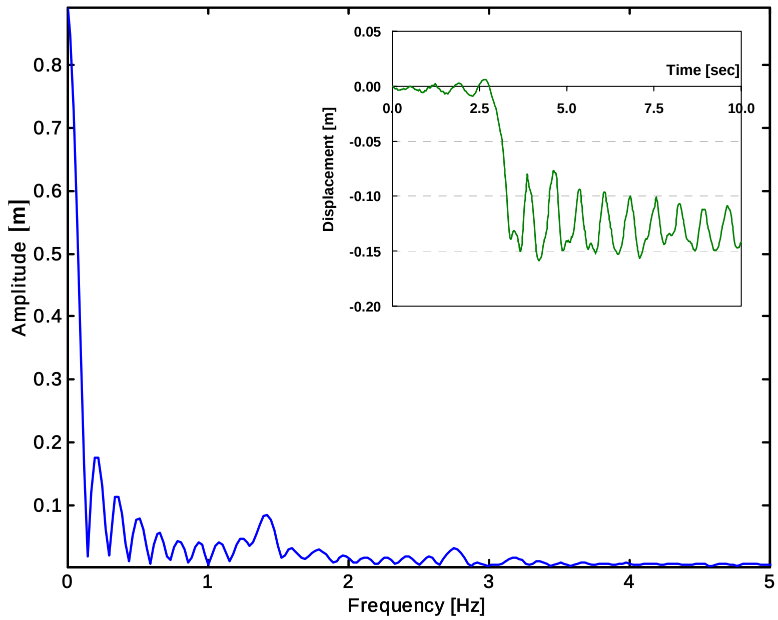

(a)

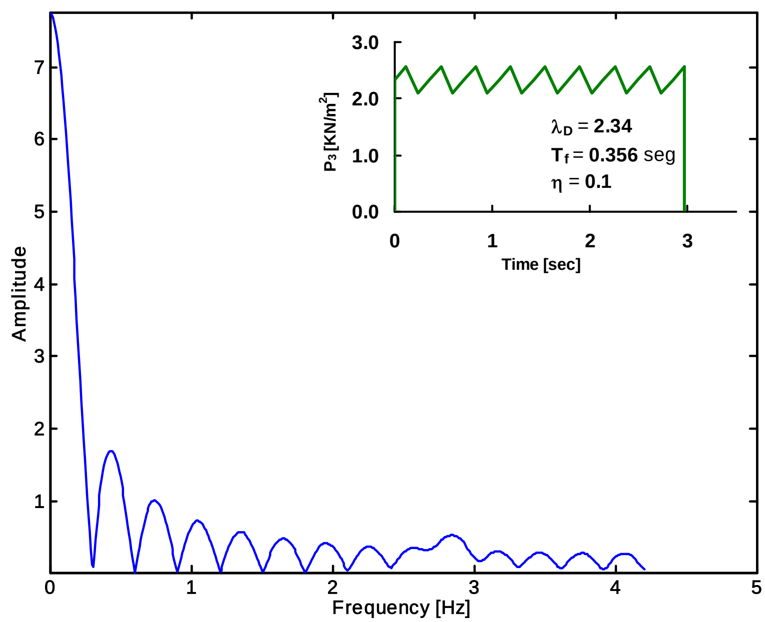

(b)

Figure 6.12. FFT of (a) Response to a fluctuating load; (b) Fluctuating load function.

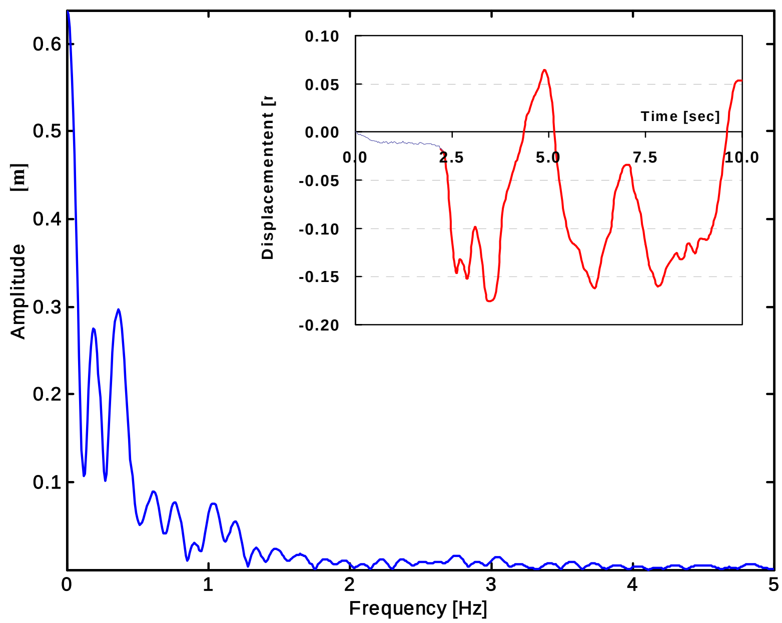

(a)

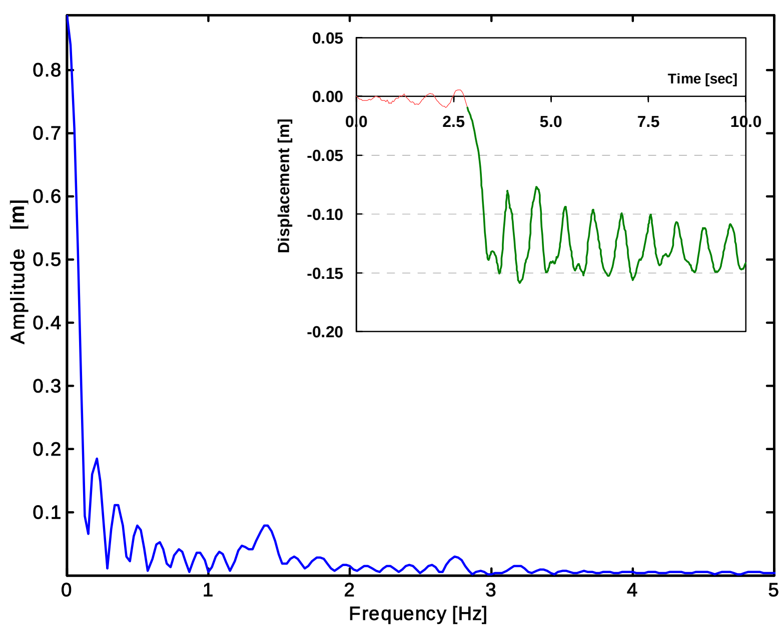

(b)

Figure 6.13. FFT of the response in the buckled state considered separately: (a) Constant load, high amplitude oscillations; (b) Fluctuating load, high amplitude oscillations.

6.7 CONCLUSIONS

The time domain results computed in this chapter indicate that for a deterministic model of velocity and pressure variations, variations in the period of oscillations do not produce a significant change in the dynamic buckling load.

For pressure fluctuations with small periods, the dynamic buckling load is close to the value obtained with a rectangular impulse of the same duration, and for periods longer than the natural period of the structure the same situation occurs. The coincidence of the period of excitation with the natural period of the tank does not induce large changes in the buckling strength.

The simpler pressure model based on a 3 sec rectangular impulse yields dynamic buckling loads only 5% higher than the worst situation considering pressure fluctuations. The small changes in the buckling load of short tanks due to a wide range of fluctuations seem to suggest that it would not be necessary to obtain a more refined record of wind velocities to account for wind changes at intervals less than 3 sec for this class of structures. The inclusion of Rayleigh damping in the model did not change the results by more than 1% for a modal damping ratio of 3%. Imperfections were found to play an important role. For imperfections with the shape of the buckling mode, the dynamic buckling load was reduced following a pattern similar to static buckling problems, with reductions of 30% for imperfections of the order of the thickness. This effect, however, is not due to the fluctuating load and is associated with the sensitivity of the shell itself; in other words, the same sensitivity is detected for tanks under pressure and analyzed statically.

The results computed in the frequency domain illustrate the close similarity between the FFT of the load and the response, for both rectangular impulse and fluctuating load. In all cases, the peaks in the FFT of load and response occur for frequency zero. For higher frequencies, within the range of the lowest natural frequencies of the tank, the peaks in the load have small amplitudes so that resonance may be ruled out as a likely effect.

The results discussed previously indicate that dynamic effects do not dominate the response for short tanks, so that static buckling models may provide a reasonable approximation to the buckling strength of the shell under deterministic wind simulations.

CHAPTER 7

CONCLUSIONS

7.1 SUMMARY OF CONTENTS

A brief summary of the results presented in this thesis is given here before conclusions are drawn. Chapter 1 describes the theme structures investigated in this work, i.e., cylindrical above-ground steel tanks. The chapter described their typical configuration, including conical roof, cylindrical shell and foundations. Motivation, scope, main objectives and methodology employed in this thesis were also presented in Chapter 1.

Chapter 2 gave an introduction to the buckling of tanks in the context of the theory of elastic stability. This chapter provided a conceptual framework to the following chapters and facilitated the explanation of the results of the computational experiments.

Chapters 3 to 6 constitute the central chapters of this thesis. Chapter 3 analyzed the effect of support settlements on a tank with a conical roof. Results using linear, geometric non-linear and bifurcation analysis were presented for a typical tank and for a small-scale model.

Chapter 4 introduced a methodology proposed in this thesis to compute lower bound buckling loads for different cylindrical tank configurations under uniform external pressure. This chapter introduced the reduced energy method to find the knock-down factor that reduces the classical critical load. Results were compared with analytical and numerical results available to validate the applicability of the proposed new procedure.

Chapter 5 is a continuation of the topics discussed in Chapter 4, in which the proposed reduced energy method was implemented for tanks similar to those considered in Chapter 4, but under a different load configuration. That chapter presented the results for wind pressures acting in different tank geometries, in order to find the variation of the knock-down factor as the geometry changes. Alternative ways to implement the reduced energy method were presented to improve the results obtained with the proposed methodology. Appendix A and B are directly related to Chapters 4 and 5, and contains detailed derivations of the constitutive model and illustrative input files used to implement the reduced energy approach.

Chapter 6 presented the results of computational experiments to evaluate the importance of dynamic effects on the theme structure under wind loads. A simplified time variation of wind gusts applied in conjunction with an adopted spatial variation, were used to compute the non-linear dynamic response. The effect of imperfections and damping were evaluated and results in the frequency domain were presented as an alternative way to explain the effect of inertial forces.

7.2 MAIN CONCLUSIONS

The results presented in this thesis show that small amplitude settlements produce large out-of-plane displacements in above-ground tanks. The buckling behavior is a stable symmetric bifurcation with only one branch, in which the post-critical path out-of-plane displacements increase with the amplitude of the vertical settlement. The results suggest that the shell buckles for a small value of the control parameter, and then deflects into a post-buckling mode that is different from what is found for buckling under pressure loads. This behavior under imposed settlements is attributed to the geometric non-linear behavior of the shell. Therefore, it does not seem adequate to establish tolerance criteria for settlements based on linear shell models, as the current engineering practice suggests.

The present research has shown that it is possible to implement a reduced energy method to estimate lower bound buckling pressures in tanks using a general purpose finite element code. The approach is accurate in predicting the knock-down factor for uniform pressures applied to different shell configurations. However, the same proposed methodology is not adequate to predict the lower bound buckling loads of tanks under wind pressures. This limitation is due to the change of the reduced critical deflected mode compared with respect to the classical critical mode. Such change in the critical modes was observed mainly in the cases for wind loads but it is almost inexistent under uniform pressures. Thus, the proposed reduced energy method can predict the lower bound load for cylindrical shells under uniform pressure distributions, but it cannot estimate the lower bound for wind pressures. The explanation is that a change in the modal shapes invalidates one of the principal assumptions made in the formulation of the reduced energy method, as originally formulated by Croll (1975), which assumes that the mode in the lower bound is the same as in the classical bifurcation analysis using the full membrane stiffness of the shell.

Concerning the influence of inertial effects on the buckling under wind pressures, it was found that changes in the period of fluctuations of the applied load do not produce significant changes in the dynamic buckling loads. The small changes in the buckling load of short tanks due to a wide range of fluctuations seem to suggest that it would not be necessary to obtain a more refined record of wind velocities to account for wind changes at intervals less than 3 sec. The inclusion of damping in the model did not change the results significantly. However, imperfections were found to play an important role, producing a drop of about 30% in the buckling load. Such drop is associated to the static imperfection sensitivity of the shell, as it is observed in tanks under pressure which are analyzed using static methods. Frequency domain results show that in all cases the peaks in the FFT of the load and response occur for frequency zero. For higher frequencies, within the range of the lowest natural frequencies of the tank, the peaks have small amplitudes so that resonance may be discarded as a likely effect. Thus, it is concluded that dynamic effects do not dominate the response for short tanks, so that static buckling models may provide a reasonable approximation to the buckling strength of the shell under deterministic wind simulations.

7.3 ORIGINAL CONTRIBUTIONS OF THIS THESIS

The main original contributions of this work are:

1- The implementation of the reduced energy method using a general purpose finite element code for cylindrical shells under uniform and wind pressures.

2- The interpretation of the response of cylindrical tanks under deterministic fluctuating loads in frequency domain.

3 - The understanding of the buckling behavior of cylindrical tanks under support settlements, and the identification of the importance of geometric non-linearity in this problem.

7.4 RECOMMENDATIONS FOR FUTURE WORK

7.4.1 ON THE REDUCED ENERGY METHOD

The reduced energy method proposed and implemented in this thesis can be applied to investigate cylindrical panels under uniform pressure. This type of structure has been studied by Yamada and Croll (1989), who reported an analytical solution to compute the lower bound buckling loads using the reduced energy method. In the implementation of the method they state that "…the eigenvalue analysis in this case is identical with the classical critical analysis of a complete cylinder simply supported at this ends…" (pp. 333). Such cylinder has been the benchmark of the proposed methodology in this thesis, reporting good agreement with the theoretical solution. Furthermore, for the cylindrical panel, Yamada and Croll state that "…a reduced stiffness critical pressure is defined as that for which all the initially stabilizing membrane energy has been eroded from the classical critical buckling mode…" (pp. 334), which is the same assumption adopted for the cases studied in Chapters 4 and 5 of this thesis. Probably the most important assumption stated by Yamada and Croll for this structures is that "…the out-plane critical mode to be unchanged…" (pp.335) in the solution of the reduced eigenvalue problem. Clearly, this seems to be a good case to be implemented using a general purpose finite element code with the methodology presented here.

7.4.2 ON FLUCTUATING LOADS IN TANKS

Concerning the consideration of fluctuations in wind loads, and since it was found in Chapter 6 that inertial effects do not play an important role in the behavior of empty tanks for short duration wind gusts, future work may be oriented to consider the fluctuations of wind loading as a stationary random process, in which the mean component is separated from the fluctuation component and applied to the structure as an equivalent quasi static or static wind loading. Introducing an influence coefficient to account for the time dependency and spatial variation of wind loads, it would be possible to represent more realistically the effect of fluctuations on the behavior of relatively large structures like the tanks considered in this thesis. Holmes and Kasperski (1996) state that for wind loads "…in some respects the dynamic effects are similar to earthquake loading; however there are two significant differences: a) in most windstorms and for most structures the frequencies of the dynamic wind forces are lower than the natural frequencies of the structures; b) the lack of correlation of the fluctuating forces which results in spatial variations in the forces acting on structures of significant dimensions…"

(pp. 1). For our purposes, windstorms are associated to hurricanes, and some of the tanks considered in this thesis may be considered structures of significant dimensions.

Holmes and Kasperski suggest that "…for the majority of the structures the resonant response is either significant but not dominant, or is negligible. For these structures the sub-resonant fluctuating loading is important and for those with significant tributary areas, the correlation effect, as described previously above is significant…" (pp. 1) Sub-resonant or 'background' wind loading is the quasi-static loading produced by fluctuations due to turbulence, but with frequencies too low to excite any resonant response. Considering the fluctuations of wind loading as a stationary random process in which the mean component is separated from the fluctuation component, Holmes and Kasperski (1996), also suggest a procedure in which "…the equivalent static peak loading distributions can be separately derived for the following three components: 1-Mean component; 2-Background or sub-resonant component; and 3-Resonant component…" (pp. 2). These researchers proposed several expressions to compute each component, assuming that the peak response is dominated by the first mode of vibration. For cylindrical tanks, Virella (2003) reported that in cone roof tanks the first modes of vibrations are cylinder modes. Considering that significant deflections occur in the cylindrical shell during hurricanes, the method proposed by Holmes and Kasperski may be implemented to compute the maximum response taking into account the fluctuations in the pressure.

Other alternative to analyze in future work is the consideration of longer wind gusts than studied in this thesis. The same procedure used in Chapter 6 to model short duration wind gusts can be extended to analyze the influence in the dynamic buckling load of longer wind gusts (> 3 sec) with the same proposed pattern of fluctuations and to examine if tanks are sensitive to load applied during a relatively extended period of time.

7.4.3 OTHER TOPICS

Considering other topics studied in this thesis, future work in the area of modeling the tank support may be oriented to model the support including the metal floor and the contact with the compacted soil foundation. During the construction of a tank, the structure is not fully restrained by the soil foundation. Sudden pressures, such as wind loads may be highly destructive, not only for the shell itself but also for the foundation. Detailed models of the foundation and of the tank floor may be useful to determine the optimal configuration to avoid a premature buckling, as reported by Jaca and Godoy (2003).

APPENDIX A

CONSTITUTIVE RELATION FOR THE REDUCED ENERGY METHOD

Classical lamination theory, based on Kirchhoff hypothesis, gives force N and moment M resultants by the following constitutive relation:

$$\begin{Bmatrix} N \\ M \end{Bmatrix} = \begin{bmatrix} \mathbf{A} & \mathbf{B} \\ \mathbf{B} & \mathbf{D} \end{bmatrix} \begin{Bmatrix} \varepsilon \\ \kappa \end{Bmatrix} \qquad \text{(A.1)}$$

The constitutive matrix in equation A.1 is a 6 × 6 matrix usually called [ABD] matrix. This matrix is composed by three sub matrices [**A**], [**B**] and [**D**] and each one is 3 × 3 in size and symmetric. Sub matrices have different functions in [ABD] matrix, they are:

- Matrix [**A**] is called in plane stiffness matrix because it directly relates in plane strains ε to in plane forces N. This matrix is also called stretching matrix.
- Matrix [**B**] is the coupling matrix and relates in plane strains to bending moments and curvatures to in plane forces. This coupling effect does not exist for homogeneous plates. This matrix is also called bending-extension coupling matrix.
- Matrix [**D**] is the bending stiffness matrix because it relates curvatures κ to bending moments M.

The coefficients A_{ij}, B_{ij} and D_{ij} of each sub matrix, are functions of the thickness, orientation, stacking sequence, and material properties of the layers. Matrix [ABD] can be expressed in an expanded form as:

$$\begin{Bmatrix} N_x \\ N_y \\ N_{xy} \\ M_x \\ M_y \\ M_{xy} \end{Bmatrix} = \begin{bmatrix} A_{11} & A_{12} & A_{16} & B_{11} & B_{12} & B_{16} \\ A_{12} & A_{22} & A_{26} & B_{12} & B_{22} & B_{26} \\ A_{16} & A_{26} & A_{66} & B_{16} & B_{26} & B_{66} \\ B_{11} & B_{12} & B_{16} & D_{11} & D_{12} & D_{16} \\ B_{12} & B_{22} & B_{26} & D_{12} & D_{22} & D_{26} \\ B_{16} & B_{26} & B_{66} & D_{16} & D_{26} & D_{26} \end{bmatrix} \begin{Bmatrix} \varepsilon_x \\ \varepsilon_y \\ \gamma_{xy} \\ \kappa_x \\ \kappa_y \\ \kappa_{xy} \end{Bmatrix} \tag{A.2}$$

where each term of the sub matrices are given by:

$$A_{ij} = \sum_{k=1}^{n} \left(\overline{Q}_{ij}\right)_k (z_k - z_{k-1}) = \sum_{k=1}^{n} \left(\overline{Q}_{ij}\right)_k t_k \qquad i, j = 1, 2, 6 \tag{A.3}$$

$$B_{ij} = \frac{1}{2} \sum_{k=1}^{n} \left(\overline{Q}_{ij}\right)_k (z_k^2 - z_{k-1}^2) = \sum_{k=1}^{n} \left(\overline{Q}_{ij}\right)_k t_k \overline{z}_k \qquad i, j = 1, 2, 6 \tag{A.4}$$

$$D_{ij} = \frac{1}{3} \sum_{k=1}^{n} \left(\overline{Q}_{ij}\right)_k (z_k^3 - z_{k-1}^3) = \sum_{k=1}^{n} \left(\overline{Q}_{ij}\right)_k \left(t_k \overline{z}_k^2 + \frac{t_k^3}{12} \right) \qquad i, j = 1, 2, 6 \tag{A.5}$$

In equations A.3 to A.5, z_k is the coordinate of each layer, t_k is the thickness of each layer, $\overline{z}_k$ is the distance to the middle surface of the k_{th} layer, and $\overline{Q}_{ij}$ are the components of the transformed reduced stiffness matrix. Those components relate strains and stresses of a lamina in plane state of stress. Explicitly, they are:

$$\overline{Q}_{11} = Q_{11} \cos^4\theta + 2(Q_{12} + 2Q_{66}) \sin^2\theta \cos^2\theta + Q_{22} \sin^4\theta \tag{A.6}$$

$$\overline{Q}_{12} = \hat{Q}_{12} \sin^2\theta \cos^2\theta + Q_{12} (\sin^4\theta + \cos^4\theta) \tag{A.7}$$

$$\overline{Q}_{22} = Q_{11} \sin^4\theta + 2(Q_{12} + 2Q_{66}) \sin^2\theta \cos^2\theta + Q_{22} \cos^4\theta \tag{A.8}$$

$$\overline{Q}_{16} = \hat{Q}_{16} \sin\theta \cos^3\theta + \hat{Q}_{26} \sin^3\theta \cos\theta \quad \text{(A.9)}$$

$$\overline{Q}_{26} = \hat{Q}_{16} \sin^3\theta \cos\theta + \hat{Q}_{16} \sin\theta \cos^3\theta \quad \text{(A.10)}$$

$$\overline{Q}_{66} = \hat{Q}_{66} \sin^2\theta \cos^2\theta + Q_{66}\left(\sin^4\theta \cos^4\theta\right) \quad \text{(A.11)}$$

where

$$\hat{Q}_{12} = Q_{11} + Q_{22} - 4Q_{66} \quad \text{(A.12)}$$

$$\hat{Q}_{16} = Q_{11} - Q_{12} - 2Q_{66} \quad \text{(A.13)}$$

$$\hat{Q}_{26} = Q_{12} - Q_{22} + 2Q_{66} \quad \text{(A.14)}$$

$$\hat{Q}_{66} = Q_{11} + Q_{22} - 2Q_{12} - 2Q_{66} \quad \text{(A.15)}$$

Each Q_{ij} in equations A.6 to A.15 are the plane-stress reduced stiffness coefficients given by:

$$Q_{11} = \frac{E_1}{1 - \nu_{12}\nu_{21}} \quad \text{(A.16)}$$

$$Q_{12} = \frac{\nu_{12}E_2}{1 - \nu_{12}\nu_{21}} \quad \text{(A.17)}$$

$$Q_{22} = \frac{E_2}{1 - \nu_{12}\nu_{21}} \quad \text{(A.18)}$$

$$Q_{66} = G_{12} \quad \text{(A.19)}$$

Notice that the plane stress-reduced stiffness coefficients involve four independent material constants, E_1, E_2, ν_{12} and G_{12}. In the implementation of the proposed reduced energy method, described in Chapter 4, a single layer laminate is used to represent the cylindrical shell. This single lamina has its local principal axis (1) coincident with axis of revolution of the cylindrical shell considered. ($\theta = 0$). With that orientation the coefficients given by equations A.6 to A.15 are:

$$\bar{Q}_{11} = \frac{E_1}{1 - \nu_{12}\nu_{21}} \tag{A.20}$$

$$\bar{Q}_{12} = \frac{\nu_{12}E_2}{1 - \nu_{12}\nu_{21}} \tag{A.21}$$

$$\bar{Q}_{22} = \frac{E_2}{1 - \nu_{12}\nu_{21}} \tag{A.22}$$

$$\bar{Q}_{66} = G_{12} \tag{A.23}$$

$$\bar{Q}_{16} = \bar{Q}_{26} = 0 \tag{A.24}$$

Coefficients given in equations A.20 to A.24 are introduced in equations A.3 to A.5 and the resultant [ABD] matrix has the following particularities: the assumed single lamina is symmetric with respect to its mid plane, so that the bending-coupling coefficients B_{ij} are zero. According to equation A.24, coefficients A_{16}, A_{26}, D_{16} and D_{26} are zero. The resultant laminate is a quasi-isotropic laminate that do not behave exactly like an isotropic plate. However, a quasi-isotropic laminate can approximate reasonable well an isotropic laminate by using a symmetric balanced laminate 0/90 and $\pm\theta$ layers and a large number of layers. With such design, using orthotropic laminas with different engineering constants in each local direction, bending coefficients are approximately $D_{11} \approx D_{22}$ and, D_{16} and D_{26} must be as small as possible (Barbero, 1998). Other alternative is assuming the same engineering constants for each local direction of a single lamina, i.e. $E_1 = E_2 = E$, $\nu_{12} = \nu_{21} = \nu$ and $G_{12} = G = E / 2\ (1+ \nu)$. This second option was used in this work and the resultant [ABD] matrix is:

$$ABD = \begin{bmatrix} A_{11} & A_{12} & 0 & 0 & 0 & 0 \\ A_{12} & A_{11} & 0 & 0 & 0 & 0 \\ 0 & 0 & A_{66} & 0 & 0 & 0 \\ 0 & 0 & 0 & D_{11} & D_{12} & 0 \\ 0 & 0 & 0 & D_{12} & D_{11} & 0 \\ 0 & 0 & 0 & 0 & 0 & D_{26} \end{bmatrix} \quad \text{(A.25)}$$

In [ABD] matrix given by equation A.25, the coefficients A_{ij} are associated to membrane stiffness and coefficients D_{ij} are associated to bending stiffness. In the proposed reduced energy method introduced in Chapter 4, the membrane stiffness is eroded in the critical state introducing a reduction factor α to reduce gradually the membrane stiffness. Such reduction factor affects only to A_{ij} terms and the membrane stiffness decreases as α increase. Then, the modified constitutive matrix to account the reduction in the membrane stiffness is:

$$ABD = \begin{bmatrix} \frac{A_{11}}{\alpha} & \frac{A_{12}}{\alpha} & 0 & 0 & 0 & 0 \\ \frac{A_{12}}{\alpha} & \frac{A_{11}}{\alpha} & 0 & 0 & 0 & 0 \\ 0 & 0 & \frac{A_{66}}{\alpha} & 0 & 0 & 0 \\ 0 & 0 & 0 & D_{11} & D_{12} & 0 \\ 0 & 0 & 0 & D_{12} & D_{11} & 0 \\ 0 & 0 & 0 & 0 & 0 & D_{26} \end{bmatrix} \quad \text{(A.26)}$$

ABAQUS (2002) allows to the user to introduce as direct input the upper triangle part of [ABD] matrix. Using this feature requires to define the shell property as *SHELL GENERAL SECTION and assigning such property to all shell elements that are part of the cylindrical shell. All computations described in Chapters 4 and 5 were performed using this constitutive model. In those cases in which the cylindrical shell is formed by courses of different thickness, for each one, a [ABD] matrix was computed and introduced in the model.

APPENDIX B

INPUT FILES FOR THE PROPOSED REDUCED ENERGY METHOD

This appendix presents input files used in ABAQUS (2002) in the implementation of the proposed reduced energy method. The computation of the knock-down factor defined in Chapter 4 is divided in two stages:

● First a classical eigenvalue analysis is performed to extract the critical buckling load and the critical mode. For this stage the material is defined as elastic isotropic.

● Next, from the first stage, the critical eigenmode is extracted and imposed as prescribed displacements in a second analysis where the strain energy is calculated for different levels of reductions in the membrane stiffness. The constitutive relation for the material at this stage of computations is defined by the [ABD] matrix described in Appendix A.

Next two pages show illustrative input files for both computation stages.

```
*HEADING
First Stage: Classical eigenvalue problem [N/m]
**GEOMETRY DEFINITION
*Node
1,12.,0.,0.
…
**ELEMENT DEFINITION
*Element, type=STRI3
1,506,4 ,5
2,522,20,21
…
**NODE AND ELEMENT SETS DEFINITION
*Nset, Nset =DESP
*Nset, Nset =BASE
*Elset,Elset=CILI
…
**SECTION AND MATERIAL DEFINITION
*Shell Section, Elset=CILI, material=STEEL
0.006, 5
*Material, name=STEEL
*Elastic
 2.06e+11, 0.3
**
**ANALYSIS DEFINITION
*Step, name=BKL, perturbation
*Buckle, Eigensolver=Lanczos
2, 0.001,
**BOUNDARY CONDITIONS
*Boundary, op=NEW, load case=1
BASE, ENCASTRE
*Boundary, op=NEW, load case=2
BASE, ENCASTRE
**LOADS DEFINITION
*Dsload
CILI, P, 1000.
**OUTPUT REQUESTS
*Node File, Nset=DESP, Global=yes
U
*Node Print, Nset=DESP
U1, U2, U3
*End Step
```

```
*HEADING
Second Stage: Energy computations [N/m]
**GEOMETRY DEFINITION
*Node
1,12.,0.,0.
…
**ELEMENT DEFINITION
*Element, type=STRI3
1,506,4 ,5
2,522,20,21
…
**NODE AND ELEMENT SETS DEFINITION
*Nset, Nset =DESP
*Nset, Nset =BASE
*Elset,Elset=CILI
…
**MATERIAL DEFINITION-ABD MATRIX
*Shell General Section, Elset=CILI
|A/alpha 0|
|0       D|
**BOUNDARY CONDITIONS
*Boundary
BASE, ENCASTRE
*AMPLITUDE, NAME=FMODAL,VALUE=RELATIVE,DEFINITION=TABULAR
0.0,0.0,1.0,0.001
**
**ANALYSIS DEFINITION: Imposed displacements
*STEP
*STATIC
*Boundary, type=displacement, amplitude=FMODAL
2,1,1, 4.7684e-003
2,2,2, 1.0000e+000
2,3,3, 4.5672e-003
…
**OUTPUT REQUESTS
*Energy Print, Elset=CILI
*End Step
```

REFERENCES

AISC (2001), "*Manual of steel construction, load and resistance design*", American Institute of Steel Construction, Chicago, IL.

ABAQUS (2002), "*User's Manuals, Version 6.3*", Hibbitt, Karlsson and Sorensen, Inc. Rhode Island.

ACI-ASCE Committee 334 (1995), "*Reinforced concrete cooling towers shells- practice and commentary*". ACI 334, 2R, 91. American Concrete Institute, New York.

API Standard 650 (1988), "*Welded steel tanks for oil storage*", American Petroleum Institute, Washington, D.C.

ASCE-7-02 (2002), "*Minimum Design Loads for Buildings and other Structures*, ASCE, Reston, VA.

Barbero, E.J. (1998), "*Introduction to composite materials design*", Taylor and Francis, Philadelphia, PA.

Batista, R. (1979), "*Lower bound estimates for cylindrical shell buckling*", Ph.D. Thesis, University College. London.

Batista, R. and Croll J.G.A. (1979), "A design approach for unstiffened cylindrical shells under external pressure", *International Conference on Thin Walled Structures*, University of Strathclyde, Crosby Lockwood, Glasgow.

Batoz, J.L., Bathe, K.J. and Ho L.W. (1980), "A study of three-node triangular plate bending elements," *International Journal for Numerical Methods in Engineering*, vol. 15, pp. 1771–1821.

Bell, R.A. and Iwakiri, J. (1980), "Settlement comparison used in tank-failure study", *Journal of the Geotechnical Engineering Division ASCE*, vol. 106 (2), pp. 153-169.

Brown, G.D. and Peterson, W.G. (1964), "Failure of an oil storage tank founded on sensitive marine clay", *Canadian Geotechnical Journal*, vol. 1, pp. 205-214.

Brush, D.O. and Almorth, B.O. (1975), "*Buckling of Bars, Plates and Shells*", McGraw-Hill, New York.

Budiansky, B. and Roth, S. (1962), "Axisymmetric dynamic buckling of clamped shallow spherical shells", *NASA Collected papers on stability of shell structures*, TN-1510, pp. 597-606.

Budiansky, B. and Sanders, J.L. (1963), "On the `best' first-order linear shell theory", *Progress in Applied Mechanics, The Prager Anniversary Volume*, Macmillan, London, pp. 129–140.

Computer and Structures, (2002), "*SAP2000 Version 8, Analysis Reference Manual*", C&S, Berkeley, California.

Clark, J.S. (1969), "Survey of oil tank failure", *Annales de l'Institute Belge du Petrol*, vol. 6, pp. 15-24.

Croll, J.G.A. (1975), "Towards simple estimates of shell buckling loads", *Der Stahlbau*, Part I, Heft, August; Part II Heft September.

Croll, J.G.A. (1995), "Towards a rationally based elastic-plastic shell buckling design methodology", *Thin Walled Structures*, vol. 23, pp. 67-84.

Croll, J.G.A. and Batista, R. (1981), "Explicit lower bounds for the buckling of axially loaded cylinders", *International Journal of Mechanical Sciences*, vol. 23, pp. 333-343.

Croll, J.G.A. and Billington, D.P. (1979), "*Cooling towers with non-axisymmetric foundation*", Princeton University, Research Report #79-SM-25, pp. 1-57.

Croll, J.G.A. and Ellinas, C.P. (1983), "Reduced stiffness axial buckling of cylinders," *International Journal of Solid Structures*, vol. 19 (No 5), pp. 461-477.

Croll, J.G.A. and Walker, A.C. (1972), "*Elements of structural stability*", Halsted Press, John Wiley and Sons, Inc, New York.

Donell, L. (1976), "*Beams, plates and shells*", Chapter 6, McGraw-Hill, New York.

D'Orazio, T., Ducan, J.M. and Bell, R.A. (1989), "Distortion of steel tank due to settlement of their walls", *Journal of the Geotechnical Engineering Division ASCE*, vol. 115(6), pp. 871-890.

D'Orazio, T. and Ducan J.M. (1987), "Differential settlements in steel tanks", *Journal of the Geotechnical Engineering Division ASCE*, vol. 113 (9), pp. 967-983.

Doyle, J.F. (2001), "*Non-linear analysis of thin-walled structures*", Springer-Verlag, New York.

Flores, F.G. and Godoy, L.A. (1998), “Buckling of short tanks due to hurricanes”, *Engineering and Structures*, vol. 20(8), pp. 752-760.

Flores, F.G. and Godoy, L.A. (1999), “Forced vibration of silos loading to buckling”, *Journal of Sound and Vibrations*, vol. 224(3), pp. 431-454.

Gavrylenko, G.D. and Croll, J.G.A. (2001), “Validation of analytical lower bounds for the imperfection sensitive buckling of axially loaded rotational symmetric shells,” *Third International Conference of Thin-Walled Structures*, Krakow, Poland, pp. 643-651.

Godoy, L.A. (2000), “*Theory of Elastic Stability: Analysis and Sensitivity*”, Taylor and Francis, Philadelphia, PA.

Godoy, L.A. and Flores, F.G. (2002), “Imperfection sensitivity to elastic buckling of wind loaded open cylindrical tanks”, *Structural Engineering and Mechanics*, vol. 13(5), pp. 533-542.

Godoy, L.A. and Méndez, J.C. (2001), “Buckling of aboveground storage tanks with conical roof”, *Thin-Walled Structures: Advances and Developments*, Ed. J. Zaras, K. Kowal-Michalska and J. Rhodes, Elsevier, Oxford, pp. 661-668.

Godoy, L.A., Portela, G., Sosa, E.M., Suárez, L.E., Virella J.C and Zapata, R. (2002), “Damage due to buckling in aboveground storage tanks”, *Proceedings of the III Int. Conf. on the Behavior of Structures with Damage, DAMSTRUC 2002*, Ed. P. Castro, Rio de Janeiro, Brazil.

Godoy, L.A. and Sosa, E.M. (2003), “Localized support settlements of thin-walled storage tanks”, *Thin-Walled Structures*, vol. 41, pp. 941-955.

Godoy, L.A., and Sosa, E.M. (2002), “Deflections of thin-walled storage tanks with roof due to localized support settlement”, *Proceedings of the II Int. Conf. on Advances in Structural Engineering and Mechanics*, Techno-Press, Seoul, Korea.

Godoy, L.A. and Sosa E. M. (2002). “Computational buckling analysis of shells: Theories and practice”, *Mecánica Computacional*, vol. 21, pp. 1652-1667.

Gopalacharyulu, S. and Johns, D.J. (1973), “Cantilever cylindrical shells under assumed wind pressures”, *Journal of the Engineering Mechanics Division*, ASCE, vol. 99(EM5), pp. 943-956.

Gould, P. (1972), “Differential settlements of hyperbolic cooling towers”, *Journal of the Structural Division*, ASCE, vol. 98(10), pp. 2207-2219.

Green, P.A. and Hight, D.W. (1964), "The failure of two oil storage tanks caused by differential settlement", *Proceedings of the Conference on Settlement of Structures*, British Geotechnical Society, Cambridge, England, pp. 353-360.

Greiner, R. (1998), "*Cylindrical shells: wind loading*", Chapter 17 in Silos, EFN Spon, London.

Greiner, R. and Derler, P. (1995), "Effect of imperfections on wind loaded cylindrical shells", *Thin-Walled Structures*, vol. 23(1-4), pp. 271-281.

Holmes, J.D. and Kasperski, M. (1996), "Effective distributions of fluctuating and dynamic wind loads", Australian Civil/Structural Engineering Transactions, vol. CE38 (2-3-4).

Hutchinson, J.W. and Koiter, W.T. (1970), "Post-buckling theory", *Applied Mechanics Reviews*, vol. 23(12), pp. 1353.

Jaca, R. and Godoy, L.A. (2003), "Colapso de un tanque metálico en construcción bajo la acción del viento", *Revista Internacional de Desastres Naturales, Accidentes e Infraestructura Civil*, vol. 3(1), pp. 73-83.

Jerath, S. and Sadid, H. (1985), "Buckling of orthotropic cylinders due to wind load", *Journal of Engineering Mechanics*, ASCE, vol. 111(5), pp. 610-622.

Jonaidi, M. and Ansourian, P. (1998), "Harmonic settlement effects on uniform and tapered tank shells", *Thin-Walled Structures*, vol. 31, pp. 237-255.

Kamyab, H. and Palmer, S.C. (1989), "Analysis of displacements and stresses in oil storage tanks caused by differential settlement", *Proceedings of Institutional Mechanical Engineers, Part C: Journal of Mechanical Engineering Science*, vol. 203, pp. 60-70.

Koiter, W.T. (1945), "*On the Stability of Elastic Equilibrium*", Ph.D. Thesis, Delft (in Dutch with English summary). H.J. Paris, Amsterdam.

Koluza, R. and Mateja, O. (1976), "Problems of the influence of irregular displacements of foundation on the state of stress and displacement of a hyperboloidal cooling tower", *Bulletin of the International Association for Shell and Space Structures,* vol. 17(3), pp. 47-79.

Krätzig, W.B and Niemann, H.J. (1996), "*Dynamics of civil engineering structures*", A.A. Balkema, Rotterdam, Netherlands.

Kundurpi, P. S., Gopalacharyulu, S. and Johns, D.J. (1975), "Stability of cantilever shells under wind loads", *Journal of Engineering Mechanics*, ASCE, vol. 101 (EM5),pp. 517-530.

Lu, W., Lin, B. and Lu, R. (1986), "Effect of unequal settlement of foundation on the stress resultants of hyperbolic cooling towers and the unequal settlement tolerance limit", *Engineering Structures,* vol. 8, pp. 39-45.

Macdonald, P.A., Kwok, K.C.S. and Holmes, J.D. (1988), "Wind loads on circular storage bins and tanks: I. Point pressure measurements on isolated structures", *Journal of Wind Engineering and Industrial Aerodynamics*, vol. 31, pp. 165-188.

Malik, Z., Morton, J. and Ruiz, C. (1977), "Ovalization of cylindrical tanks as a result of foundation settlement", *Journal of Strain Analysis*, vol. 12, pp. 339-348.

Marr, A., Ramos, J.A. and Lambe, T.W. (1982), "Criteria for settlement of tanks", *Journal of the Geotechnical Engineering Division*, ASCE, vol. 108(8), pp. 1017-1039.

Maderpach, V. and Kamat, M.P. (1979), "Buckling of open cylindrical tanks due to wind loading," *Der Stahlbau*, H. 2, pp. 53-56.

Myers P. (1997), "*Aboveground Storage Tanks*", McGraw-Hill, New York.

Pandey, M.D. and Sherbourne, A.N. (1991), "Imperfection sensitivity of optimized laminated composite shells: a physical approach", *International Journal Solid and Structures*, vol. 27, pp. 1575-1595.

Portela, G. and Godoy, L.A. (2005), "Wind pressures and buckling of cylindrical steel tanks with conical roof", *Journal of Construction Steel Research*, vol. 61, No. 6, pp 786-807.

Purdy, D.M., Meher, F.J. and Frederik, D. (1967), "Model studies of wind load on flat-top cylinders," *Journal of the Structural Division*, ASCE, vol. 93(ST2), pp. 379-395.

Rish, R.F. (1967), "Forces in cylindrical shells due to wind," *Proceedings of the Institution of Civil Engineers*, vol. 36, pp. 791-803.

Riks, E. (1972), "The application of Newton's method to the problem of elastic stability", *Journal of Applied Mechanics*, vol. 39, pp. 1060-1065.

Riks, E. (1979), "An incremental approach to the solution of snapping and buckling problems", *International Journal of Solids and Structures*, vol. 15, pp. 529-551.

Sabransky, I.J. and Melbourne, W. H. (1987), "Design pressure distribution on circular silos with conical roofs". *Journal of Wind Engineering and Industrial Aerodynamics*, vol. 26, pp. 65-84.

Sosa, E.M. and Godoy, L.A. (2005a). "Non-linear dynamics of above-ground thin-walled tanks under fluctuating pressures", *Journal of Sound and Vibration*, vol. 283, pp. 201-215.

Sosa, E.M. and Godoy, L.A. (2005b). "Computation of lower-bound buckling loads using general-purpose finite element codes", *Proceedings of 3rd International Conference on Structural Stability and Dynamics*, June 19-22, Kissimmee, Florida.

Virella, J.C., Godoy, L.A. and Suárez, L.E. (2003). "Influence of the roof on the natural periods of steel tanks", *Engineering Structures*, vol. 25, pp. 877-887.

Virella, J.C. (2004). "*Buckling of steel tanks subject to earthquake loadings*", Ph.D. Thesis, University of Puerto Rico, Mayagüez, Puerto Rico.

Yamaki, N. (1984), "*Elastic stability of circular cylindrical shells*", North-Holland, Amsterdam.

Yamada, S. and Croll, J.G.A. (1989), "Buckling behavior pressure loaded cylindrical panels", *Journal of Engineering Mechanics*, ASCE, vol. 115(2), pp. 327-344.

Yamada, S. and Croll, J.G.A. (1993), "Buckling and post-buckling characteristics of pressure-loaded cylinders", *Journal of Applied Mechanics*, ASME, vol. 60, pp. 290-299.

Yamada, S. and Croll, J.G.A. (1999), "Contributions to understanding the behavior of axially compressed cylinders", *Journal of Applied Mechanics*, ASME, vol. 66, pp. 299-309.

Zintilis, G.M. and Croll, J.G.A. (1982), "Pressure buckling of end supported shells of revolution", *Engineering Structures*, vol. 4, pp. 222-232.

Zintilis, G.M. and Croll, J.G.A. (1983), "Combined axial and pressure buckling of end supported shells of revolution", Engineering Structures, vol. 5, pp. 199-206.